

## Distribution Agreement

In presenting this thesis or dissertation as a partial fulfillment of the requirements for an advanced degree from Emory University, I hereby grant to Emory University and its agents the non-exclusive license to archive, make accessible, and display my thesis or dissertation in whole or in part in all forms of media, now or hereafter known, including display on the world wide web. I understand that I may select some access restrictions as part of the online submission of this thesis or dissertation. I retain all ownership rights to the copyright of the thesis or dissertation. I also retain the right to use in future works (such as articles or books) all or part of this thesis or dissertation.

Signature:

---

Harrison Watters

---

Date

# Infraslow dynamics of the default mode network and a spectrum of external to internal attention

By  
Harrison Watters

Doctor of Philosophy  
Graduate Division of Biological and Biomedical Science  
Neuroscience

---

Sheila Keilholz, PhD  
Advisor

---

Kate McCann, PhD  
Committee Member

---

Malavika Murugan, PhD  
Committee Member

---

Dieter Jaeger, PhD  
Committee Member

Accepted:

---

Kimberly Jacob Arriola, Ph.D, MPH  
Dean of the James T. Laney School of Graduate Studies

---

Date

# Infraslow dynamics of the default mode network and a spectrum of external to internal attention

By

Harrison Watters  
B.A., Biology, University of Utah

Advisor: Shella Keilholz, PhD

An abstract of  
A dissertation submitted to the Faculty of the  
James T. Laney School of Graduate Studies of Emory University  
in partial fulfillment of the requirements for the degree of  
Doctor of Philosophy in Neuroscience  
Graduate Division of Biological and Biomedical Science  
2024

## Abstract

# Infraslow dynamics of the default mode network and a spectrum of external to internal attention

By Harrison Watters

Early efforts to understand the human cerebral cortex focused on localization of function, assigning functional roles to specific brain regions. More recent evidence depicts the cortex as a dynamic system, organized into flexible networks with patterns of spatiotemporal activity matching attentional demands. In functional MRI (fMRI), dynamic analysis of such spatiotemporal patterns is highly promising for providing non-invasive biomarkers of neurodegenerative diseases and neural disorders. However, there is no established neurotypical spectrum to interpret the burgeoning literature of dynamic functional connectivity from fMRI across attentional states. Here, we apply dynamic analysis of network-scale spatiotemporal patterns in a range of fMRI datasets across numerous tasks including a left-right moving dot task, visual working memory tasks, congruence tasks, multiple resting state datasets, mindfulness meditators, and subjects watching TV. Additionally, we compare QPP detection methods and explore the effects of prolonged behavioral training on cortical network dynamics, using a dataset of musical training. In our task vs rest datasets, we find that cortical networks show dynamic functional connectivity across a spectrum that tracks external vs internal attention. Dynamics of networks often grouped into a single task positive network show divergent responses along this axis of attention, supporting evidence that definitions of a single task positive network are misleading. Somatosensory and visual networks exhibit strong phase shifting along this spectrum of attention. Results from the multi-dataset task study were robust on a group and individual level, further establishing network dynamics as a potential individual biomarker. Finally, we explore the application of these results to biomarker discovery using an Alzheimer's Disease dataset as an example.

To our knowledge, this represents the first study of its kind to generate a spectrum of dynamic network relationships across such a breadth of tasks and brain states, representing a significant advance towards implementing dynamic functional connectivity as a biomarker.

# Infraslow dynamics of the default mode network and a spectrum of external to internal attention

By

Harrison Watters  
B.A., Biology, University of Utah

Advisor: Shella Keilholz, PhD

A dissertation submitted to the Faculty of the  
James T. Laney School of Graduate Studies of Emory University  
in partial fulfillment of the requirements for the degree of  
Doctor of Philosophy in Neuroscience  
Graduate Division of Biological and Biomedical Science  
2024

## Acknowledgements

I must express my gratitude to Dr. Shella Keilholz, who adopted me into her lab of biomedical engineers and MRI physicists when I had virtually no computational or fMRI experience. After failing to find a good fit across multiple lab rotations at Emory, I was in discussions with program leadership about quitting the doctoral program or seeking a terminal master's. Shella placed intellectual faith in me that was scarcely deserved. At every step she encouraged my creativity, my curiosity, and cultivated my growth as a scientist. I hope the work presented here is of some value to the broader scientific community, but if not, then at least to my friends and colleagues in the Keilholz lab.

I must also begrudgingly thank the late Dr. Carl Sagan, who lured me into believing that science was something beautiful, noble, and innately human. If it weren't for Carl encouraging me to step onto a ship of imagination in a goofy turtleneck, I probably wouldn't be living on an academic stipend as a 34-year-old graduate student while going gray with stress over a research document that five humans might ever read. As much as it pains me to admit, however, I do not regret my long voyage on this ship of imagination and will be forever grateful to Carl for sparking my curiosity to explore the cosmos without, and the cosmos within.

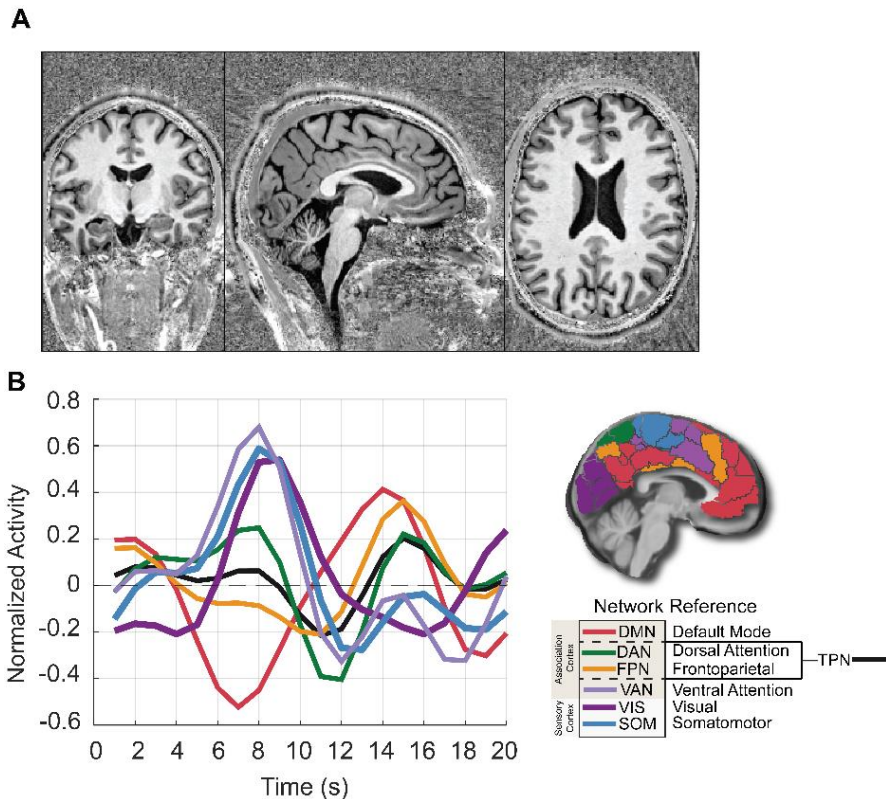


Figure: A) T1-weighted structural MRI of neuroscience graduate student in 3 planes (from left to right): coronal, sagittal, axial. B) Resting-state infraslow quasi-periodic pattern from the same subject, plotted as normalized blood oxygen level dependent (BOLD) fMRI activity for several major cortical networks. Thanks to Dr. Gopi for accepting me as a test subject for the 7T scanner at Emory University.

# Table of Contents

- **Chapter 1:** Introduction and Background: Anticorrelated dynamic patterns of the default mode and task positive networks – Quasi-Periodic Patterns
  - 1.1 Intrinsic brain activity and cortical networks
  - 1.2 Default mode and task positive networks
  - 1.3 Quasi-periodic patterns (QPPs) of cortical networks
  - 1.4 The goal of a multi-dataset application of QPP analysis across attentional states and disorders
  
- **Chapter 2:** Networks beyond the default mode and task positive networks show changes in quasi-periodic patterns that track an axis of external vs internal attention
  - 2.1 Introduction
  - 2.2 Methods
  - 2.3 Results
  - 2.4 Discussion
  - 2.5 Conclusions
  
- **Chapter 3:** QPP methods comparison and the effects of prolonged behavioral training on resting state cortical network dynamics, an example based on musical training data
  - 3.1 Introduction
  - 3.2 Methods
  - 3.3 Results
  - 3.4 Discussion

- 3.5 Conclusions
- **Chapter 4: Conclusions and future directions**
  - 4.1 Conclusions
  - 4.2 Discussion and Future directions – QPPs in Alzheimer’s Disease, cortical networks as attractor states
- Appendix A: CPAC processing pipeline
- Appendix B: Supplemental Tables
- Appendix C Supplementary Figures
- Funding Acknowledgements

# Chapter 1

Introduction and Background: Anticorrelated dynamic patterns of the default mode and task positive networks – Quasi-Periodic Patterns

1.1 Intrinsic brain activity

1.2 Default mode, task positive, and other cortical networks

1.3 Quasi-periodic patterns (QPPs)

1.4 The goal of a multi-dataset application of QPP analysis across attentional states and disorders

## 1.1 Intrinsic brain activity and cortical networks

**T**he brain consumes ten times the energy by weight of other organs in the human body on average, despite only accounting for 2% of body weight (1). The brain's high energy demand, 20% of all glucose metabolism in adult humans (1), is perhaps not surprising given that it is composed of the hundreds of billions of neurons and glia that form the biological basis of all conceivable sensation, behavior, and cognition.

What is more surprising is the relative energetic cost of task-related activity vs on-going **intrinsic activity** in the brain. Intuitively, one might predict that the greatest energy expenditures would accompany goal-directed behavior, task-related activity, or cognitive effort. However, when imaging with modalities such as positron emission tomography (PET) or functional magnetic resonance imaging (fMRI), even highly demanding perceptual, cognitive, or motor tasks cause no more than a 5% increase in regional blood flow or energy consumption (1, 2). In other words, most of the energy consumed by the most energy demanding organ goes not to facilitating goal-directed behavior or task activity, but to maintaining on-going activity and blood flow that happens independent of any task – intrinsic activity.

Not only does intrinsic activity consume a disproportionate amount of energy, but it is also organized in a decidedly non-random fashion into intrinsic cortical networks. Foundational fMRI work conducted by Biswal and colleagues in 1995 demonstrated that this type of intrinsic, or resting state, brain activity showed high functional correlation within canonical cortical networks, such as sensory and motor networks (3, 4). This means that even at rest the brain is organized into distributed cortical networks; the same networks that show organization during task activity. Subsequent work has

continued to validate these original findings, demonstrating that cortical networks show correlation and organization at rest, not merely in response to tasks. (1, 2, 5-8).

### 1.2 Default mode, task positive, and other cortical networks

There is no agreed upon universal taxonomy to describe cortical networks, with different groups and methods arriving at overlapping but distinct definitions (5). However, based on anatomical and functional criteria, several canonical cortical networks have emerged in the common vocabulary of brain imaging literature (5, 9, 10). In the present study, we use the Yeo's 7 network definitions which are estimated based on intrinsic functional connectivity, and we focus primarily on the following networks: default mode network (DMN), the task positive networks - dorsal attention (DAN) and frontoparietal (FPN) - ventral attention network (VAN), visual (VIS), and somatomotor (SOM) networks (10).

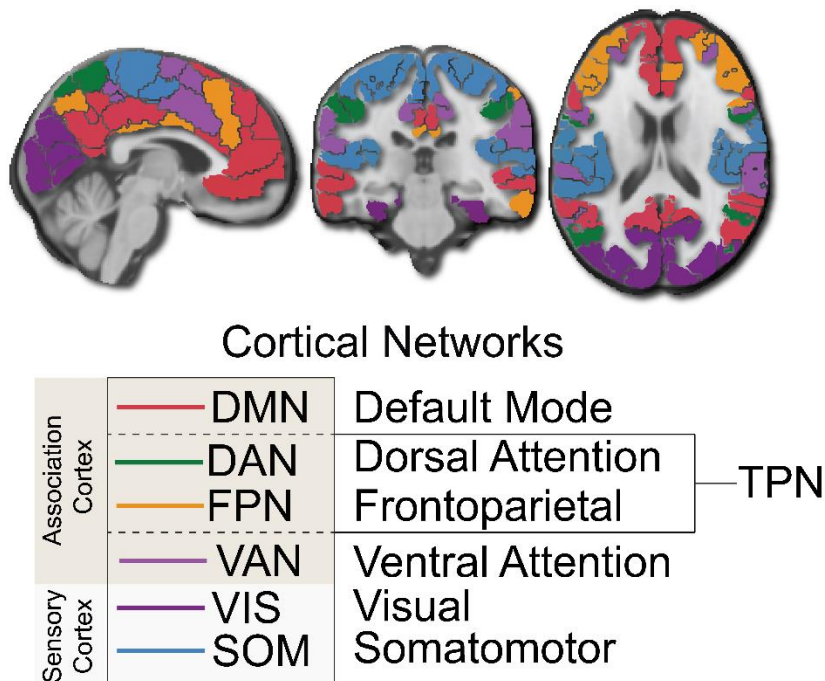


**Figure 1.1.** 6 of the primary intrinsic cortical networks of the human brain, which are the primary focus of the present study (the 7<sup>th</sup> network, the limbic network, is not shown). The DAN and FPN are

often grouped as the TPN. Networks are Yeo's networks (10) shown on an example parcellation and structural template from the Montreal neurological institute (MNI) 152 atlas.

These cortical networks, which can be grouped roughly into two categories, sensory-motor cortex and association cortex (Figure 1.1), also scale with phylogeny (11). This means that across mammals the relative size of cortical networks tracks the adaptive needs of the organism. In humans, highly social primates with one of the largest relative brain sizes, the massive evolutionary expansion of the neocortex corresponds to disproportionate growth of association networks such as the default mode network (11), while the relative change in area dedicated to primary sensation and motor cortex is minimal.

Foundational efforts in fMRI often focused on activation and functional connectivity (FC) of the sensory and motor cortical networks (12, 13). This makes good sense, as these studies were concerned with measuring changes in blood oxygen level dependent contrast (BOLD) signal in response to simple tasks like finger tapping. In the 2000's, attention turned to understanding the role of distributed cortical networks such as the **default mode network** (DMN) and the **task positive network** (TPN) (7, 14). Based primarily on task and resting state fMRI studies, the DMN shows increased activation during internally focused tasks while the TPN shows activation during goal-directed or external focus (15, 16). In global signal regressed fMRI time series (17), the relative activation of these two networks appears to work in opposition, meaning they show anticorrelated activity (7, 8, 14, 18). When one network's activation is high the other is low. The DMN, as its name implies, was originally thought to represent a sort of default or task-negative brain state that becomes dominant in the absence of any clear task (7, 15, 19). This thinking has been modified, as it is now clear that the DMN is also highly involved in a number of tasks, chiefly (but not exclusively) those tasks that involve internally directed attention such as mind wandering, memory encoding and recall, and maintenance of internal thought trains (7, 15, 20-24).

Based on traditional time-averaged FC analysis, which compares the averaged activity with respect to a seed or between networks across the entire scan, it has been demonstrated that the balance of anticorrelated activity between the DMN and TPN regions is related to healthy arousal, attention, and cognition (25, 26). This appears to be especially true of the typical anticorrelated activity seen between the DMN and the dorsal attention network (DAN), a task positive network that shows increased functional activation in response to externally focused and visual tasks (27-30). In time-averaged fMRI studies, loss of anticorrelation between the DMN and DAN is associated with poor task performance, aging, dementia, and sleep deprivation (28, 31-34). In congruence tasks, which present distractor or incongruent stimuli to demand increased cognitive effort during a task, deactivation of the DMN during the task has been shown to scale with task difficulty (35). Studies like these demonstrate that anticorrelated activity between the DMN and task positive regions is a feature of neurotypical development, as well as a critical feature of cortical resource allocation underlying attentional control.

Activity balance between DMN and task networks may have also been critical to the evolution of humans, social primates who rely heavily on generating and understanding shared narratives (15, 36). Beyond merely an internal attention or mind wandering network, the DMN may be critical for integrating information across domains of memory, language, and symbolic meaning for the purpose of constructing internal narratives, a sense of self, and theory of mind (37). Consistent with the understanding that the DMN is key to generating a sense of self, substances that can induce ego dissolution such as psilocybin, LSD, and THC, have all been found to affect DMN activity and/or reduce DMN/DAN anticorrelation (26, 38-41). Notably, in phylogenetically close primate relatives such as macaques, marmosets, and lemurs, the DMN lacks integration of the medial prefrontal cortex (mPFC), which may be key to increased regulation of DMN activity in humans, helping to set them apart in terms of social cognition (42). A growing body of evidence indicates that the DMN helps

us make sense of the world by integrating intrinsic information (memory) with incoming extrinsic information to form narratives and shared neural representations essential for building communal meanings and societies (43). For example, Zadbood and colleagues found that subjects viewing movies during fMRI had similar DMN activity in response to viewing and recalling the same narrative (44). In a storytelling task, subjects more successfully transmit and comprehend stories the more similar their DMN activity is - termed neural alignment or neural coupling (43, 45, 46). Additionally, the closer friends are in a social network, the more similar their DMN activity appears at baseline (47), and the more similar their DMN responses to viewing audiovisual movies are, an effect that decreases with decreasing closeness in a social network (48). In summary, the DMN, one of the major human cortical networks, has been implicated in a range of processes critical to human attention, cognition, and socialization.

### **1.3 Quasi-periodic patterns (QPPs)**

Most of the previously mentioned work explored the activity of the DMN and other networks using traditional time-averaged functional connectivity methods, which compare the averaged activity across a whole scan. While time-averaged, or seed-based FC methods have been foundational and incredibly valuable in identifying cortical networks and patterns of FC during task, rest, and disease, they do not capture any recurring or periodic patterns within a scan that could be highly informative (49-52). Cortical network activity is increasingly conceived of as a dynamic phenomenon, with spatiotemporal patterns occurring across scales and modalities (53). Unlike static or time-averaged FC methods, dynamic methods focus on identifying recurring patterns of co-variation or anticorrelation between networks. Such spatiotemporal patterns of cortical activity could provide valuable non-invasive biomarkers of attention and cognitive disorders missed by traditional fMRI analysis (54-57).

Several types of spatiotemporal patterns have been identified, including co-activation patterns and infraslow **quasi-periodic patterns** (QPPs) (55, 56, 58). The work in the present study focuses on the QPP, an infraslow ( $>0.1\text{Hz}$ ) pattern directly involving anticorrelation of the DMN and task positive regions. QPPs repeat quasi-periodically and last approximately  $\sim 20$  seconds in humans (59, 60). QPPs appear to be a highly robust phenomenon of infraslow anticorrelated network activity, having been detected across species (54-56) (mice, rats, non-human primates, and humans) and with sliding window algorithm (Figures 1.2-1.3) and complex principal components analysis (PCA) methods (49, 59). Abbas and colleagues reported in 2019 using sliding window-based methods that QPPs significantly contribute to FC in the brain, particularly in the observed FC relationships between default mode and task positive areas (59), a finding consistent with previous work in rodents and humans (55, 61). Using complex PCA (Figure 1.4), a method that is not constrained by a user selected window length or sliding window algorithm, Bolt and colleagues demonstrated that the QPP is one of 3 primary components that explain most of the time varying fluctuation in intrinsic brain activity (49). Not surprisingly, given traditional FC analysis findings implicating DMN-TPN anticorrelation in neurotypical attentional processing, QPPs are weaker in individuals with attention deficit hyperactivity disorder (ADHD) (62), and increased DMN-TPN anticorrelation during the QPP has been associated with “in the zone” type attentional performance in healthy subjects (63).

Given the large contribution of QPPs in directing intrinsic whole brain spatiotemporal patterns, and evidence that the relationship between networks in the QPP could provide valuable biomarkers of healthy and maladaptive brain states, further exploration of QPP network relationships is warranted. In particular, a more fine grained network approach that looks beyond the grouping of the TPN is needed, as there is evidence from both static and dynamic measures of FC indicating that TPN activity is better understood not as a single network, but as separate networks such as the dorsal attention network (DAN), frontoparietal control network (FPN), and the ventral attention network

(VAN) (27, 63-67). Additionally, as is discussed below, though all cortical networks, including sensory networks, seem to participate strongly in QPPs, only the role of the DMN and “TPN” have been explored.

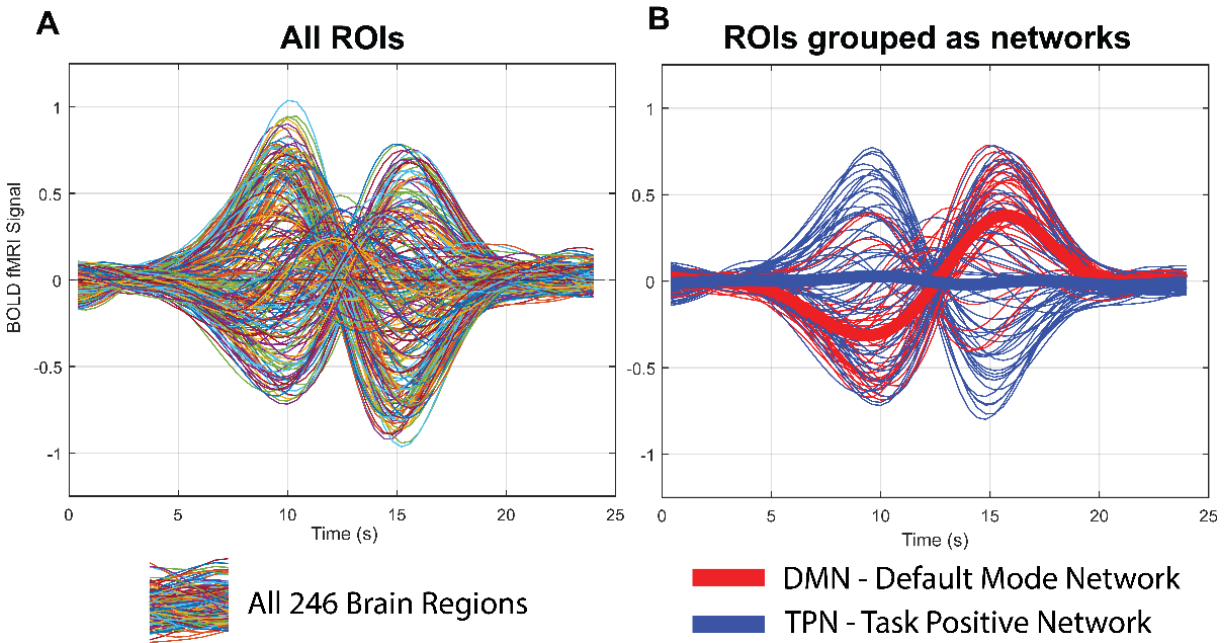


**Figure 1.2.** Example of a single full QPP cycle as detected with a sliding window algorithm on resting state fMRI time series. A) All 246 regions of interest (ROIs) from the Brainnetome 246 atlas used in the present study and B) the subsets of those regions as they appear after being grouped into the DMN and TPN, respectively. Note the generally anticorrelated relationship between DMN and TPN regions during the QPP. Also note the time course on the x-axis, though the x ticks cover 0-25 seconds, from beginning to end the pattern itself spans 15-20 seconds.

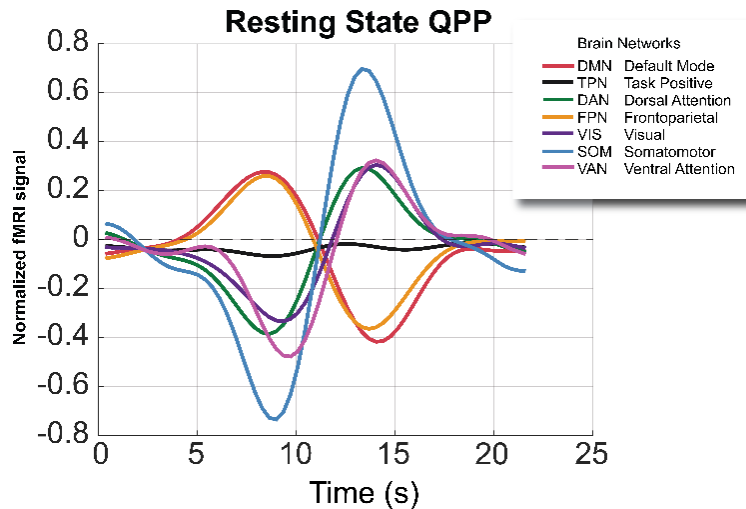


**Figure 1.3.** QPP network activity detected on resting state data from the human connectome project (n = 50, half male half female). Note that all major cortical networks, not only the default mode and task positive networks, participate in the QPP, meaning they also show anticorrelation.

#### 1.4 The goal of a multi-dataset application of QPP analysis across attentional states and disorders

So far the following has been established: intrinsic activity accounts for most brain activity (2), this intrinsic activity is organized into anticorrelated networks that subserve divergent functions related to the balance of external and internal attention (3, 7), and the quasi-periodic pattern appears to be the dominant pattern of this intrinsic anticorrelated activity (49). Finally, dynamic analysis methods, including analysis of QPPs, have become a major point of interest (7, 49, 50, 52, 54, 58, 59, 62, 63, 68-73).

However, significant gaps in our understanding of QPPs remain before they might serve as useful biomarkers or provide insight into the etiology of neurological disorders. First, there exists no neurotypical reference of the internetwork relationships of the various networks that participate in the QPP. Most studies of QPPs have focused on the relationship between the DMN and the TPN,

though all the major cortical networks, including sensory and motor networks, participate in the anticorrelated pattern of the QPP (Figure 1.2). An exploration of the dynamic connectivity between the DMN and all major cortical networks would be much more informative.

Regarding the application of QPP analysis to neural disorders, Abbas and colleagues explored how QPPs might be altered in individuals with ADHD (62), but other neural disorders remain largely unexplored, including Alzheimer's Disease (AD), which is known to heavily affect DMN-DAN anticorrelation in traditional time-averaged FC methods (74-77). It is very likely that QPPs will also be disrupted in AD, and it is possible QPPs could provide a non-invasive biomarker of AD. The effects of prolonged behavioral training on internetwork QPP relationships are also virtually unexplored. Processing approaches and the application of dynamic analysis methods also varies widely between research groups, complicating interpretation of possibly related findings between groups.

To address these gaps, the present study implements a multi-dataset approach to apply QPP analysis uniformly to a wide range of datasets. By using a streamlined processing approach and uniform application of the same QPP methods across many datasets, we seek to eliminate some of the noise generated by inter-study differences in methodology. The datasets detailed in each chapter were selected to capture a range of brain states across tasks and rest in healthy neurotypical subjects.

The following chapters seek to: A) establish how internetwork relationships change across task vs rest in many neurotypical subjects from different datasets, and B) explore how prolonged behavioral training may alter QPP network dynamics, using musical training as a proxy for prolonged behavioral training.

### QPP as detected with cPCA

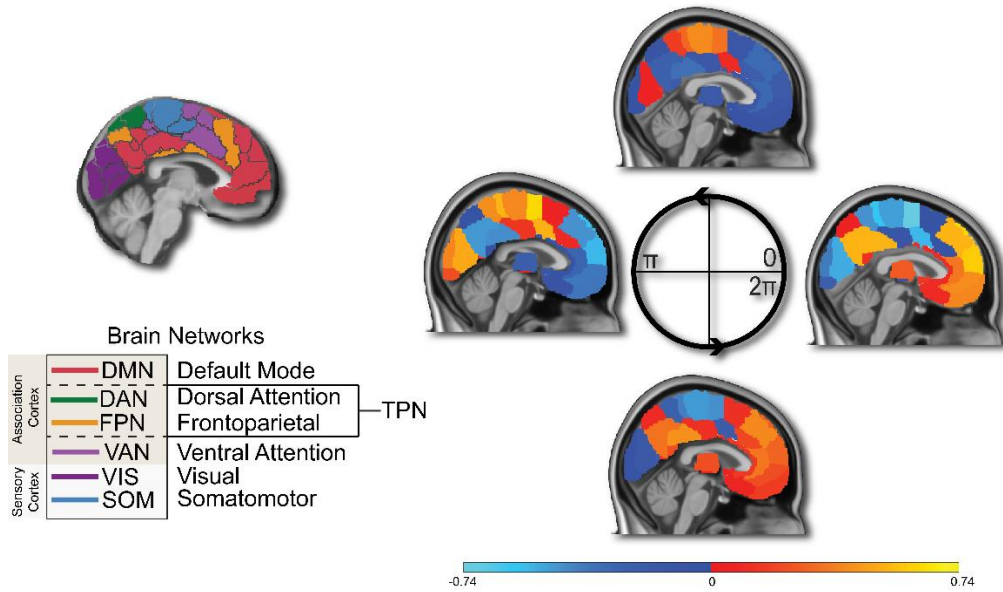


**Figure 1.4.** QPP detected with cPCA from resting state HCP data, shown on sagittal plane of MNI template. Note the strong anticorrelation between default mode and task positive regions throughout the cycle (heat bar shows normalized BOLD signal). Compare with the anatomical reference for DMN and other networks on the left.

The chapter on musician data (chapter 3) also serves as a cautionary tale regarding the interpretation of group vs individual application of QPP detection methods, with an example of how group vs subject-wise QPP results can differ, especially in smaller datasets with shorter scan lengths. Additionally, the musician chapter includes a comparison of group level results between QPP detection with a sliding window based QPP vs complex PCA detection. In the final chapter, we report preliminary results of QPP analysis applied to subjects from the Alzheimer's Disease Neuroimaging Initiative (ADNI) database. We also discuss how these results provide possible biomarkers and how these results are consistent with an intuitive explanation based on basins of attraction for why anticorrelated network dynamics may be adaptive and necessary for neurotypical cognition.

## Chapter 2

Networks beyond the default mode and task positive network show changes in quasi-periodic patterns that track an axis of external vs internal attention

2.1 Introduction

2.2 Methods

2.3 Results

2.4 Discussion

2.5 Conclusions

This chapter is from the first author manuscript *Infraslow dynamic patterns in human cortical networks track a spectrum of external to internal attention*, which has been accepted for publication at Human Brain Mapping.

Citation: H. Watters *et al.*, Infraslow dynamic patterns in human cortical networks track a spectrum of external to internal attention. *bioRxiv* 10.1101/2024.04.22.590625 (2024).

Full Author List: Harrison Watters, Aleah Davis, Abia Fazili, Lauren Daley, TJ LaGrow, Eric H. Schumacher, Shella Keilholz.

## 2.1 Introduction

The human cerebral cortex, which, to quote Geschwind & Rakic, “considers itself the crowning achievement of evolution”, is marked by significant expansion compared to other mammalian brains (78), with the majority of volume increase accounted for by disproportionate representation of non-sensory association cortex (11, 79, 80). Expansion of the association cortex paralleled the evolution of highly interconnected brain networks that became untethered to direct sensory stimuli and adapted novel functions related to attentional control, memory, cognition, and social interaction (11).

These flexible but distinct cortical networks (9), originally detected in positron emission tomography (PET) and later functional magnetic resonance imaging (fMRI) (7, 18), largely maintain their organization at rest, in the absence of any externally directed task (4, 51). One way to view these distributed cortical networks is along an axis of external to internal attention (11, 15, 81, 82). At one end of the spectrum, regions of the default mode network (DMN) become less active during externally focused tasks, and more active during memory recall, mind-wandering, the maintenance of internal thought trains, and other internally directed processes (6-8, 16, 18-20, 83-85). At the other end of the spectrum, regions showing task related activation, opposite the DMN, have been referred to as the task positive network (TPN), which typically is considered to include the dorsal attention network (DAN) (27, 86), the frontoparietal network (FPN)(81), and sometimes the ventral attention or salience network (VAN) (5, 87). The DMN seems to work in opposition with networks that exhibit increased activity during externally directed tasks, showing anticorrelated activity with the DAN specifically (15, 21, 66, 88, 89). As measured with fMRI when subjects are at rest, anticorrelated activity between the DMN and DAN appears to be a hallmark of neurotypical cognition. DMN-DAN anticorrelation declines in aging and dementias (28, 32, 68, 74, 90, 91). Diminished DMN-DAN

anticorrelation has also been seen in sleep deprivation (33, 34), is associated with attention deficit hyperactivity disorder (ADHD) in children (25, 26), poor task performance in adults (31), and the use of exogenous neuromodulators that negatively affect working memory performance, such as delta9-tetrahydrocannabinol (39, 92, 93).

Anticorrelated DMN-DAN activity may have evolved as an adaptation to allocate cortical resources based on a spectrum of external vs. internal attention, and to allow for more elaborate construction of internal thoughts and narratives (15, 22, 43, 94, 95). Weber et al reports that subjects engaged in a congruence task showed DMN deactivation that scaled with the difficulty of the task (35), indicating a relationship between task difficulty and increasing allocation of cognitive resources. In other words, when the external task was easier, the default mode network could afford to become more active. This interpretation of DMN-DAN anticorrelation fits with anecdotal human experience: when unrelated thoughts interrupt external tasks, we tend to perform the tasks poorly. Conversely, when external stimuli are overwhelming or distracting, maintaining an internal train of thought is difficult. Importantly, this model of network resource allocation also implies that underlying networks such as the DMN may show dynamic changes related to external vs internal attentional demand.

Seminal fMRI studies of cortical network activity, including DMN-DAN anticorrelation, relied on traditional time-averaged measures of activity, which represent the averaged correlation between reference-informed regions across the entire scan. While this time-averaged analysis approach is incredibly valuable for exploring external vs internal attention, it misses recurring dynamic patterns that capture time-varying relationships between networks within the fMRI signal (50, 70). A subject's attention may shift repeatedly over the course of a single scan, and time-averaged approaches fail to capture network dynamics that may correspond to such attentional fluctuations. Across imaging modalities, there is increasing evidence that dynamic spatiotemporal patterns are related to arousal,

attention, and cognition (49, 53, 55, 58, 59, 61-63, 73, 96, 97). Several types of dynamic spatiotemporal patterns have been described in fMRI literature (52, 53, 60, 72, 98). The work in the current study focuses on the quasi-periodic pattern (QPP): a repeating, whole brain spatiotemporal pattern of alternating activity between the DMN, TPN, and other networks that happens quasi-periodically on the infraslow timescale (lasting about 20 seconds in humans), and has been directly implicated in attention and arousal (55, 57, 59, 61, 73, 99). Consistent with previously mentioned time-averaged FC studies regarding the DMN, QPPs are disrupted in individuals with ADHD (62) and low frequency waves of DMN activity (<0.1Hz) disrupt task performance (100). More recently, work from collaborators showed that the amount of anticorrelation in the QPP between DMN and the frontoparietal network (FPN) decreases along with task performance (63).

Considering the important evolutionary role of the DMN, its critical functions in attention and cognition, and the potential for inter-network DMN dynamics as a biomarker of healthy brain function across task and rest states, we tested whether the dynamic relationships of networks in infraslow QPPs reflect the axis of external vs. internal attention. Here, we detected QPPs in a range of datasets (Figure 2.1) obtained from a mix of open sources and collaborators (Supplemental table 1). We employed inter-network correlation analysis (Figure 2.3) between the DMN and DAN, as well as all other major attentional networks of the cortex (Figure 2.2) during the QPP. We hypothesized that 1) key attentional networks would show task related shifts in their correlation with the DMN. 2) These effects would be robust when QPPs were detected at both the group averaged and individual level. 3) The constituent networks of the so-called task-positive network (i.e., DAN, FPN, VAN) would show divergent results with respect to their correlation with the DMN in the QPP. And finally, 4) sensory cortices would also participate in dynamic shifting of DMN correlation in response to the task-rest spectrum.

This is one of the first studies connecting such a breadth of datasets for spatiotemporal analysis in relation to an axis of attention. The results provide significant theoretical insight into the role of inter-network DMN dynamics in the balance of external vs internal attention. Additionally, the resulting dynamic DMN fingerprints for each task type can be used as a reference to guide future studies, to interpret disparate findings related to dynamic functional connectivity, and to help identify shifts in inter-network DMN activity to be used as a biomarker in health and disease.

## **2.2 Materials and Methods**

### **2.2.1 Code**

All code is Open-Sourced and available online. QPP code referenced in the methods section is available on github: [https://github.com/BnzYsf/QPP\\_Scripts\\_v0620](https://github.com/BnzYsf/QPP_Scripts_v0620)

Preprocessing code and pipeline are open source and available here: <https://fcp-indi.github.io/>

All code used for quasi-periodic pattern detection was run in Matlab (Mathworks Inc. 2023) with some plots generated using R studio (Posit team, 2024).

### **2.2.2 Study design and participants**

A range of functional MRI task types were obtained, totaling 327 participants across 788 scans (**Figure 2.1A**). For a full summary of datasets used, scan type, scans per subject, sources, and the available scan parameters for T1 and functional scans see **Supplemental table 1**. In brief the following task types were used: a left-right moving dot task (101) originally used to measure reaction times in a study of gamers vs. non-gamers; two n-back visual working memory tasks - one from OpenNeuro (102), and one from the Human Connectome Project (103); three types of congruence tasks – Stroop (104), Flanker (105), and Simon (106); a dataset of meditators during resting state and

a mindfulness meditation task (107), and a dataset of subjects watching an episode of the Twilight Zone (108).

### **2.2.3 Quasi-Periodic Pattern Acquisition, TR, and Window Lengths**

Recurring infraslow spatiotemporal patterns (quasi-periodic patterns) were detected using an updated version of the QPP detection algorithm originally employed in rats (55, 56) and more recently in humans (57, 59, 61, 99). For full details on the pattern detection algorithm see the preceding studies, especially Xu and colleagues 2023 (99). In the present study, a robust version of the pattern algorithm was used that starts at the beginning segment and then iterates through the entire time series, correlating the initial segment with all other segments (**Figure 2.1C**). The pattern finding algorithm uses a segment of data the length of one QPP, which is on the order of ~20 seconds in humans and set by choosing a window length that when multiplied by the repetition time (TR) for a given scan is equal to a final length of 20 seconds (49). For example, with a TR of 2 seconds, 10 timepoints would represent an elapsed time of 20 seconds, therefore the window length would be set at 10 such that  $TR \times WL = 20$  seconds. The algorithm starts with this segment length at the beginning of the time series then moves through the time series and correlates the QPP template segment with every time point from beginning to end of the time series. Segments which exceed a threshold of correlation (0.2) with the initial QPP template are then averaged. The averaged-updated template is then fed back into the algorithm loop in place of the initial segment, and sliding correlation is repeated until change is negligible between iterations, producing a convergent QPP pattern (57, 61).

One complication arising from a multidataset approach is that datasets have variation in spatial and temporal resolution. While the voxel sizes used in the present studies were relatively uniform

(3-4mm range, supplemental table 1) the TR in various datasets varied from 0.535 - 2.25 seconds (table 1). To account for this variation, it becomes necessary to employ different window lengths in the sliding window QPP algorithm to capture equivalent patterns across time. The established QPP length is in the range of 20 seconds in humans (49, 57, 59, 61-63, 73, 109). This means that one full cycle of the QPP, one peak and one trough of DMN anticorrelation for example, takes about 20 seconds. Therefore, if the final pattern length (20 seconds) is divided by the TR (the effective temporal resolution) the appropriate window length for datasets of different TRs can be estimated. Based on this logic, we selected window lengths for each dataset that resulted in a final QPP length as close to 20 seconds as possible, while still attempting to adjust for window lengths that best captured a whole phase of the QPP with minimal inter-QPP phase. The chosen window lengths and resulting final QPP lengths are shown in **Table 1**.

It is important to emphasize that small changes in window length do not change the overall internetwork correlation patterns observed in the QPP. For example, in work by Abbas and colleagues (59), various window lengths capturing a final pattern anywhere from 16 – 30 seconds were applied and still found the same anticorrelated pattern between the DMN and TPN. However, if the window length is too small, less than one full cycle will be captured. When the window length is too long, the final pattern captured will show more of the tails of the pattern or begin to show another peak from another cycle. In other words, altering the window length slightly doesn't change the final pattern, just how much you see of the pattern. To further illustrate this point, we repeated all group level QPP detection with alternate window lengths in addition to those listed in table 1. The additional window lengths used did not change the overall patterns detected or their internetwork correlations and are shown in supplementary figures 2.1 and 2.2, with new window lengths shown in supplementary table 3. QPPs were detected on a group and individual level. That

is, the algorithm was employed on concatenated time series for each group and individually for all 788 scans using the same TR-window length combination from each subject’s respective group. This allowed us to compare inter-network QPP dynamics at both the group and individual level (see **Figure 2.3**).

**Table 2.1. Datasets, TRs, and QPP parameters**

<b>Dataset</b>	<b>OpenNeuro o VWM</b>	<b>VG: Gamer Task</b>	<b>HCP Task/ Rest</b>	<b>Flanker</b>	<b>Simo n</b>	<b>Stroop</b>	<b>CABI Rest</b>	<b>Meditator s</b>	<b>Twilight Zone</b>
<b>EPI TR (s)</b>	2	0.535	.72	2.5	2	1.5	2.25	1.5	1.5
<b>QPP Window Length</b>	10	32	30	8	10	12	10	10	12
<b>Final QPP Length (s)</b>	20	17.12	21.6	20	20	18	22.5	15	18

#### **2.2.4 Processing pipeline and global signal regression**

To minimize noise introduced by processing variation, all datasets were uniformly processed with the configurable pipeline for the analysis of connectomes (CPAC) (110). CPAC is run via Docker container and contains many formerly separate fMRI tools and processing packages housed within a single software, allowing for streamlined processing. These include but are not limited to steps for skull stripping, functional to anatomical registration, and motion correction. As the name implies, the pipeline has a default version but has a wide range of parameters which are configurable to meet the needs and experimental interests of the researcher. For this study, an identical version of the configurable pipeline was used for all datasets, which included motion correction, slice-timing correction, global signal regression, and registration to an anatomical template. The complete version of the pipeline used can be made available upon request.

The default CPAC pipeline automatically generates processed time series with and without global signal regression (GSR). In the present study the primary findings are in the global signal regressed data, as anticorrelated patterns between the default mode and other networks only tend to emerge after GSR (15, 49, 57). However, we recognize that the global signal contains meaningful functional information (111) and could be possibly informative, and thus repeated all group level QPP detection and analysis without using GSR. The results of non-GSR internetwork analyses, as expected (49), showed positive global correlation between all networks and are shown in supplementary figures 2.3 and 2.4.

#### **2.2.5 Grouping ROIs into networks for inter-network QPP analysis**

The output of the QPP detection algorithm is a ~20 second pattern dominated by reliable and strong anticorrelation between the DMN and TPN. However, as mentioned, the TPN itself is composed of multiple cortical networks depending on the study (DAN, FPN, and/or VAN) (5, 63). And other regions and networks, whose dynamics across task type have not been thoroughly explored, also participate in this strong pattern of anticorrelation (57, 61). To analyze broader network relationships across task types in the QPP and compare them to existing network-based FC findings in the literature from seed-based and dynamic methods, we employed a network-based approach grouping all ROIs into canonical association and sensory networks. QPP outputs were plotted as 246 ROIs assigned to Yeo's 7 networks (9), which assigns cortical ROIs into 7 major association and sensory cortices, plus subcortical regions (See supplemental table 2 for a key used to group Brainnetome ROIs into Yeo's 7 networks). As we were focused primarily on generating an spectrum of inter-network QPP dynamics for the major attentional and sensory networks we excluded the limbic or subcortical networks. The following networks were used: default mode network (DMN), frontoparietal network (FPN), dorsal attention network (DAN), ventral attention network (VAN), somatomotor network (SOM), visual network (VIS) (see Figure 2.1B for anatomical location of these networks). The task positive network (TPN) is also plotted and included in our analyses but note that this network is just the combination of the DAN and FPN, which show divergent results in our data depending on the task (see figures 2.3 and 4). As indicated in the following sections, the primary factor driving DMN/TPN anticorrelation across brain states appears to be DMN/DAN anticorrelation, while the DMN/FPN have more flexible correlation.

### **2.2.6 Measures of inter-network QPP relationships**

Waveform plots were generated showing the normalized BOLD signal during the QPP for all networks (Figure 2.2). Waveform plots were chosen as they allow qualitative inspection of major shifts in

network behavior based on task (Figure 2.2A-F upper panels). Corresponding network correlation plots were generated to capture these shifts quantitatively for each dataset (Figure 2.2A-F lower panels). Tasks were categorized based on the type of activity. These task categories were reinforced qualitatively based on clear trends we saw in our preliminary results that seemed to indicate a spectrum of inter-network shifts related to external vs internal attention (see Figure 2.3). This resulted in datasets being categorized as either “visual task” (for visual working memory and the visual reaction time moving dot task), “congruence task” (for congruence tasks such as Flanker, Simon, and Stroop), “rest” (for resting state scans), “meditators rest” (practitioners of mindfulness meditation at rest), “meditation” (same practitioners but during a meditation task), or “Twilight Zone”. Note that Twilight Zone and Meditators are the only datasets in their categories as they did not fit with other tasks categorically or empirically (in terms of their inter-network dynamics, see results).

To generate a spectrum of inter-network DMN dynamic fingerprints as a potential biomarker, focused analysis was made with respect to the DMN (Figures 2.4-5). Initially, the correlation between all networks and the DMN was calculated at the group level (Figure 2.3A). As notable differences immediately became apparent across the task spectrum in several networks, we repeated all DMN-to-network correlations at the individual level for comparison (Figure 2.3 A-B). DMN-to-network correlation from individual QPPs (Figure 2.3B) was used for statistical comparison (Figure 2.3C), as group level correlations lack variance and mean. Scans were grouped by task category to test differences between “visual task”, “congruence task” and “rest” QPPs. Note that meditator and Twilight Zone groups were excluded from statistical comparison as they have much smaller sample sizes and showed empirically different trends from the other categories. These miscellaneous groups show interesting trends however, informative for interpreting task vs rest and for guiding future experiments, and were therefore included for visual comparison. Statistical comparisons of DMN-

to-network correlations (Figure 2.3C) were made using the Kruskal-Wallis test for multiple comparisons. All correlation values were Fisher transformed before statistical comparison to account for non-normal distribution. Multiple comparison correction was done using the conservative Bonferroni method (112) and assuming 7 comparisons between the 8 canonical networks used. (Standard  $\alpha = .05$  was adjusted for 7 comparisons ( $.05/7$ ) to  $\alpha = .007$ ). To capture the idea of DMN-to-network correlations in the QPP as a “fingerprint” that can be used as a neurotypical reference to compare to future studies, we generated a DMN-to-network QPP fingerprint for each category of scan (Figure 2.4). The qualitative differences between infraslow QPP fingerprints are discussed in the results section, while the underlying statistical differences are captured network by network in Figure 2.3C.

### **2.2.7 Plotting internetwork QPP correlations without qualitative grouping and comparing visual tasks**

The exact protocols of the visual working memory (VWM) and moving dot video gamer task (VG) are quite different. Furthermore, congruence tasks are certainly a very *visual* task as well. Thus, to overcome a purely qualitative definition of visual task based on the attention spectrum shown in Figures 2.3 and 4, we also separated all data out by subject and Fisher transformed correlation to DMN. We then assigned subjects/scans into quartiles based on their degree of correlation to DMN regardless of dataset or task type (Figure 2.5 A) to see if the spectrum of attention that becomes apparent in qualitative data would survive. Additionally, while the VWM and VG tasks could both be categorized as a type of cued response task, they are different tasks and required separate analysis. In Figures 2.5 and 2.6 the category of “visual task” is therefore broken into VWM and VG, respectively, so that a finer grained groupwise comparison can be made. Based on the normalized distribution of the fisher transformed values, a one-way ANOVA comparison was made with respect to the

correlation-to-DMN factor for the groupings Rest, Congruence, VWM, and VG, with corresponding pairwise Tukey analysis of significance reported in a p-value table in the same figure (Figure 2.6).

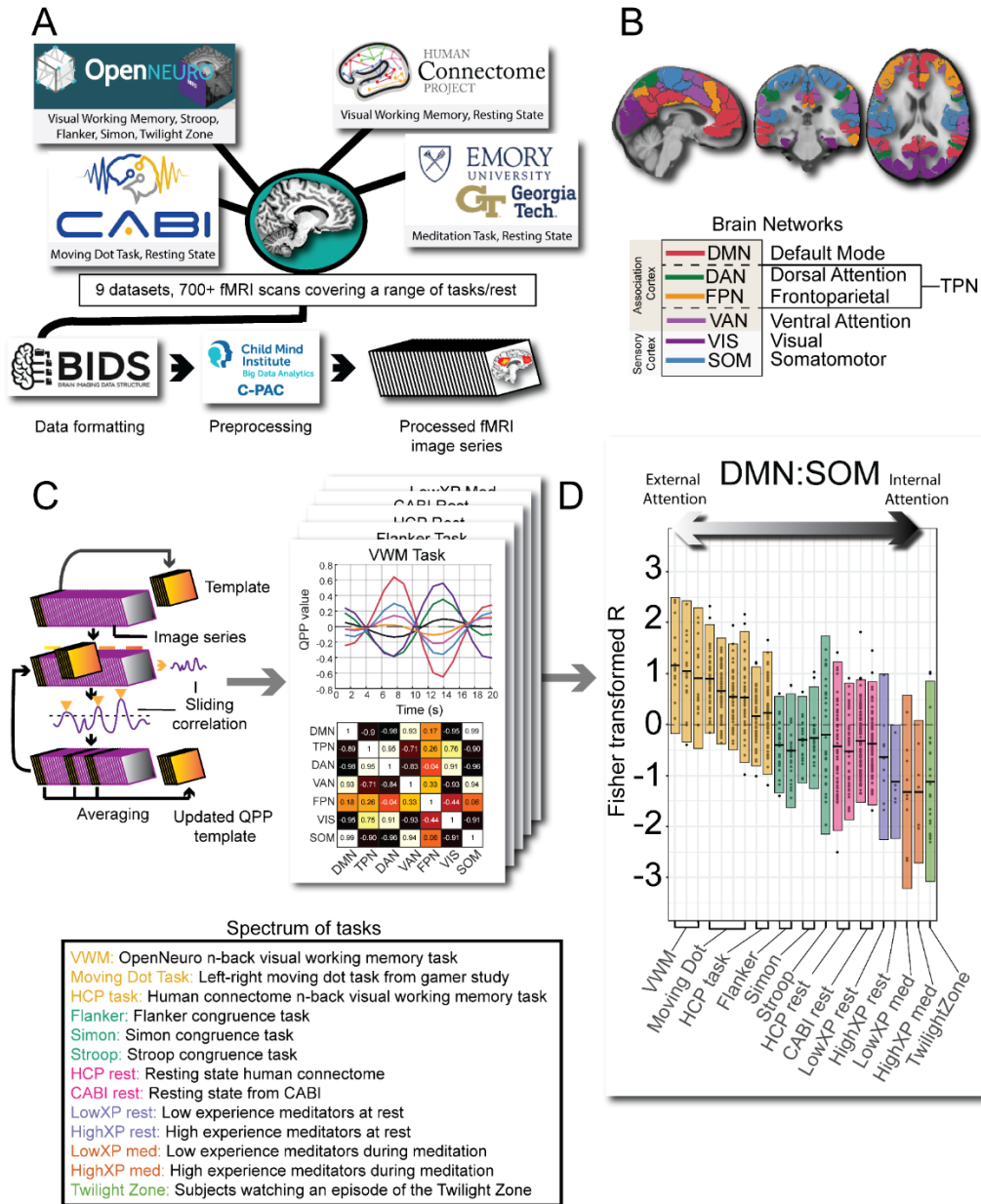


**Figure 2.1.** (A) Data sources to CPAC processing. (B) Example of Yeo’s network used in the present study, shown in a 3-plane slice of standard MNI 152 space. Note that the task positive network (TPN) is the combination of DAN and FPN networks. (C) Process of QPP detection, network waveforms,

and inter-network correlations. (D) Example of inter-network analysis specific to DMN. Note the change in correlation to the DMN across an axis of external to internal attention.

## **2.3 Results**

Our results reflect the dynamic relationships of cortical networks within QPPs, spatiotemporal patterns of activity, expressed as the correlation between networks (for example movies of such QPPs see other work by our group (49, 61)). The reported correlation structure simply summarizes the behavior of specific networks within these patterns. Overall, QPPs showed a strong pattern of DMN/DAN anticorrelation, consistent with previous literature, using both seed-based and dynamic FC methods, describing strong anticorrelation between default and task positive brain networks (15, 16, 19, 49, 59, 61, 63, 73). Group level QPP waveforms and inter-network group correlations are reported first followed by subject-wise DMN QPP correlations and statistical comparisons. For both group and individual analysis, we find that a spectrum of inter-network DMN shifting emerges based on task type that seems to track a spectrum of external to internal attention.

### **2.3.1 Group level QPP waveforms and qualitative network differences across task type**

Several major qualitative differences and trends were quickly apparent in the group level QPP waveforms (Figure 2.3). First, in the visually demanding tasks (moving dot task and visual working memory, see methods), the phase of the VAN and somatosensory (SOM) networks is completely switched compared to the other task types (compare Figure 2.3A to other task types). That is, rather than showing positive correlation with the DAN they are instead strongly correlated with the DMN. This VAN and SOM phase switching is not apparent in congruence tasks, though they do trend more positively in DMN correlation (Figures 2.2 and 2.3A).

The FPN also shows a major shift corresponding to the spectrum of tasks (Figure 2.2 and Figure 2.3A-B). Specifically, across all resting groups and during meditation and TV watching the FPN is strongly in phase with the DMN. For both visual and congruence tasks the FPN becomes more positively correlated with the DAN than the DMN. The more externally directed the current task is (further left on task spectrum in Figure 2.3A), the stronger the FPN-DAN alignment in the QPP appears to be on average. This is consistent with previous seed-based FC findings characterizing the frontoparietal control network as a flexible network that can shift between modulating the DAN or DMN, respectively, depending on task type (22, 113).

The DMN-TPN relationship at the group level is somewhat more variable across the datasets, trending towards positive in the meditation and TV watching datasets, and more negative correlation in the visual task sets. The increased DMN-TPN anticorrelation during tasks found here is consistent with literature indicating that externally focused tasks increase separation between the DMN and TPN (97). However, as mentioned, the TPN described in this study and in others is just the combination of the DAN with other attentional networks such as the FPN and VAN, which show divergent results in our QPP data with respect to their DMN correlation.

When inspecting the results of the DAN and FPN across the task and rest spectrum reported in the present study, it is apparent that shifts in activity of the FPN are primarily responsible for the overall TPN inter-network correlation shift. In the group level QPP, the DMN-DAN correlation is universally negative with minimal variability, only trending towards the positive in the Twilight Zone set. The FPN, however, shows dynamic switching in the QPP that corresponds strongly to the amount of externally directed task demand the subjects are engaged in (Figure 2.3A). In other words, in the group level QPP, the DAN exhibits only small change in DMN anticorrelation based on task, where the FPN seems

highly responsive to the task-rest spectrum, shifting flexibly between the DMN at rest and the DAN during externally directed tasks.

### **2.3.2 Individual level QPP correlations for Visual, Congruence, and Rest states**

Subject-wise inter-network DMN correlation results were largely consistent with group level findings (**Figure 2.3 A-B**). Specifically, means of the individual DMN-to-network correlations for all networks showed the same trends found at the group level. That is, in both group and individual QPPs the TPN, DAN, FPN, and VIS showed significantly decreased DMN correlation during visual tasks compared to rest and congruence, while the VAN and SOM showed significantly increased DMN correlation for visual tasks compared to rest and congruence (**Figure 2.3C**). In summary, both group and individual results indicate that with respect to infraslow QPP dynamics, the VAN and SOM exhibit task-negative-like responses, shifting phase to be more in line with the DMN, a network associated with internal mentation, memory retrieval, mind-wandering, and perceptual decoupling (6, 18, 19, 21, 95). Meanwhile, the DAN, FPN, and VIS networks exhibit task-positive-like responses.

It is important to highlight the results of the HCP dataset within the task-rest spectrum, as they act as a reference point to validate the other datasets analyzed here. Most of the datasets have subjects with either a task or a rest scan, not both. For example, the CABI rest subjects were only scanned during rest, and the VG and VWM subjects were only scanned during tasks. The HCP subjects, however, were each scanned twice at rest and twice during a visual working memory task (114). Thus, the HCP subjects plotted in the task and rest categories are the same subjects. Importantly, these same subjects compared at task and rest recapitulate the same results of network phase shifting and correlation changes for each DMN-to-network comparison made between tasks in the other datasets (note HCP task and rest results in Figure 2.3A-B).

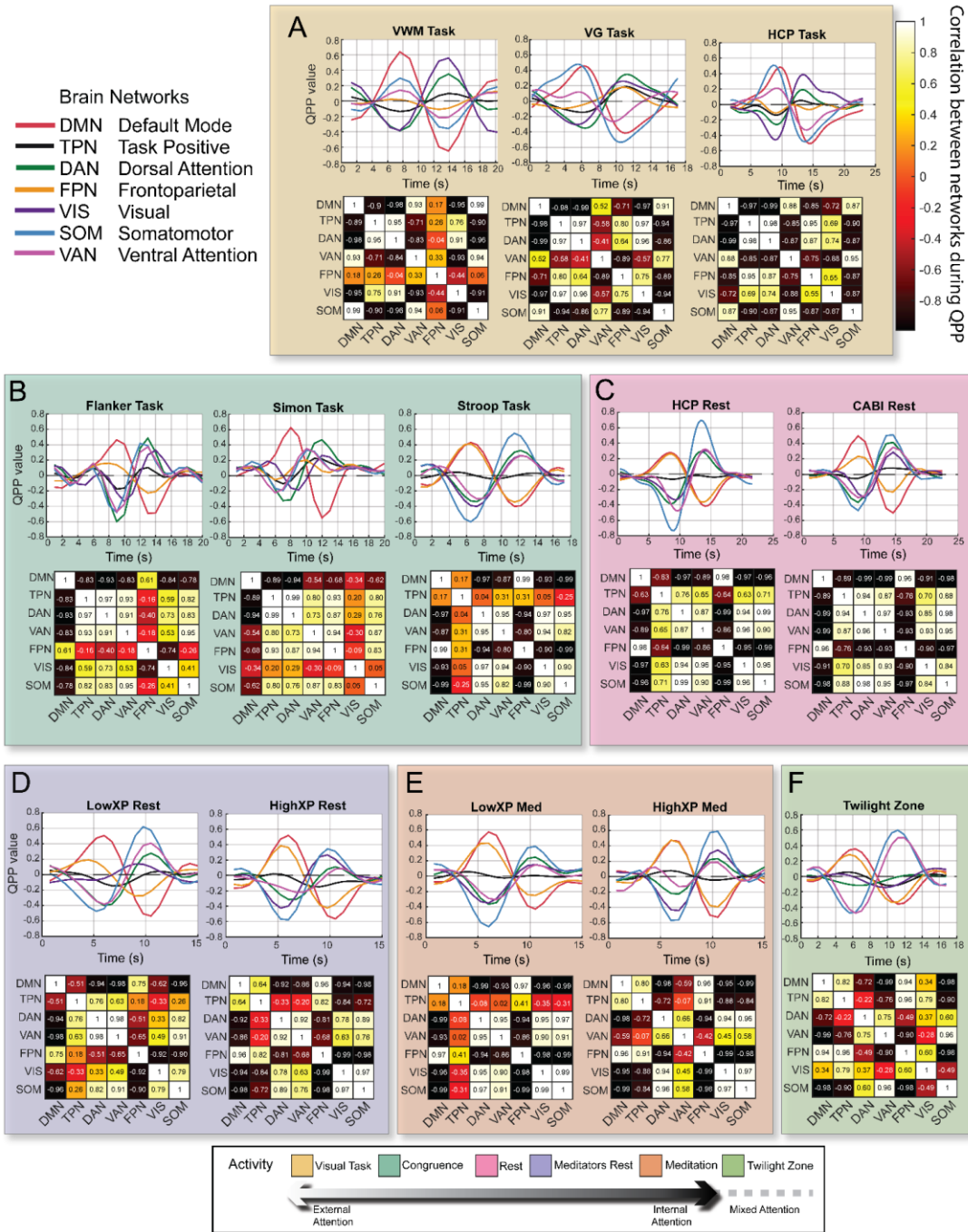


**Figure 2.2.** (A-F) QPP waveforms and heatmaps showing correlations between all networks during QPP across task spectrum. Note switching of SOM and VAN from negative DMN correlation at rest/congruence to positive DMN correlation in visual tasks. FPN becomes more negatively correlated with DMN in visual and congruence tasks compared to rest.

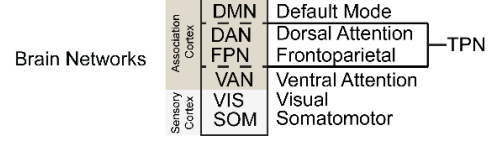
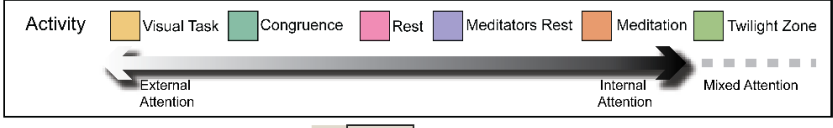
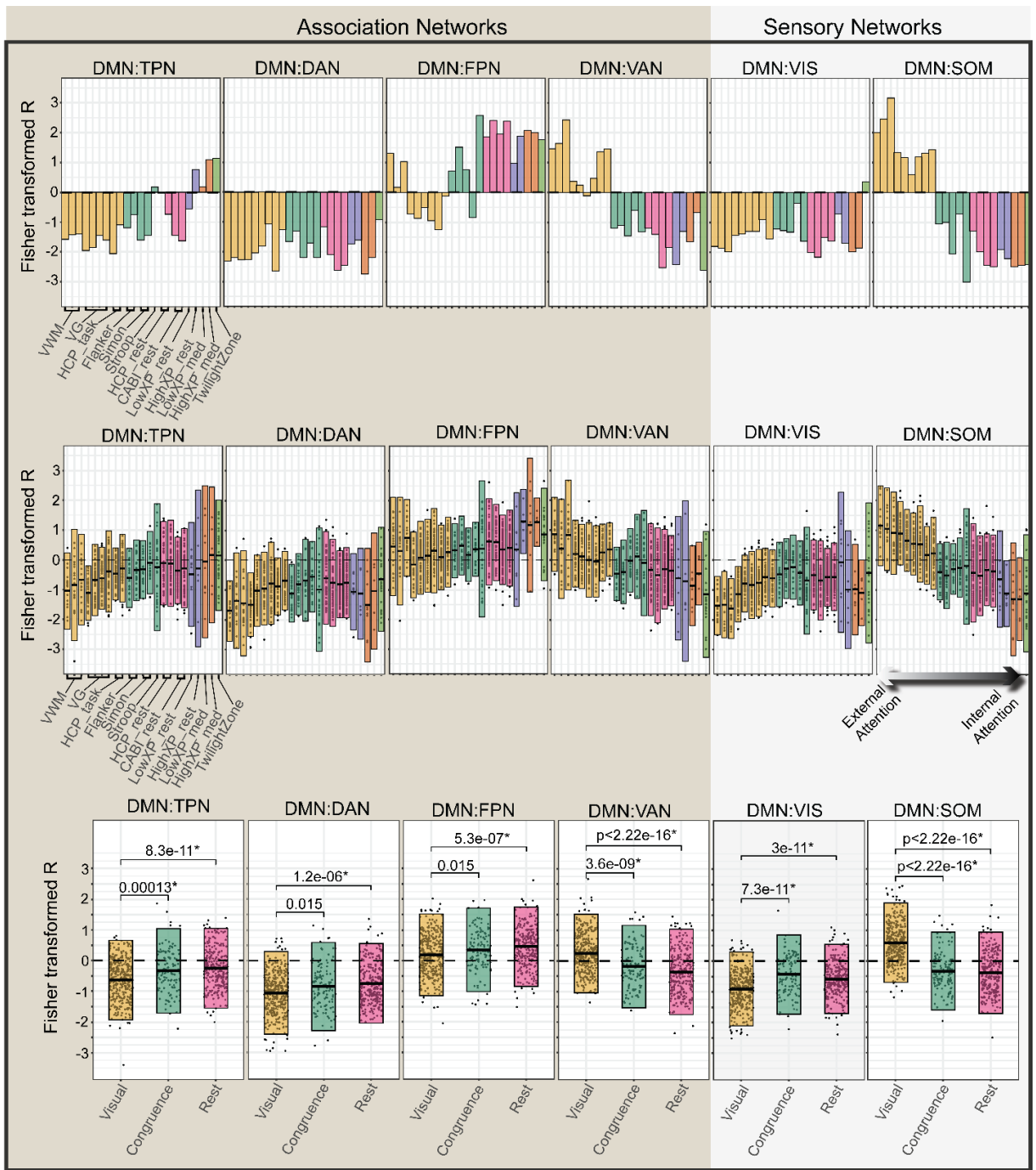


**Figure 2.3.** Shifts in DMN-to-network correlations along the spectrum of fMRI tasks, shown as Fisher transformed correlation R values on y-axis vs task type on x-axis. Group (A), Individual (B), and Stat Comparisons (C). Note that DAN, FPN, and VIS networks show task-positive-like responses moving from rest towards visual tasks (right to left), while VAN and SOM show the opposite trend, becoming positively correlated with the DMN during visual tasks.

### **2.3.3 Meditators and Twilight Zone DMN correlations during the QPP**

While meditators and Twilight Zone groups contained much smaller sample sizes and thus were not included in the statistical comparison with the visual, congruence, and rest groups, they exhibited notable trends that inform the other datasets. The high experience meditation group, actively meditating subjects, and the Twilight Zone group trended much higher than resting state subjects in their DMN-DAN correlation, at the opposite extreme from external visual tasks. A similar but opposite trend is seen in the DMN-SOM correlation, with the high experience meditation group, actively meditating subjects, and the Twilight Zone group showing a much more negative DMN correlation, resembling extreme rest. For networks such as the DAN, VAN, and SOM, these miscellaneous datasets (meditators/Twilight Zone) suggest that activities related to a high degree of internal focus or narration cause inter-network DMN shifts that fit on the resting state end of the attention spectrum. Or rather, that tasks involving heavy internal focus or narration overlap heavily in their inter-network DMN dynamics with resting states.

### **2.3.4 Inter-network DMN fingerprints during QPP**

Inter-network DMN correlations for all networks were co-plotted on polar plots to capture a functional connectivity fingerprint for each task state (Figure 2.4). The overall fingerprints are notably similar between congruence tasks and rest (Figure 2.4), while the visual task varies significantly (captured in Figures 2.2/4 qualitatively and statistically in network-by-DMN comparisons in Figure 2.3C). Meditation and Twilight Zone DMN fingerprints also trend strongly away from typical rest. In conjunction, the results of inter-network DMN dynamics during the QPP in Figures 2.3 and 2.4 indicate a spectrum of network shifting with respect to the DMN that corresponds heavily to the balance of external vs internal attention in each task.

### **2.3.5 The attention spectrum without qualitative grouping, and comparison of visual task type**

While a DMN vs non-DMN alignment spectrum is apparent in Figures 2.3 and 2.4 when grouping the tasks into the categories of “visual task”, “congruence task”, etc., these groupings were primarily made on a qualitative basis. However, when breaking the visual task further into finer categories of visual working memory (VWM) and the moving dot video gamer task (VG) and plotting all subjects together only by their correlation to DMN values, the spectrum of external to internal attention is equally apparent (Figure 2.5 A). Separate comparison of the cued visual tasks VWM and VG also shows that the tasks show largely similar responses with respect to DMN alignment during the QPP (Figure 2.5 and 2.6). The VG task showed significantly different correlation to DMN for all networks analyzed compared to rest (Figure 2.6). The VWM and VG tasks showed the same general trend for all networks (Figure 2.6), and only different significantly with respect to the VAN response, where the VWM showed greater DMN alignment than the VG task (see Figure 2.6 p-value table).

## **2.4 Discussion**

We generated a spectrum of inter-network DMN dynamics from infraslow QPPs across a range of task types in neurotypical human subjects. Most whole brain spatiotemporal analysis projects advanced by our group and others have focused on single datasets and only on the relationship between the DMN and TPN. To our knowledge, this represents the first study of its kind to generate a spectrum of dynamic infraslow network relationships across such a breadth of tasks and networks. Additionally, as the effects of the various stimuli across tasks on QPPs were unknown, it represents an investigation of stimuli dependent effects on infraslow QPP dynamics. We propose that the detected shifts in spatiotemporal network patterns tracks an axis of external to internal attention, with certain networks exhibiting dynamic task-positive-like behavior (DAN, FPN, VIS) and others showing task-negative-like dynamic shifting (DMN, VAN, SOM) during the QPP. This work has broad implications for the interpretation of dynamic FC findings and their implementation in preclinical research. For example, these neurotypical network dynamic results can be used as a reference as we and other groups apply QPP analysis to datasets of pathology and neurodivergence, helping us to identify biomarkers and understand how aberrant network dynamics contribute to the etiology of neural disorders. Additionally, these findings contribute important evidence to theory regarding the evolution of flexible cortical networks and attentional resource management. The robustness of the inter-network DMN shifting across group and individual level QPP analysis also indicates that QPPs have potential as a biomarker for individual subjects despite considerable intersubject variability.

### **2.4.1 Relation to other models of network topography**

The observed network shifts in QPPs across task type reported here may be related to a hierarchy of unimodal vs transmodal network topography reported by Margulies and colleagues, where highly integrated association networks such as the DMN sit at the highest level of abstraction and

multimodal integration (115) and unimodal sensory regions like the SOM and VIS networks are at the other extreme of the hierarchy processing primary sensation. Cortical network activity has been found to exhibit a temporal hierarchy as well, with Golesorkhi (116) and colleagues finding that “core networks”, or the association networks more distant from periphery sensation, are more influenced by activity in slower frequency ranges. Cortical organization by unimodal to transmodal hierarchy across timescales has been found across modalities, and such intrinsic neural time scales shape cognition and affect the integration of information between peripheral sensory networks and core association networks such as the DMN (117). Further exploration of why infraslow sensory network activity becomes more aligned with the DMN, such as between the DMN-SOM as reported here, could help to bridge the understanding of how cortical dynamics across timescales reconfigure to accommodate task demands.

The results of the present study could also support a recent “baseline model” interpretation of intrinsic cortical activity. Northoff and colleagues argue that rather than DMN and TPN regions underlying separate internal vs task states (the dual mode), respectively, ongoing global cortical activity is argued to drive a shared neural code for both internal and external attention (118). The findings from the present study seem to support the baseline model interpretation of intrinsic activity, as we find that flexible interactions with the DMN are important in task and rest between various networks, including sensory networks. Additionally, we observe that at least in the infraslow

frequency range, activity between the DMN and TPN is largely stable between task and rest, while other networks such as FPN, VAN, and SOM seem to shift flexibly depending on task needs.

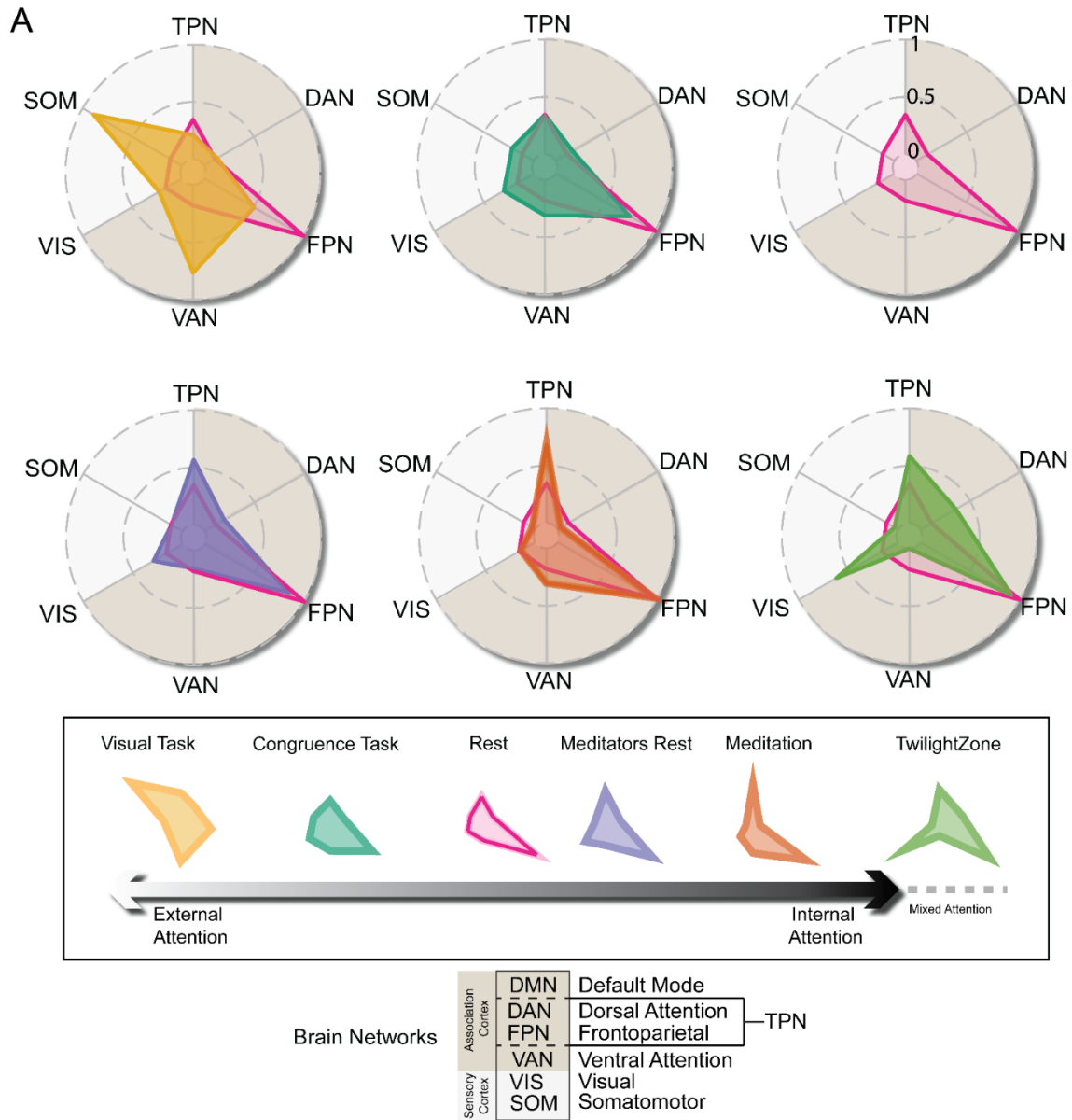


**Figure 2.4.** DMN-to-network dynamics for each category of task, plotted as correlation to DMN for each network normalized to a scale of 0 (minimum) to 1 (maximum). Note that all tasks are co-plotted with rest as a reference state. Correlational structure for each task may represent a

dynamic fingerprint for whole brain dynamics corresponding to the mix of external vs internal attention demanded by a task.

#### **2.4.2 Consideration of different stimuli**

The exact parameters of the various stimuli from the task datasets differ significantly. For example, the moving dot task from the gamer study required subjects to react quickly to a pair of moving dots, with one dot being a distractor color and one being a cued color they were prompted to react to. The n-back working memory tasks from the OpenNeuro and HCP are similar to the gamer task in that they were also based on prompting the subjects to direct their attention to certain “cued” stimuli” before being presented the stimuli on a 4x4 grid. Stimuli were then shuffled and presented after disappearing for some delay, with subjects having to report the location of the cued stimuli. The tasks we have grouped as congruence tasks all fall within the category of some type of congruence reaction task, where there is some type of mismatch introduced in the cue stimuli. The Stroop task prompts subjects to correctly respond when text is displayed that is incongruent with the color of the word, the word blue in red text, for example. The Simon and Flanker tasks represented similar types of cued stimuli mismatch. The meditation task required subjects to attempt to engage in mindfulness based meditation while in the scanner, and is described in full detail in the original study by Hasenkamp and colleagues (107). Lastly, the Twilight Zone dataset is one of several fMRI datasets available on OpenNeuro that represent subjects engaged in audiovisual media watching. In this case, the time series represents subjects watching the same 15 minute segment an episode entitled “The Lateness of the Hour.” To be clear, beyond the hypotheses described in the introduction, we had no idea how these varied stimuli might relate to or alter network activity in infraslow QPPs, and

the mix of datasets represents an effort to explore how such dynamic patterns might change in relation to these different stimuli.

As most task datasets were obtained from open sources we were limited in access to behavioral and other non-imaging data. Reaction time data were only available in the gamer vs non-gamer datasets shared with us by the Dhamala lab at Georgia State University, which was based on reaction time to a moving dot task (101), and were only accessible as averaged reaction times across all trials per subject. Given these limitations to accessing behavioral data, the present study focused on the functional imaging data from each dataset.

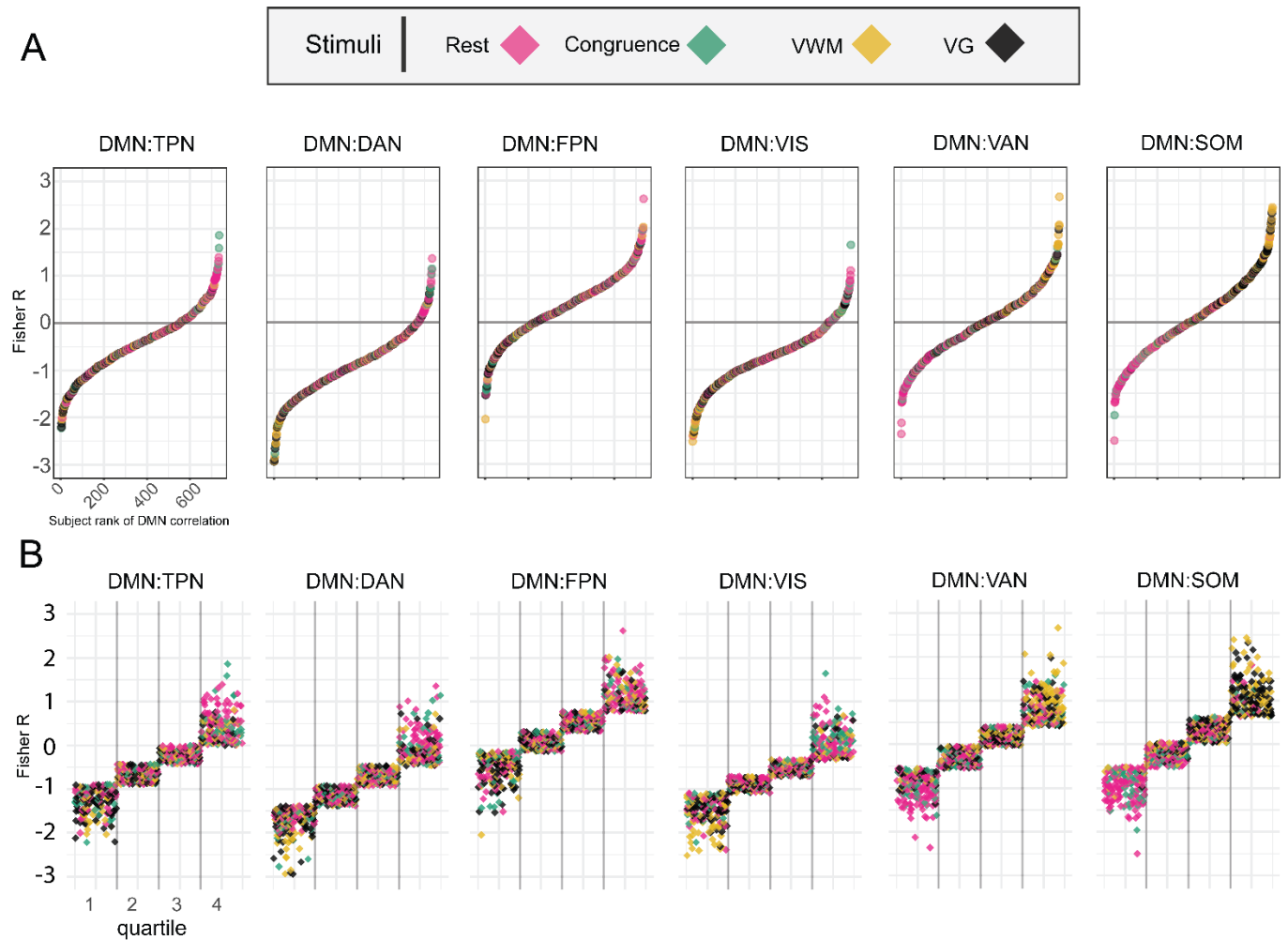


**Figure 2.5. A)** DMN correlations from QPPs plotted from lowest to highest for all subjects and scans instead of qualitative grouping based on dataset of origin. B) The same DMN correlations assigned into quartiles for visual aid. Note in both A and B that the VAN and SOM show highest correlations during the VWM and VG tasks, while the other networks trend towards higher DMN correlation during rest and congruence tasks. Despite differences in the protocol of VWM and VG tasks, both tasks seem associated with similar changes with respect to network correlation to DMN during the QPP.

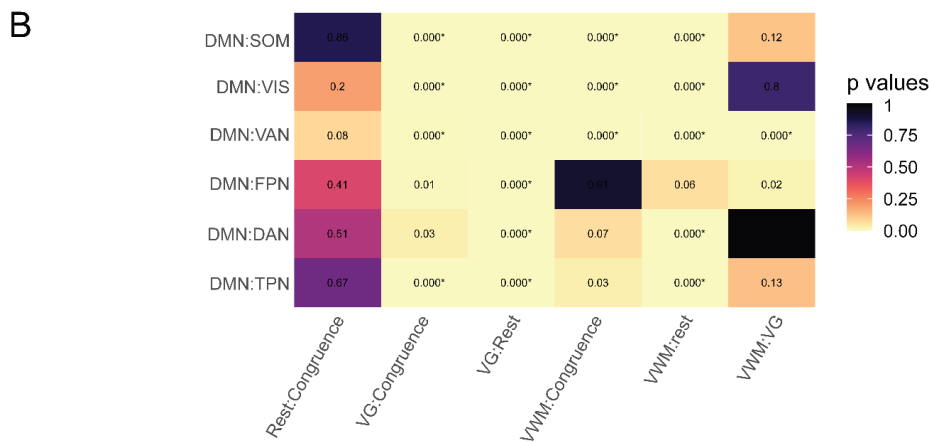
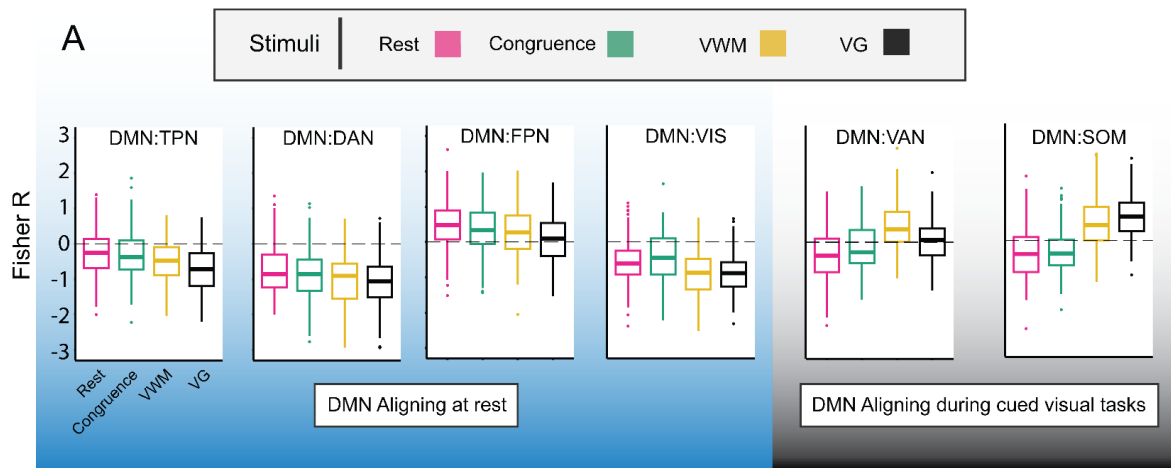


**Figure 2.6.** Separate analysis of visual working memory (VWM) and moving dot task from video gamer study (VG) shown as correlation to DMN in box plots with mean and variance. While the tasks are

somewhat different, in both tasks the subjects are presented with a cued stimuli that they must then react to. In the VG task, the subject's goal is to react quickly to a cued dot color after it begins moving. In the VWM tasks, subjects must hold a cued visual stimulus in their working memory after it disappears from a grid and then correctly identify it after it disappears for some amount of time. Despite differences in these types of cued stimuli tasks, with respect to DMN correlation in the QPP the tasks seem associated with the same trends for all the major cortical networks analyzed. These differences are tested at the group level with a one-way ANOVA on the box plots shown in A, with corresponding pairwise Toker analysis and resulting p-values between groups and networks shown in B). In B, note that the VG task differs from rest for all networks, but that VG and VWM only differ significantly with respect to the VAN.

### **2.4.3 Discussion of changes by network:**

#### **Dorsal attention network**

DMN-DAN anticorrelation significantly increased during visual tasks compared to rest but not congruence tasks. Our results add further evidence that definitions of a single "task positive" network can be misleading, given the divergent task responses shown by the DAN, FPN, and VAN along the DMN vs non-DMN spectrum. (c.f., (61, 63). Our results are corroborated by recent work from collaborators. Employing QPP analysis to a finger tapping task, Seeburger and colleagues found consistent results with respect to DMN-DAN anticorrelation. Subjects engaged in the finger tapping task were assessed for time spent "in the zone" vs "out of the zone". Subjects who performed better showed significantly greater DMN-TPN anticorrelation, with some of this effect accounted for by increased DMN-DAN anticorrelation (63). Also consistent with our results, Seeburger found that the

shifting in TPN anticorrelation was primarily driven by changes in the amount of FPN anticorrelation, not DAN.

### **Frontoparietal control network (also referred to as executive control network)**

We found that the FPN exhibits decreased DMN correlation in the infraslow QPP depending on the task, becoming more positively correlated with the DMN during rest and more anticorrelated with the DMN during congruence and visually demanding tasks. This result lines up with a considerable body of evidence from fMRI and seed-based analysis that the FPN, or frontoparietal control network, acts to flexibly modulate the DMN and DAN depending on the degree of internal to external attention involved in a task (22, 65, 113, 119-123). For example, Smallwood and colleagues proposed that increased DMN-FPN alignment during rest, when attention is often directed inward or to mind-wandering, is critical for buffering internal thought trains to prevent interruption by intruding thoughts or external stimuli (22, 94, 95, 124, 125). Morin and colleagues, which employed the same Yeo's 7 network definitions used in the present study, also reported flexible reconfiguration of the FPN resulting in increased DAN-FPN alignment and decreased DMN-FPN alignment during symbolic visual tasks (123). The FPN has also been further parcellated into subregions based on preferential connectivity with either the DMN and DAN, with these FPN subdivisions showing flexible change in DMN FC based on task type (65). While there are disparate results and many open questions regarding the role of DMN-FPN connectivity in neurotypical subjects, our QPP based results taken with the broader evidence support a theory of DMN-FPN interaction that points to generally increased DMN-FPN connectivity during rest and internal attention, and decreased DMN-FPN connectivity during externally directed or visual tasks.

## **Ventral attention network**

Throughout fMRI literature, the VAN (also referred to as the salience network or reorienting network) is characterized as critical for redirecting attention to salient incoming stimuli (5, 51, 87, 126-128). Across our QPP task spectrum, the VAN exhibited the opposite trend of the DAN and FPN, becoming strongly correlated with the DMN during visual tasks, and more negatively correlated during internally focused tasks. Both categories of visual task in this study (n-back visual working memory and left-right moving dot task) require a high degree of focused external attention and the suppression of distracting stimuli. The VAN becomes more suppressed during external goal-directed tasks, but transiently active when a distracting or novel stimuli is introduced to redirect attention (126, 127, 129). Seeburger and colleagues further corroborate our results, reporting the DMN and VAN to be more positively correlated when task performance was high and more negatively correlated when performance was low (63). DMN-VAN dynamics could provide a valuable biomarker for attentional disorders (62, 130). Considering seed-based findings of increased DMN-VAN FC in ADHD subjects (130), the aberrant DMN-TPN dynamics reported in Abbas et al (62), and the QPP results in the present study of increased DMN-VAN connectivity during external tasks, it could be the case that ADHD subjects exhibit task-like infraslow brain dynamics (QPPs) even at rest.

## **Sensory networks (SOM/VIS) across the task-rest spectrum:**

The somatomotor network showed a strong shift across the spectrum of external-internal attention in the group and individual QPP results. Somatomotor and visual networks showed opposite trends across the spectrum, with SOM becoming much more correlated with the DMN during visual tasks,

and the VIS becoming more anticorrelated with DMN during task. Increased alignment between the visual network and DAN during a visually demanding task fits an understanding of the DAN as directing top-down goal directed visual attention (15, 27, 66, 67). Likewise, perceptual decoupling is thought to be essential to the maintenance of internal trains of thought, when the DMN is generally most active (94, 124, 131). The need for perceptual decoupling, the separation of intruding somatosensory perception from internal thought processes, might explain why we see high DMN-SOM anticorrelation in the resting state QPPs.

Our results support an updated understanding of sensory areas as being key to cognition and consciousness (132, 133) and not merely evolutionarily ancient substrates of primary sensation (134, 135). Of course, while expansion of the human cortex is disproportionately represented by association areas (11) this does not mean that sensory cortices remained static over the course of millions of years of evolution. Rather, sensory networks coevolved with association cortex and underwent selection suited to human behavior (for another good discussion on this topic see “Your Brain Is Not an Onion With a Tiny Reptile Inside”) (136). Dynamic inter-network relationships between the DMN and sensory networks could provide novel insight into our understanding of cortical function as well as a potential biomarker for conditions with altered sensory network activity like autism spectrum disorder (137-139)

#### **2.4.4 Limitations**

A primary limitation is that the data analyzed in the current study was obtained from a range of different subjects, from different scanners, with slightly different parameters. However, as mentioned in the results section, subjects scanned on the same scanners with identical parameters (HCP data) recapitulated the same task vs rest inter-network changes seen in the other datasets,

indicating that the signal of inter-network dynamic changes was greater than noise from dataset-to-dataset variability. Age and sex are factors that have long been known to affect baseline FC (32, 140). While effort was made to include datasets with similar age and sex ratios, these are important biological variables that surely contribute noise to data analyzed here. Demographic variables such as socioeconomic status, a variable that was not included in these datasets, can also have a major impact on FC (26). The inter-network correlation values reported here are on functional time series processed with global signal regression (GSR). There is no consensus on the use of GSR in fMRI preprocessing, with some arguing that GSR increases the possibility of detecting spurious anticorrelations (17, 141). There is also evidence that GSR reveals information in FC patterns missed without GSR (17).

It has been demonstrated that variation in DMN activity, CAPs, and global signal are related to physiology and behavior (111). As behavioral, physiological, and psychological data were not available for the subjects of the present study, the DMN vs non-DMN network spectrum was only analyzed using fMRI data. However, Seeburger and colleagues explored the interaction between moment-to-moment changes in QPPs as they relate to behavior using a finger tapping sustained attention task, and found results that are consistent with findings from the previous study with respect to DMN-to-network connectivity (63). Future studies could include regression analysis of more behavioral task performance data or other subject data to compare with changes in these reported infraslow DMN dynamics.

#### **2.4.5 Conclusions**

We applied QPP analysis to compare dynamic inter-network correlations between major attentional and sensory networks with the default mode network, a cortical network crucial for neurotypical

cognition whose aberrant activity has been implicated in numerous disorders. Using a range of datasets comprising a spectrum of task and rest and external-to-internal attention, we found that DAN, FPN, and VIS networks exhibit task-positive-like responses to visually demanding tasks during QPPs, while the VAN and SOM networks exhibit task-negative-like responses, becoming more aligned with the DMN during visual tasks. These findings based on spatiotemporal dynamics offer additional evidence that the brain does not possess a single task positive or task negative network (142). Rather, cortical networks are in a constant state of dynamic interaction that can flexibly change. The brain is never truly at rest and is constantly integrating external and internal models of reality, a process mediated by the DMN (37, 43). Our results suggest that as the locus of attention shifts from external to internal tasks, cortical network dynamics shift with respect to the DMN in a way that corresponds to the balance of task demands. This is consistent with the literature at large and makes evolutionary sense. The brain is a flexible behavioral system that evolved to produce adaptive behavior in the face of constantly shifting environmental variables. It is not surprising then that cortical networks underlying human behavior should themselves show dynamic shifts tracking task demands.

#### **2.4.5 Future Directions**

The results presented here provide a reference for comparing altered and pathological cortical dynamics to healthy subjects that can be used to gain insight into disease etiology and to identify diagnostic biomarkers. Specifically, given the evidence of altered DMN-DAN anticorrelation in attentional disorders and mild cognitive impairment, this type of analysis could be applied to datasets of ADHD and Alzheimer's Disease. The evidence presented here for dynamic shifting of sensory networks with respect to the DMN also suggests that application of this type of QPP analysis to autism spectrum disorder (ASD) could be fruitful, given the altered sensory network activity in

subjects with ASD. Considering the growing evidence that the DMN is central to capacities amplified in humans such as theory of mind, advanced language, and the construction of shared neural representations of the world (43), the application of QPP analysis to experimental datasets of subjects engaged in storytelling, problem solving, or economic game theory is also an active area of interest.

### **Acknowledgments**

We would like to acknowledge the Dhamala lab at Georgia State University and Dr. Jordan for collaborating and making available their moving dot task data. We also thank Dr. Wendy Hasenkamp and Dr. Larry Barsalou for sharing their meditation scans with us. Finally, we want to acknowledge that this study was made possible by OpenNeuro, the Human Connectome Project, and CABI, for promoting large scale open data sharing of fMRI scans. This research was funded by grants from the National Institutes of Health: 1R01Ns078095, 1R01AG062581, 1R01EB029857.

## Chapter 3

QPP methods comparison and the effects of prolonged behavioral training on resting state

cortical network dynamics, an example based on musical training data

3.1 Introduction

3.2 Methods

3.3 Results

3.4 Discussion

3.5 Conclusions

This chapter is from the first author manuscript *Creative tempo: Spatiotemporal dynamics of the default mode network in improvisational musicians*, which is pending submission after revisions.

Citation: H. Watters et al., Creative tempo: Spatiotemporal dynamics of the default mode network in improvisational musicians. bioRxiv 10.1101/2024.04.07.588391 (2024).

Full Author List: Harrison Watters, Abia Fazili, Lauren Daley, Alex Belden, TJ LaGrow, Taylor Bolt,

Psyche Loui, Shella Keilholz

### **3.1. Introduction:**

Intrinsic brain activity is dominated by alternating activity between brain regions associated with internal and external attention (7, 8, 19, 59). The primary network known to increase activity in the absence of externally directed attention is the default mode network (DMN), which is typically considered to include the posterior cingulate cortex (PCC), medial prefrontal cortex (mPFC), and precuneus (19, 21). The DMN shows increased activity during internally directed processes such as memory replay, mind wandering, imagination of future scenarios, social inference, and the construction of shared and individual internal narratives (15, 37, 43, 44). In global-signal regressed data from resting state functional magnetic resonance imaging (rsfMRI), activity in default mode regions is strongly anticorrelated with regions that show task-related increases in activity during externally directed attention (15, 88). These task positive regions have been referred to as the task positive network (TPN), which typically includes dorsal and frontoparietal cortical regions, or the dorsal attention network (DAN) and frontoparietal network (FPN) (15, 86).

This anticorrelated relationship between the DMN and TPN has been implicated in attentional control, and DMN FC is disrupted in pathologies such as attention deficit hyperactivity disorder (62, 143-147). Increased default mode network activity has also been associated with resting state mind-wandering (84, 125, 148, 149) and increased rumination, both thought to be predictors of unhappiness (150).

However, while increased DMN activity may drive spontaneous thoughts in the form of mind-wandering and maladaptive rumination, it may also signal an increase in all types of spontaneous cognition, including creativity (125). Several groups have reported a link between increased activity in the primary nodes of the DMN and creativity, including mPFC and PCC (151-153). An increase in functional connectivity between the DMN and the frontoparietal/executive control network (FPN) and

the DMN and ventral-attention/salience network (VAN) has also been implicated in creativity, specifically in the domain of musical improvisation (153-155). Such alterations in DMN-FPN or DMN-VAN connectivity may represent an increased capacity for flexible cognitive control driving creativity (156, 157).

Based on the known relationship between DMN-FPN FC and creativity, Belden et al., 2020 explored changes in resting state functional connectivity (FC) depending on creative musical training, using seed-based functional connectivity and graph-theory analysis to compare changes in the DMN, FPN, and other networks (158). Belden et al., 2020 found that improvisational musicians showed an increase in resting state FC between the visual network and both the DMN and FPN, as well as increased intrinsic FC in the ventral DMN when compared to classical musicians and controls.

While traditional time-averaged functional connectivity analysis employed by Belden et al., 2020 can identify seed-based correlations during resting state fMRI, analysis of dynamically recurring patterns such as co-activation patterns or infraslow quasi-periodic patterns (49, 53, 55, 57, 58, 61, 96) may provide deeper insight into the relationships between networks involved in creative improvisation. Also, the original study conducted analysis based on group level concatenated scan data, or aggregate data. As has been documented in the public health space, aggregated data can lead to misleading conclusions about the variance of individual subjects that belong to a group, a phenomenon which has sometimes been referred to as the ecological fallacy or aggregation bias (159). In this study, we seek to expand upon the analysis made by Belden and colleagues by applying multiple methods of dynamic FC pattern detection at both the group (aggregated scans) and individual scan level. Thus, this study also represents an exploration of the robustness of the methods themselves, and the validity of using purely aggregated group level data to make inferences about subject level dynamic functional connectivity.

Multiple types of recurring dynamic patterns have been detected and described in rsfMRI data (52, 53, 60, 72, 98). The present study focuses primarily on the dominant resting state pattern of anticorrelated activity between the DMN and the task positive regions, which occurs quasi-periodically on the infraslow timescale (with 1 cycle lasting about 20 seconds in humans) (59). This pattern, which has been described as the primary quasi-periodic pattern (QPP) of dynamic FC, was first quantitatively detected in blood-oxygen level dependent (BOLD) fMRI in anesthetized rats (56) and was subsequently detected in human rsfMRI (55). The original QPP detection in Majeed et al., 2009 and Majeed et al., 2011 employed a sliding window-based algorithm that converged on a reliable pattern of DMN/TPN anticorrelation. More recently, this QPP has been replicated using complex principal components analysis (cPCA) on rsfMRI (49) and appears to be one of the three dominant spatiotemporal patterns that account for most of the time lagged connectivity structure in intrinsic brain activity observed across methods.

Given the relation of default mode QPP dynamics to attention, we predicted that prolonged focused musical training, like that experienced by classical musicians, may lead to altered DMN and DAN anticorrelation dynamics when compared to musicians who are primarily improvisational. The established role of the DMN in spontaneous cognition makes it a useful reference network for making functional correlations that may implicate other networks in creative cognition. We primarily measured the amount of correlation between other canonical networks and the DMN at the group and individual level, over the full cycle of the QPP. QPP analysis allows us to capture whole brain dynamics and the time lag structure between other cortical networks based on musical training, and to compare with the inter-network results originally reported in Belden et al., 2020 in networks such as the visual network and frontoparietal network. Thus, while our analysis was primarily focused on exploring functional correlation to the DMN during the QPP, we also followed QPP results that differed in regions beyond the DMN.

In addition to QPP detection using the QPP-finding algorithm, we repeated part of our group level QPP network analysis using cPCA, a type of dimensionality reduction method originally pioneered in geological and climate sciences to detect the components that explain most of the variance within propagating patterns (160). More recently, Bolt and colleagues demonstrated that in global signal regressed data, the first component from cPCA in rsfMRI is equivalent to the QPP of DMN/TPN activity. To our knowledge, this is the first study to apply both the pattern-finding algorithm and cPCA to the same dataset to detect group-wise dynamic FC differences. By applying both methods, we hoped to uncover any differences in the sensitivity of each approach to group level changes in QPP network dynamics. To compare group-average vs individual QPP network trends, we repeated all algorithm-based QPP detection on a subject-wise level.

Using these two methods, a QPP-finding algorithm and cPCA-based QPP detection, we hypothesized that: (1) DMN network activity in the QPP may be higher in improv musicians than improv or MMT subjects, given the association between DMN activity and mind-wandering/spontaneous cognition, (2) the visual network in the QPP would be more strongly correlated with the DMN and FPN, given the seed-based connectivity results in Belden et al., 2020, (3) group level differences in QPP network correlations would be consistent across both the sliding window and cPCA methods, (4) the application of QPP waveform analysis may detect groupwise differences in time-lagged information missed by traditional seed-based FC analysis.

The findings in this study add to growing evidence that infraslow patterns of anti-correlated DMN-TPN activity, sometimes referred to as quasi-periodic patterns, are a robust phenomenon in resting state data. They also provide cautionary results related to the overinterpretation of inter-network correlations based purely on aggregate level detection of dynamic FC patterns.

### **3.2. Methods:**

All code is Open-Sourced and available online. QPP code and cPCA code referenced in the methods section is available on GitHub: (1) [https://github.com/BnzYsf/QPP\\_Scripts\\_v0620](https://github.com/BnzYsf/QPP_Scripts_v0620), and (2) [https://github.com/tsb46/complex\\_pca](https://github.com/tsb46/complex_pca)

All code used for sliding window quasi-periodic pattern detection was run in Matlab 2023a (161). Visualizations were generated through R, version 4.3.2 (162), and FSL (163). Code for cPCA was run in Python on a Linux operating system.

#### **3.2.1 Participants**

Structural and functional MRI scans were obtained from Alex Belden and Psyche Loui at Northeastern University. All original scan acquisition adhered to best practices for ethical human data collection and informed consent in accordance with local institutional review boards. For a full description of participants and MRI acquisition see their original study Belden et al., 2020.

In brief, 48 young adult subjects were recruited from universities and schools in the Boston area and classified into three groups based on musical training background: classical training, improvisational training, or minimal-musical training (MMT). Final groups consisted of 16 subjects each (n = 4 females, n = 12 males). To the extent possible, the groups were matched in age, general cognitive ability, pitch discrimination, duration of musical training, and age of onset of musical training.

#### **3.2.2 Data acquisition and pre-processing**

T1 weighted structural scans and resting state functional scans were obtained on 3T Siemens scanners at Northeastern Biomedical Imaging Center and the Olin Neuropsychiatry Research Center. T1-weighted sequences were 3D magnetization prepared rapid-acquisition gradient-echo

(MPRAGE) with a voxel size of  $0.8 \times 0.8 \times 0.8 \text{ mm}^3$  (TR = 2.4 s, TE = 2.09 ms, flip angle =  $8^\circ$ , FOV = 256 mm).

Resting state scans had a duration of 7.5 minutes and were obtained with an echo-planar imaging (EPI) sequence with 947 volumes (TR = 475 ms; TE = 30 ms; flip angle =  $90^\circ$ , 48 slices; FOV = 240 mm; acquisition voxel size =  $3 \times 3 \times 3 \text{ mm}^3$ ). Following typical resting state protocol, participants were instructed to keep their eyes open and fixated on a cross for the duration of the scan.

For processing, scans were formatted according to Brain Imaging Data Structure (BIDS: <https://bids.neuroimaging.io/>. Poldrack et al., 2024). All pre-processing was run in Linux (Ubuntu 22.04.3 LTS) using the configurable pipeline for the analysis of connectomes (C-PAC: <https://fcp-indi.github.io/>). Outputs for algorithm based QPPs were generated with and without global signal regression (GSR); non-GSR results are available in supplemental material. As part of the default C-PAC pipeline, anatomical scans were registered to the 2mm Montreal Neurological Institute MNI 152 Atlas. Resting state functional scans were also registered to standard MNI space and then extracted as timeseries to the Brainnetome 246 atlas, a 246 region-of-interest (ROI) parcellation based on MNI space. The first 10 volumes of each scan were truncated for all subjects, resulting in a final 937 timepoints by 246 ROI 2-dimensional timeseries for each subject.

### **3.2.3 Quasi-Periodic Pattern Acquisition window**

Recurring spatiotemporal patterns (quasi-periodic patterns) were identified using an updated version of the sliding window pattern detection algorithm from Majeed et al. 2011 and other work from the Keilholz group. For a more detailed description of the original algorithm see Majeed et al. 2011. Previous versions of the algorithm were based on a user-defined or random starting point within the time-series and would conduct a sliding correlation of the initial segment with other segments in the scan that exceeded a threshold of correlation (0.2) with the initial template. In this

study, we used a robust version of the pattern algorithm that starts at the beginning timepoint and then iterates through each timepoint, updating until a convergent pattern is produced (57, 73).

While the QPP algorithm we used no longer has a user defined start point, it still requires a user defined window length. Previous work indicates that QPPs last approximately 20s in humans (49, 59, 73) but we ran the QPP algorithm with various window lengths (WL) to determine empirically which WL most reliably captured a full phase of the QPP in this dataset. After trying a range of window lengths between 15-40 seconds, we found that a WL of 24 time points most reliably captured a full phase of the QPP in this dataset and used that WL for all algorithm based QPP analysis. Given that the TR of the functional scans was .475 seconds, this means that the QPPs displayed in the results section are on the order of 12 seconds ( $TR \times WL$ ,  $.475 \text{ seconds} \times 24 \text{ second WL} = 12 \text{ seconds}$ ).

Initial QPP analysis was conducted at the group level: we ran the QPP algorithm on the concatenated time series for 16 subjects at a time (classical, improv, MMT, respectively) and an average group level QPP was detected. QPP analysis was then conducted between group-level QPPs based on canonical networks (described below). Individual QPPs were also run for all 48 subjects. Statistical comparisons at the individual level were only made for the network correlations found to be most different at the group level, including the visual network and parts of the subcortical network (amygdala).

#### **3.2.4 Network based analysis of QPP functional connectivity**

Analyzing QPP dynamics with canonical network definitions generated results that could be easily compared with the default mode network literature as it relates to creativity, including Belden et al.'s original seed-based analysis findings (158). We therefore decided to employ canonical network definitions after applying the QPP pattern detection algorithm.

After QPP detection, the QPP was mapped to network space (9, 10) (Yeo et al., 2011). ROIs from the Brainnetome 246 parcellation were assigned into 7 canonical cortical networks plus subcortical, resulting in QPP waveforms for the following 8 canonical networks: default mode network (DMN), frontoparietal network (FPN), dorsal attention network (DAN), ventral attention network (VAN), somatomotor network (SOM), visual network (VIS), limbic network (LIM), and subcortical network (SCN).

From these time series, waveform plots were then generated plotting the normalized BOLD signal for one full cycle of the QPP for all defined networks. We then compared the correlations, the amplitude, phase, and squared difference between networks of each group-level QPP against all other groups. As the present study was focused on dynamics relative to the DMN, the focus of these comparisons was with respect to the DMN. As the improv group showed an altered amygdala-DAN FC, we reported differences with respect to the DAN instead of the DMN. Because the DMN and DAN are strongly anticorrelated in all group QPPs, either the DMN or DAN provide convenient reference networks to compare the remaining Yeo's cortical networks.

For statistical measures, group level network correlation comparisons were made using the cocor R library (164). Subject-wise statistical comparisons of network correlations were made in R studio using Kruskal-Wallis test for multiple comparisons (162). All correlation values were Fisher transformed. Subject-wise statistical comparisons were made after Fisher transform. Correction for multiple comparisons was made using the conservative Bonferroni correction (112) based on the assumption of 7 underlying comparisons between the 8 canonical networks used. Thus, the standard significance threshold of  $\alpha = .05$  was adjusted for 7 comparisons ( $.05/7$ ) to an  $\alpha = .007$ .

### **3.2.5 Complex Principal Components Analysis**

Bolt et al, 2022 demonstrated that the majority of variance in low-frequency spatiotemporal BOLD patterns can be explained by three principal components (49). In global signal regressed data, the first of those principal components is equivalent to the QPP or task-positive vs default mode anticorrelated pattern. Note that in Bolt et al. the primary results are reported without global signal regression, and thus in that study the first component is global signal while the second component is equivalent to the QPP. Using the same methodology of Bolt et al., we applied Complex Principal Components Analysis (cPCA), a dimensionality reduction method, to identify the principal component of low-frequency BOLD signal in our dataset equivalent to the QPP.

The same 2-dimensional timepoint by ROI preprocessed CPAC outputs that were the QPP algorithm input were used for cPCA. cPCA was run in Python on a Linux operating system on concatenated scans on a groupwise basis for the 3 respective music groups (classical, improv, MMT).

cPCA was run initially with 10 components; consistent with Bolt et al., 2022, the majority of variance in our dataset was explained by the top 3 components (Figure 3.4A). We then plotted the top 3 components across 937 timepoints to generate histograms of the proportion of the components across subjects (Figure 3.4B) and total proportion of the top 3 components (Figure 3.4C). Note that components 2 and 3 of GSR data possibly correspond to additional types of QPPs, QPP2 and 3 specifically (61), but as the present study focuses on the dominant QPP of DMN/TPN anticorrelation the other QPPs/components were not used for analysis.

After confirming that the relative proportion of time spent in the QPP component was similar across groups (Figure 3.4B-C), component 1 (QPP1) for each musical group was then reconstructed as a 4-dimensional nifti file for visualization in FSLeyes. We then plotted the QPP component as a reconstructed time series into brain space and generated network activity waveforms for comparison to the sliding window algorithm results (Figure 3.5).

cPCA based waveforms were generated in FSLeyes (163) by selecting voxels in key nodes of ROIs corresponding to each network of interest (DMN, DAN, VIS, AMYG) based on the Brainnetome parcellation (table 1) and then plotting the timeseries in bins representing the length of one full cycle through the QPP. The default number of bins is 30 for the reconstructed time series. 100 bins were used instead for increased temporal resolution for plotting the phase aligned components. For any number of bins used in the reconstructed component time series, the total number of bins represents one full cycle through the QPP, corresponding to radial distance between 0 and  $2\pi$ . Like the algorithm based QPP, one full cycle of the cPCA based QPP takes approximately 20 seconds in humans (49). Note that in the algorithm based QPP we used a window length of 24 time points, which was determined empirically by trying a range of window lengths between 15-40 time points.

As with the algorithm based QPP networks, we then made group-level comparisons of the correlations between the networks of interest and the default mode network. For the cPCA QPP analysis, only group level comparisons were made, no subject-wise waveforms or correlation values were generated. When plotting ROI based correlation of cPCA based time courses in FSLeyes, we found that all voxels within a given Brainnetome ROI were highly correlated, near 1 (see supplemental figure 2), and thus plotting the time course from a representative voxel within each ROI was roughly the same as plotting a mask for each ROI. Thus, for each network of interest a representative voxel was selected and used to generate waveform plots (Figure 3.5 B-C). To account for interhemispheric differences, voxel-based time courses were plotted from both left and right hemispheres. No qualitative differences were noted in left vs right hemisphere time courses from the chosen voxels, so the average time course between left/right was calculated and plotted to compare with QPP pattern algorithm results (Figure 3.5 B). All voxels and their corresponding Brainnetome ROI numbers are shown in table 3.1.

Network	MNI coord. left hemisphere	MNI coord. right hemisphere	Brainnetome ROI	Brainnetome ROI numbers
DMN	87 85 107	95 85 107	PCC	175,176
FPN	70 151 124	113 151 124	Dorsolateral area 8	3, 4
DAN	72 125 139	110 125 139	Dorsolateral area 6	7, 8
VIS	77 26 63	107 26 63	Occipital polar cortex	203, 204
AMYG	70 125 51	114 125 51	Medial amygdala	211, 212

**Table 3.1:** MNI and Brainnetome coordinates for all seeds used to generate cPCA waveforms

**3.3. Results:**

**3.3.1 Network analysis of QPPs**

QPPs detected in our groups were similar to those in prior studies (49, 59) showing a strong pattern of anticorrelation between default mode and dorsal attention/task-positive areas (Figure 3.2). Group level QPPs are discussed first followed by a comparison with subject-wise QPP results.

DMN/TPN anticorrelation is shown to be associated with changes in cognition and arousal, specifically attentional control and mind wandering (33, 54, 59, 141, 148, 165). Given the prolonged hours of repetitive musical training undergone by classical musicians, we initially speculated there may be differences in resting attentional control and thus looked for differences in correlation between default mode and task positive regions (DAN, FPN, and VAN) in classical musicians. However, we did not find significant differences in correlations specifically between the DMN/TPN regions in the classical musicians (Figure 3.2 A). Instead, we found significant differences in the time lagged network correlations between the DMN and other networks in the improv group. Additionally, the amplitude of QPPs in improv musicians trended much lower than classical and MMT groups.

As captured by the squared difference between networks, the overall amplitude of the anticorrelation between the DMN-DAN in the improv group trended far below the classical and minimally trained musicians (Figure 3.2, C-D). For the improv musician group, the squared difference between DMN-DAN was 0.076, roughly half of the classical group's 0.132 and the MMT group's 0.149 (note that squared differences between normalized network activities were measured at the group level and thus lack a standard deviation).

In addition to changes in overall QPP amplitude, the improv group also showed an altered QPP progression in the visual and subcortical networks. More specifically, the network waveform plots (Figure 3.2C) and their underlying correlations showed increased correlation between visual-DMN and decreased correlation between amygdala-DMN activity in the improv group QPP (Figure 3.3B). Given the strong anticorrelation between the DMN and DAN in the QPP, decreased amygdala-DMN FC also means increased amygdala-DAN FC. As previous literature implicates amygdala-DAN FC as an area of interest for behavior and cognitive control (166, 167) we decided to report the difference in extrinsic amygdala FC as between amygdala-DAN and not amygdala DMN. We found no clear group-wise differences in other subcortical structures such as the hippocampus, which was highly

varied between groups, or in the thalamus and basal ganglia, which seem to show almost no QPP-like activity in this frequency range (0.1-1 Hz). This is consistent with Yousefi et al., 2021, which reported very weak thalamic QPP activity only revealed by substantial averaging (61).

Given that the improv group's visual network and amygdala seemed to be the most different, plots and statistical comparisons were made for the improv group's visual network-DMN and amygdala-DAN correlations compared to the other training groups. The improv musicians showed an increased correlation between both the visual network and DMN and the amygdala and DAN relative to the classical and minimally trained musicians (Figure 3.3, A-B, left).

Group-level QPP waveforms were also generated on time series processed without global signal regression (GSR). Waveform results without GSR exhibited positive global correlation between all of Yeo's networks used in the present study (supplemental Figure 1).

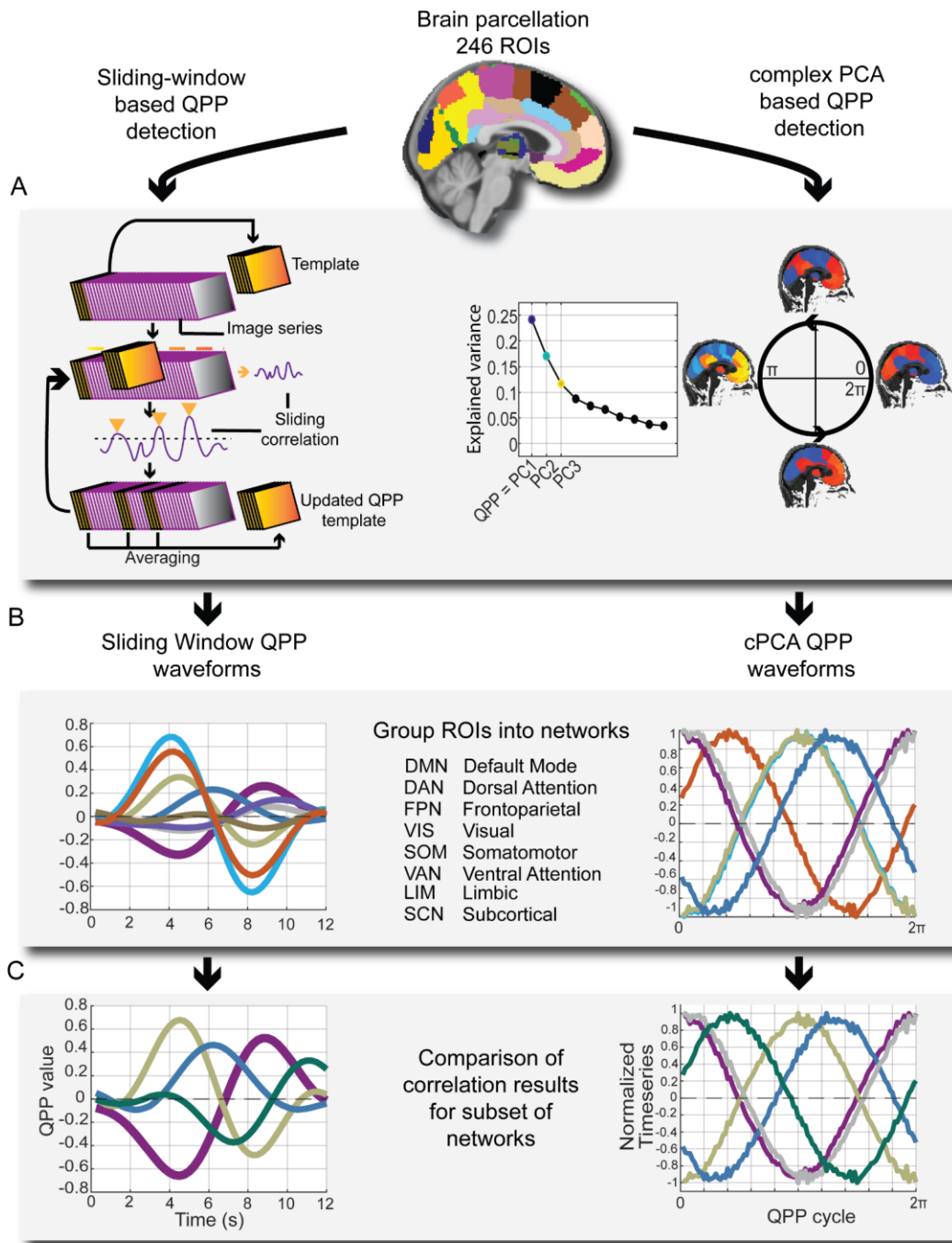


**Figure 3.1:** Parcellation of pre-processed resting state fMRI time series into Brainnetome 246 ROIs.

A) Detection of quasi-periodic patterns (QPPs) using a sliding window based algorithm and complex principal components analysis, respectively. B) Grouping of 246 ROIs into 8 canonical networks for C) comparing correlations and squared differences of network activity during the QPP.

### 3.3.2 Subject level QPPs for comparison of selected networks

Group level analysis is commonplace in seed-based and dynamic FC studies but obscures individual variability. To explore how dynamic DMN FC differs at the subject-wise level, we also applied the QPP algorithm individually to all 48 subjects. We then again plotted the fisher-transformed correlation values between the DMN and all other networks for each subject (Figure 3).

The purpose of the individual QPP comparison was two-fold. First, we wanted to know how similar the mean network correlation values of all networks in the individual QPPs were to the correlations detected at the group level. Previous work from Yousefi et al., 2018 using neurotypical subjects from human connectome data suggests that DMN/TPN anticorrelation is consistent within individual subjects, and between the individual and group level. However, Yousefi et al., 2018 did not apply QPP analysis to detect group-wise differences based on training or pathology and focused on DMN/TPN without considering other networks. Having individual correlation values allowed us to more easily make statistical comparisons as they provide a distribution and variance.

We found notable differences between the group and subject level QPP analysis. First, at the group level (Figure 3, A-B) the improv musicians showed a much higher correlation between the DMN and visual network (Fishers  $r = 1.187$ ) than classical (Fishers  $r = -0.218$ ) and non-musicians (Fishers  $r = -1.068993262$ ). This DMN-VIS correlation increase is not present in the subject level analysis. Second, improv musicians also showed a significantly higher Amyg-DAN correlation at the group level (Fishers  $r = 1.365$ ) compared to classical (Fishers  $r = 0.215$ ) and non-musicians (Fishers  $r = 0.0142$ ). Once again, when the QPP algorithm was run on a subject-wise basis this increased Amyg-DAN correlation was not present (Figure 3 B).

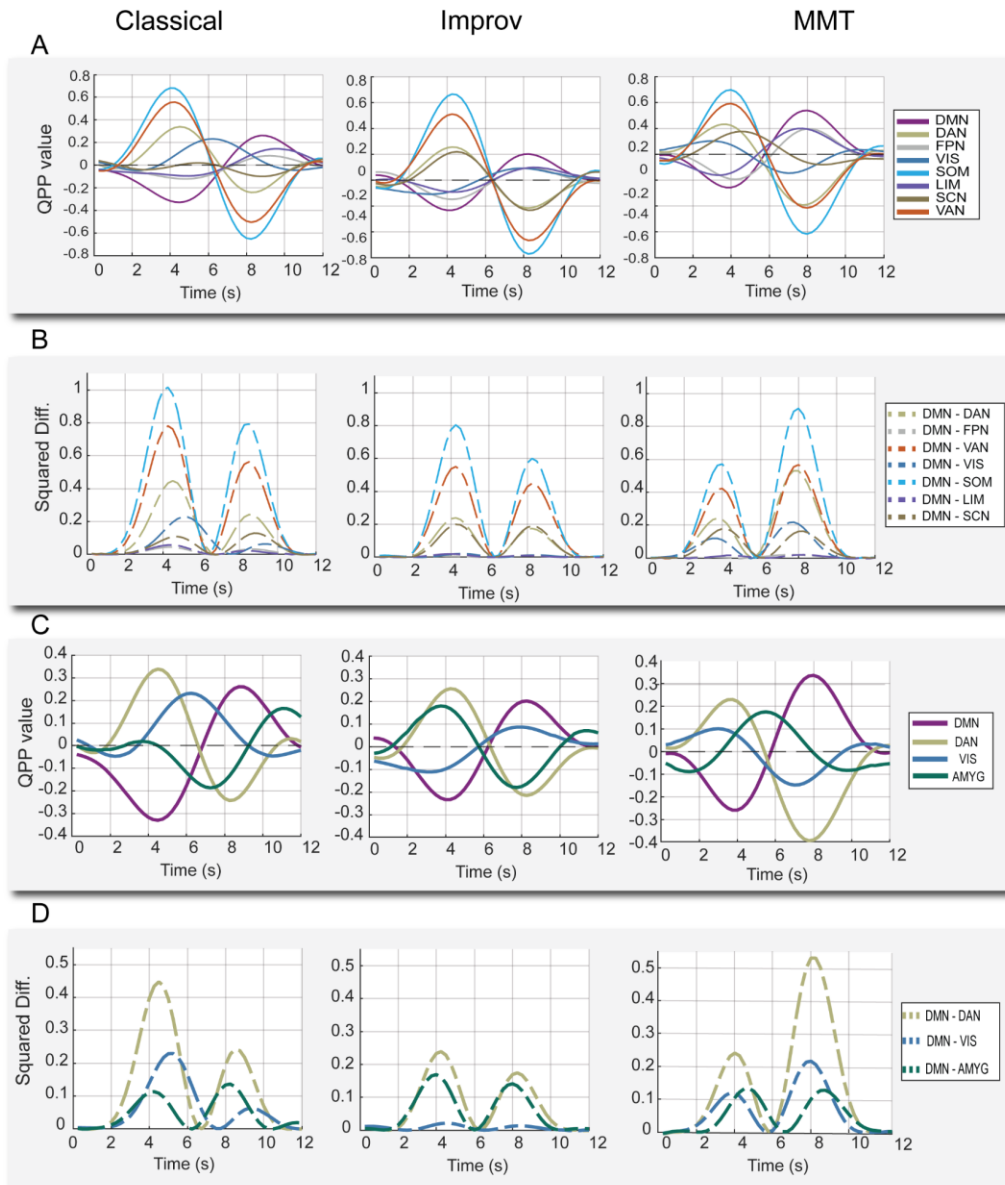


**Figure 3.2:** QPPs from sliding window pattern detection algorithm. A) QPP waveforms during 1 full cycle for all 8 cortical networks. DMN: default mode network, DAN: Dorsal attention network, FPN: frontoparietal network, VIS: visual network, SOM: somatomotor network, LIM: limbic network, SCN: subcortical network, VAN: ventral attention network. B) Squared difference between each network and the DMN for the same cycle. C) QPP waveforms for the DMN, DAN, and the two regions where group-level differences were noted in improv musicians: the visual network and amygdala. D) Squared difference between the same subset of networks for each group.



generated with Kruskal-Wallis test for multiple comparisons in R studio. A Bonferroni adjusted significance threshold of .007 was used for both subject-wise and group comparisons, assuming a multiple comparison correction of .05/7 (assuming 7 network comparisons between the 8 networks defined).

### **3.3.3 Complex Principal Components Analysis of QPPs**

As in Bolt et al., 2022, the top 3 components explained most of the variance and there is a strong elbow in the explained variance after the first 3 components (Figure 4A). We found the proportion of the top 3 components across all 937 timepoints for each subject and group to be very similar (Figure 4 B-C). For all 3 training groups, the first component (representing the QPP) was the dominant brain state for approximately 40-50% of all timepoints (Figure 4C). Note that the other components (2-3) were not used for further comparison as they represent different spatiotemporal patterns (49).

The cPCA results are aligned in several ways with the QPP algorithm results. First, the peak amplitude of the QPP component is noticeably less in the improv group, roughly half that of the other training groups, just as it was with the DMN-DAN amplitude in the algorithm-based pattern detection. Specifically, improv musicians normalized cPCA timeseries (BOLD signal) showed a decreased peak amplitude range in the QPP of -0.462 to 0.462, compared to the classical musicians' range of -0.816 to 0.816 and the MMT range of -0.772 to 0.772 (Figure 5A). Second, when mapping the cPCA-based QPP back to brain space we noticed that in the improv group, the occipital/visual regions were positively correlated with the posterior cingulate cortex ( $r = 0.371$ ), a primary node of the default mode network (Figure 5A). The classical ( $r = -0.549$ ) and MMT ( $r = -0.960$ ) groups showed typical visual-DMN anticorrelation, consistent with the sliding window QPP waveforms. Thus, based on the reconstructed time series in brain space, the improv musicians showed increased visual-DMN correlation just as they did in the QPP algorithm approach. Additionally, the improv musicians also

showed a much higher correlation between the amygdala and DAN ( $r = 0.878$ ) compared to the classical ( $r = 0.215$ ) and MMT ( $r = 0.014$ ) groups, again consistent with the QPP algorithm results (Figure 5 B-C).

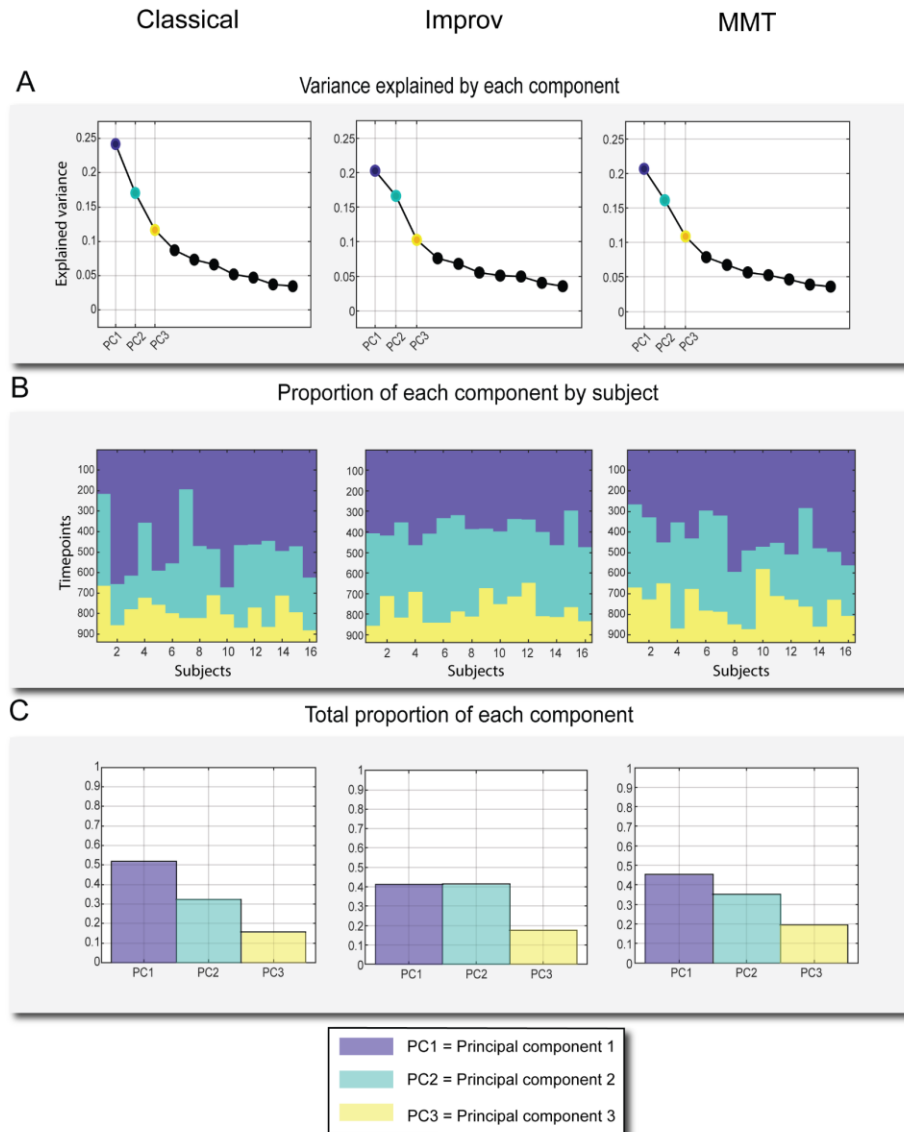


**Figure 3.4:** Explained variance and occurrence of top three components from complex PCA. A) Explained Variance of the top 10 components, top 3 highlighted. B) Top 3 components' respective proportions plotted against 937 timepoints. C) Proportion of each of the three components over the course of the scan out of 1.

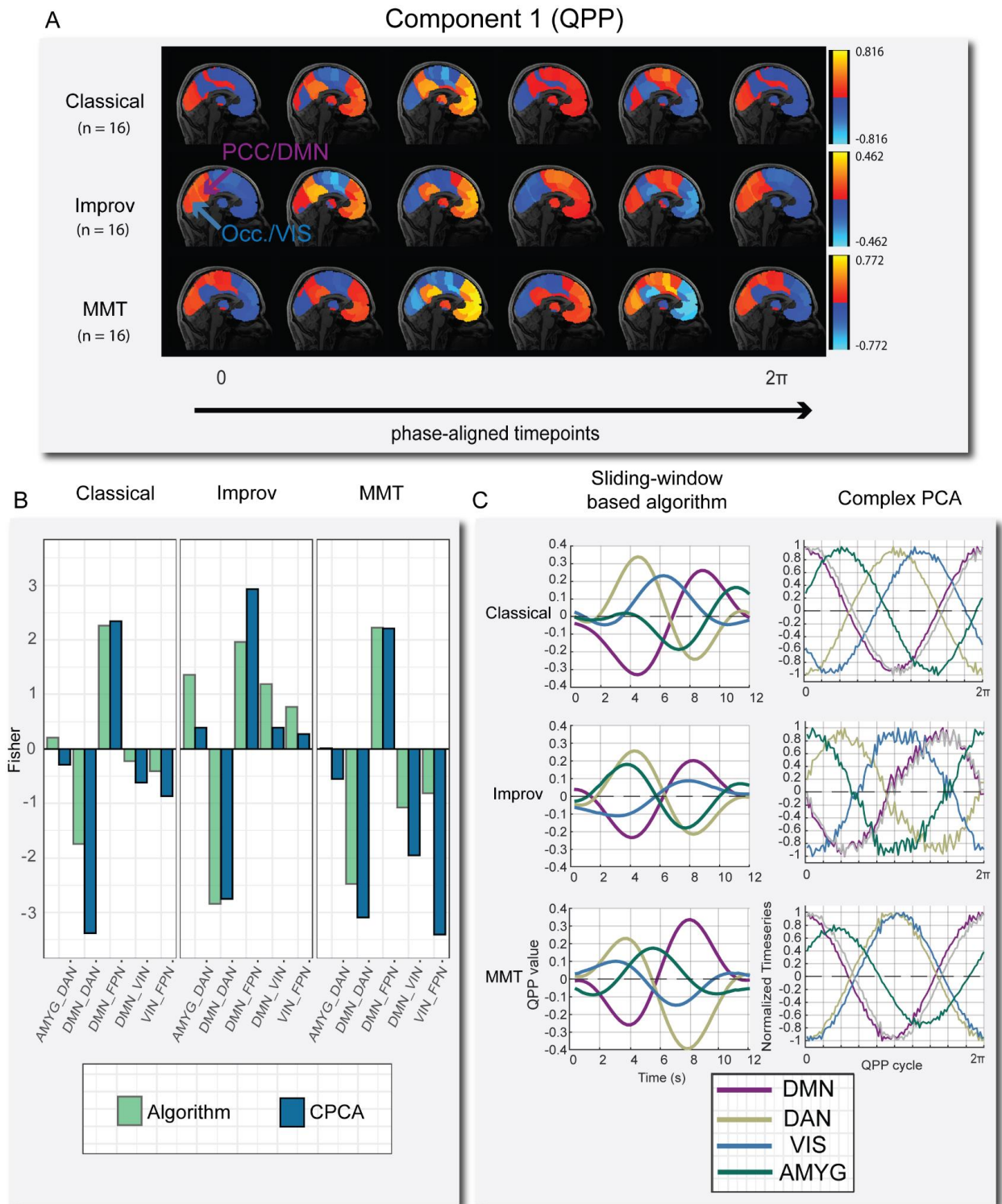


**Figure 3.5:** A) One full phase (zero to  $2\pi$ ) of group-level cPCA detected QPP time-courses mapped onto brain space. Time-courses were manually phase adjusted into 6 time points. Note that in the

improv group the posterior-cingulate cortex (PCC) is highly correlated with primary visual cortex (occipital lobe) at various time points, where in the classical and minimally trained musicians these two regions are always anticorrelated. B) Comparison of group-level correlation results between the sliding window-based algorithm and cPCA for selected networks. The overall network trends are very similar in both approaches. C) Waveform plots of normalized BOLD activity from QPP algorithm (left) and cPCA approach (right) for one full cycle of the QPP.

In summary, we found that the three main group level differences detected in improv musicians were consistent between the pattern detection algorithm and complex PCA methods. (1) The overall amplitude of the QPP between DMN-DAN trends much lower in the improv group. (2) The visual network in the improv musicians has a positive correlation with the default mode network at the group level, whereas for the classical and MMT groups the visual network-DMN were anticorrelated. 3. The amygdala is more correlated with the dorsal attention network in the improv musicians than in classical musicians or in MMTs.

### **3.4. Discussion:**

This study applied two methods of dynamic functional connectivity analysis to a dataset of human subjects based on musical training. **Our primary finding** is that sliding window and cPCA based QPP detection show convergent results. Both dynamic FC analysis methods detected an increased FC between the visual network and both the DMN and FPN, respectively, in improv musicians compared to classical and untrained musicians. With both methods, a trend of decreased QPP amplitude was detected in the improv group. Importantly, these inter-network correlation differences detected at the group level were not replicated when the sliding-window algorithm was applied on a subject-by-subject basis. Thus, our results indicate that interpretation of group level findings as they relate to a hypothesized link to creativity could be very tenuous. In general, one interpretation of our results is

that substantially greater individual scan lengths may be needed to find consistency between group averaged and individual infraslow dynamic pattern detection. The possible implications for these findings are discussed below.

### **3.4.1 Consistency between sliding-window and cPCA methods, and a consideration of group vs individual level QPP discrepancy:**

Inter-network correlations during the QPP were very consistent between the sliding window and cPCA QPP detection methods, with both approaches finding that the improv group showed increased correlation between the DMN-VIS and DAN-Amyg during the QPP. This finding is one of the first cross-method comparisons to demonstrate consistent sensitivity to the same group-wise correlation differences across the two methods of QPP detection. Our results add to a growing body of evidence that the QPP phenomenon is a robust feature of time-varying infraslow intrinsic activity, and that the QPP phenomenon is sensitive to group level changes in such patterns.

However, the large discrepancy between inter-network correlations detected at the group and individual level with QPP analysis warrants further discussion.

On one hand, differences in functional connectivity results between group-averaged and individual level analyses have been well documented in the FC literature and should not be entirely surprising given the high degree of individual variability in neuroanatomy and functional networks (15). On the other hand, as demonstrated in the chapter 2 multi-dataset approach, results appear to be very consistent between group and individual QPP detection with many scans and subjects.

Additionally, the QPP algorithm converges on an average pattern no matter what time series it runs on, so it should be no surprise that the group level QPP and underlying network dynamics are not fully recapitulated when running the QPP on a subject-wise level. At the group level, the QPP algorithm was run on the concatenated time series for all 16 subjects from a group at once (14,992

timepoints at once). This means the group QPP converged on an average pattern for all 14,992 timepoints for each group. The individual scans' QPP (937 timepoints per scan) resulted in a distribution of correlations largely consistent with the group level analysis (Figure 3.3A). However, the group level algorithm may converge on altogether different results depending on the underlying subjects, and because there is much less data in an individual image series. When considering group vs subject-wise QPP results it is also important to note that global signal regressed data has been shown to produce QPPs that may be more like one another in terms of individual DMN-TPN correlations (57).

#### **3.4.1.2 Short scan length and QPPs**

Another important consideration with respect to group vs individual pattern detection is the scan length in the present study. Each subject only had one scan that was 5 minutes in length. The original dataset authors used a TR of 0.475 ms, which they correctly point out results in a time series with many more timepoints to sample than a typical TR of 2-3 seconds employed in other fMRI studies. However, the effective temporal resolution of 0.475 ms is faster than the temporal resolution of the BOLD signal which is on the order of several seconds in humans (4, 168). Also, the QPP phenomenon itself, as pointed out, lasts about 20 seconds on average when the waves of activity occur. Thus, sampling at a much faster rate than the fundamental signal (BOLD) and the phenomenon being tracked (QPPs) does not increase the amount of data or the fidelity of the QPP detection algorithm. As with any BOLD based fluctuation in activity, the QPP detection algorithm benefits from longer scan times. For a pattern that happens quasi-periodically and lasts on the order of 20s, the pattern in a 5-minute scan for any individual subject may happen only a handful of times in the entire scan. Thus, when detecting concatenated data, individuals who happen to have more occurrences of QPPs during a short scan will necessarily have a greater influence on the end QPP than the algorithm

converges on. The short scan length of the present dataset therefore likely contributes to the large discrepancy between group and individual correlation results.

#### **3.4.2 Default Mode - Visual Network Connectivity and a Tenuous Link to Creativity:**

In both QPP detection methods the visual network/occipital lobe activity of improv musicians was more in phase with the DMN and FPN compared to classical and MMT groups, resulting in a significantly higher VIS-DMN and VIS-FPN correlation. This finding is consistent with the seed based connectivity analysis employed by Belden et al., 2020. The robustness of this finding across two dynamic QPP methods, in addition to the original static FC analysis, seems to indicate that an increased VIS-DMN/FPN connectivity is a very strong feature of this dataset. Whether increased VIS-DMN connectivity is a real feature of improvisational musical training or related to an increased capacity for creativity is a much more difficult question to answer conclusively with these findings alone.

However, these dynamic FC results contribute to a growing body of evidence indicating that visual-DMN connectivity may drive domain general creativity by way of increased mental imagery (158). A link between visual network activity and creativity was originally supported by findings from EEG (169) and white matter tractography (170, 171). For example, Petsche found increased coherence between frontopolar and occipital/visual regions during visual, verbal, and musical acts of creative thinking. More recent rsfMRI findings also indicate that spontaneous visual network activity and connectivity to the DMN are related to visual creative cognition (172).

Considering the role of activity in V1 and V2 in the generation of mental imagery (173), it seems intuitive that creativity may be linked to visual imagination. However, the combination of visual imagination and musical creativity, a process presumably dominated by audition more than vision, is less intuitive. At the same time, visual activity has already been linked to spontaneous imagery and

creativity in non-waking states of consciousness. Dreaming during REM sleep for example, another type of spontaneous cognition, is heavily linked to both default mode network (125) and spontaneous visual network activity (174). Dreaming itself has also been linked to creativity (175, 176). Given the available evidence, it seems reasonable that increased synchrony between two networks heavily implicated in the generation of spontaneous thoughts could explain an increased capacity for domain general creativity.

Of course, even if the increase in dynamic VIS-DMN FC in this dataset is related to creative cognition, and not merely an artifact, the direction of causality is unclear. In other words, from the analysis in this study it is unclear whether years of creative musical improvisation cause an increase in VIS-DMN connectivity or whether people who are more creative and exhibit such dynamic FC in the first place are simply more drawn to certain types of creative expression.

### **3.4.3 Dorsal Attention - Amygdala Connectivity:**

The improv group QPP also displayed increased correlation between the amygdala and DAN for both QPP detection methods. It is difficult to make strong interpretations of increased amygdala-DAN connectivity based on the analysis from this study alone. However, there is related evidence from rsfMRI studies that an increased amygdala-DAN correlation could underlie important behavioral and attentional changes. For example, one rsfMRI study using the same canonical networks from the present study (Yeo's 7 networks) found that increased amygdala-DAN FC was negatively correlated with trait anxiety (166). If our results of increased amygdala-DAN functional connectivity were to be replicated in other datasets measuring creativity, this would establish a potential link between creativity training and anxiety.

More recently, Sylvester et al., 2020 empirically defined three amygdala subsections based on their respective functional connectivity with major cortical networks: identifying a default mode

subdivision, dorsal attention subdivision, and a subdivision that did not display a preferred connectivity with the DMN or DAN (167). In the present study, the amygdala section used would have fallen within what Sylvester et al., 2020 described as the centromedial amygdala, or DMN connected amygdala subdivision. However, in our improv musicians, despite the selected amygdala seed being in the DMN-associated region, the amygdala was instead highly correlated with the DAN. In contrast, the classical and MMT groups displayed positive DMN correlation from the same amygdala voxel (or DAN anticorrelation), consistent with the neurotypical trend described in Sylvester et al., 2020. Again, the direct implications for this altered amygdala functional connectivity are unclear. But as Sylvester et al., 2020 points out, the subsections of the amygdala with high DAN functional connectivity may regulate top-down attentional and spatial processing (like that typically associated with the DAN). If increased amygdala-DAN FC is a real feature of increased creativity or improvisation, it could be the case that the amygdala's role in modulating the DAN becomes altered in creatively trained subjects.

There is also some anatomical evidence that the amygdala is related to increased creative cognition, with Bashwiler et al., 2016 reporting that increased volume in the left amygdala was significantly correlated with higher scores of creativity in their subjects (177). In a study specifically using jazz musicians and improvisation, the amygdala showed increased activity during musical improvisation inspired by positive images (178). Whether increased amygdala activity or amygdala-DAN FC at rest could signal increased creativity will require further replication in future studies.

#### **3.4.4 Limitations**

Small sample size is a common limitation in resting state and task-based fMRI interpretation (179, 180). Given the group sample sizes of  $n = 16$  for this study, it is difficult to draw strong general conclusions regarding creativity. With this type of niche study however, sample size will likely

continue to hamper interpretation for the foreseeable future as it is difficult to recruit a large number of age-matched volunteers for a variable such as musical or creative training. Even within this study there is significant heterogeneity of creative training within each group. For example, not all of the improv musicians have the same primary instrument, or the same number or training hours, or the same age of onset for musical training. Attempting to obtain an even larger sample size of musicians would introduce even more variation in the subjects' respective training backgrounds. However, while small sample size may hinder generalization, in our case it may be beneficial as it shows that our QPP and cPCA methods are robust in a very typical fMRI dataset in terms of sample size.

While the groups used in this study all had the same ratio of male and female subjects (12 and 4, respectively), it would be ideal to have an equal number of male and female subjects overall, as sex differences in rsfMRI have been widely reported (140).

Our primary dynamic FC correlation values are presented on data that were processed with global signal regression (GSR). There is still no consensus on global signal regression as a pre-processing step, but the use of global regression has been argued to increase the possibility of detecting spurious anticorrelations (17, 141). At the same time, GSR may reveal valid insights into FC patterns missed without GSR (17).

Finally, as noted previously, the primary group level findings were not recapitulated when the QPP algorithm was run on a subject-wise basis. While this is not entirely surprising, the discrepancy between group and individual results shows that we require further understanding of individual FC dynamics. It is possible that individual noise or anatomical variation may very well be greater than subtle but real shifts in network dynamics due to creative training.

### **3.4.5 Conclusions**

This study represents the first simultaneous application of algorithm based and cPCA based QPP analysis to detect group-wise differences in rsfMRI network dynamics. Using cPCA to detect QPPs yielded convergent group level results to those of algorithm-based QPP detection. Improvisational music training was found to be associated with increased visual network and DMN connectivity during quasi-periodic infraslow network dynamics. This is consistent with Belden et al.'s previous static functional connectivity analysis results and extends upon their findings. Both QPP analysis methods support a potential relationship between visual network-DMN connectivity and human creativity. The two methods also found that improvisational music training is associated with higher amygdala and DAN connectivity, further implicating the amygdala in creative cognition.

### **3.4.6 Future Directions**

While the subjects' age of onset of musical training was available for each subject, the present data are purely cross-sectional. Performing a longitudinal study with two or more scans over the course of musical training would help clarify whether there is a causal link between creative training and altered network dynamics by comparing dynamic DMN FC at different phases of learning. Additionally, comparing the dynamics of artists, writers, or other creatively trained individuals with musical improvisers would help clarify whether the effects of creative training are domain general or differ depending on the creative discipline.

The trend of decreased QPP amplitude in improvisational musicians seems counter to our initial hypothesis that improv musicians may exhibit increased DMN activity. However, the squared difference between DMN and DAN only represents the amplitude of those networks in the infraslow frequency range analyzed in the present study. To better understand the findings of amplitude change in improv musicians, future studies could apply additional band passes for internetwork analysis, or

include individual comparison of all ROIs within each respective network to provide a sense of which ROIs show altered amplitude during infraslow QPPs or patterns of other frequency ranges.

Because increased amygdala-cortical connectivity is related to anxiety (166), investigating a correlation between trait anxiety, creative training, and dynamic amygdala activity is another opportunity for future studies of dynamic FC and creativity. Creativity and anxiety have been tentatively linked in the literature for some time (181-183). Such a study of dynamics could be guided using the three amygdala subdivisions established in Sylvester et al., 2020, that is, the default mode, dorsal attention, and unspecified amygdala, to elucidate their respective dynamic FC with cortical networks implicated in creativity.

### **Data and Code Availability**

QPP algorithm scripts are available at the Keilholz MIND Lab github here: [https://github.com/BnzYsf/QPP\\_Scripts\\_v0620](https://github.com/BnzYsf/QPP_Scripts_v0620)

cPCA scripts provided by Taylor Bolt (Bolt et al., 2022) are available at his github here: [https://github.com/tsb46/complex\\_pca](https://github.com/tsb46/complex_pca)

Structural and rsfMRI scans were provided by Alex Belden from the MIND lab at Northeastern and can be made available upon request to the authors and original data collectors.

### **Author Contributions**

Conceptualization, data preparation, data processing, formal analysis, figure drafting, paper writing, review, editing: HW and AF. Data visualization, analysis, review, and editing: LD. Data preparation and curation: AB, PL. Supervision, review, and editing: SK. Preprocessing troubleshooting, review, and editing: TJL.

## **Chapter 4**

### Conclusions, Discussion, and Future Directions

4.1 Conclusions

4.2 Discussion and Future Directions – QPPs in Alzheimer's Disease, cortical networks as attractor states

## 4.1 Conclusions

This multi-dataset study produced several novel insights into the dynamic functional connectivity of cortical networks across behavioral states, as well as cautionary information regarding the application of dynamic analysis on the individual level or to smaller samples.

### 4.1.1 DMN vs non-DMN axis of attention

In neurotypical subjects from a wide range of task and rest states, we report that cortical network dynamics during the QPP follow a **DMN vs non-DMN alignment axis**, which appears to closely track the degree of external attention demanded by tasks. At one end of the spectrum, subjects engaged in resting states or tasks requiring a high degree of internal attention such as mindfulness meditation, show a strong correlation between the DMN-FPN. This DMN-FPN connectivity weakened during congruence tasks and became significantly weaker during external visual tasks. These findings were consistent with literature portraying the FPN as a flexible executive control network that modulates and buffers the activity of other networks depending on attentional demands (119, 141, 184). These results also suggest that decreased DMN-FPN alignment in the QPP could serve as a biomarker of atypical executive control or attentional processing at rest. The DMN-VAN correlation also exhibited a strong shift corresponding to internal vs external attention, but in the opposite direction, showing a flip from negative to positive correlation to the DMN during externally focused tasks. Surprisingly, the somatomotor (SOM) network participated more strongly than any other network in shifts related to external vs internal attention, switching from very negative DMN-SOM correlation during internal tasks to very positive correlation during external tasks. Overall, the spectrum of attention from internal-to-external that we observe generates a tool that can be used to help interpret the burgeoning literature of dynamic FC results, which so far have lacked a neurotypical reference to link results across datasets. We propose that this DMN vs non-DMN axis can serve as a reference point

to establish biomarkers in future dynamic FC studies, where results can be compared to this reference spectrum to identify atypical internetwork dynamics.

#### **4.1.3 QPP Methods comparison and musical training as a proxy for the effects of prolonged behavioral training on QPPs**

To explore the hypothesis that prolonged behavioral training, especially that which may heavily engage attentional networks over time, might change internetwork QPP dynamics, we applied QPP analysis to a dataset of musicians.

Comparing internetwork dynamics in classical, improv, and non-musicians, we initially hypothesized that classical musicians, given years of disciplined practice and focus on musical training, might exhibit greater anticorrelation between the DMN and DAN, a characteristic of improved performance (31, 63). Instead, in the group level QPP results, we observed greater DMN-DAN anticorrelation in improv musicians compared to both classical and non-musician groups. We also explored the feasibility of breaking down networks into sub-ROIs to make comparisons between ROIs that seem to most explain observed network level effects. Specifically, we compared amygdala to DAN connectivity, as we found this to be significantly greater in improv musicians than the other groups.

As we applied two methods of QPP detection to the musician data, sliding window and cPCA, comparison of the results between these two approaches was one of the most valuable findings. Specifically, sliding window and cPCA methods showed convergent results at the group level, indicating the same group level changes to networks. The use of cPCA is validating as it is not constrained by a user defined window length and is thus less influenced by user-controlled parameters.

The musician study also generated cautionary information regarding sample size and the comparison of group level to individual QPP results. When repeating our inter-network analysis on

correlational values from individual QPPs, all the group level findings from this study washed out, and no significant differences were observed between the groups. These results indicate that caution should be taken when drawing conclusions from group level QPP analysis alone.

At the group level, the findings from this study suggest that behavioral training may alter infraslow network dynamics, but the effects could be very subtle. To make strong interpretations of such subtle effects, we expect a much greater sample size would be necessary. This would likely require documentation of musical training on subjects from a much larger database, with sample sizes more than 100 (180, 185).

#### **4.2 Discussion and Future Directions**

The results reported here reflect a considerable advance in understanding how inter-network dynamics in QPPs change in response to a spectrum of external vs internal attention, exogenous neuromodulators, and prolonged behavioral training. As alluded to in previous sections, we propose that this initial survey of QPP results across datasets leads logically to the comparison of these results with datasets representing neural disorders and pathologies for biomarker discovery.

Specifically, as the results from the present study provide more evidence that strong anticorrelation between the DMN and DAN is a feature of healthy cognition and attentional performance, neurodegenerative diseases marked by a loss of cognitive function should hypothetically exhibit a loss of typical anticorrelation between the DMN and other networks. Consistent with this hypothesis, this is exactly what we found when analyzing inter-network QPP dynamics on subjects from the Alzheimer's Disease Neuroimaging Initiative (ADNI) database (Figures 4.1-5.3).

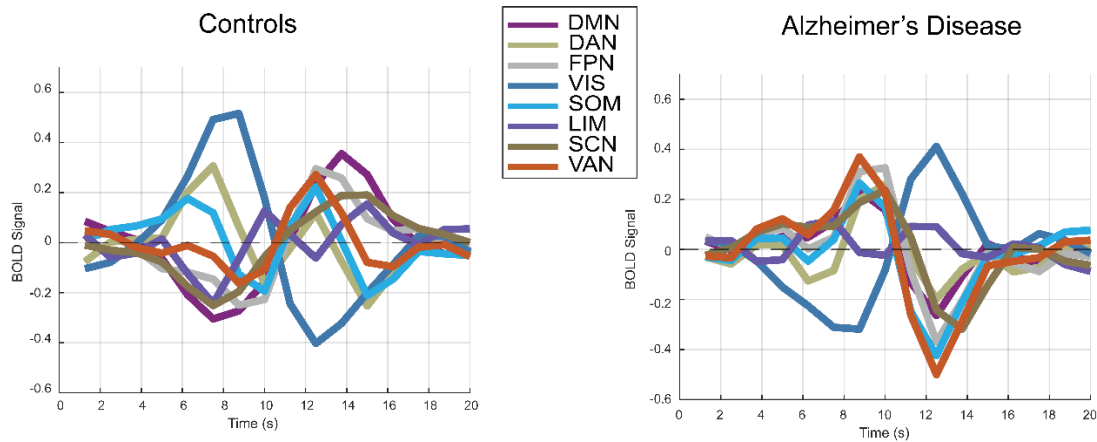


**Figure 4.1.** QPP waveforms showing the normalized BOLD captured by sliding window QPP algorithm in age matched healthy controls (n=20 per group, 10/10 male/female, mean age 72).

Inspecting the QPP waveform of 7 Yeo's networks through one cycle of the QPP (Figure 4.1), it becomes apparent that all networks except the visual and subcortical networks show a loss of anticorrelation with the DMN. This difference becomes especially clear when focusing on the attention networks specifically (Figure 4.2), those that are sometimes grouped as the TPN. This includes DAN, FPN, and VAN.

While the data shown in Figure 4.2 are merely qualitative and represent preliminary results, they show more of an obvious change in anticorrelation than any other dataset or condition we have observed so far. Importantly, the loss of anticorrelation seen in the ADNI group is consistent with a large body of evidence from existing fMRI literature based on traditional seed-based and time-averaged methods pointing to a loss of DMN-DAN anticorrelation in aging and AD (28, 68, 74-77).

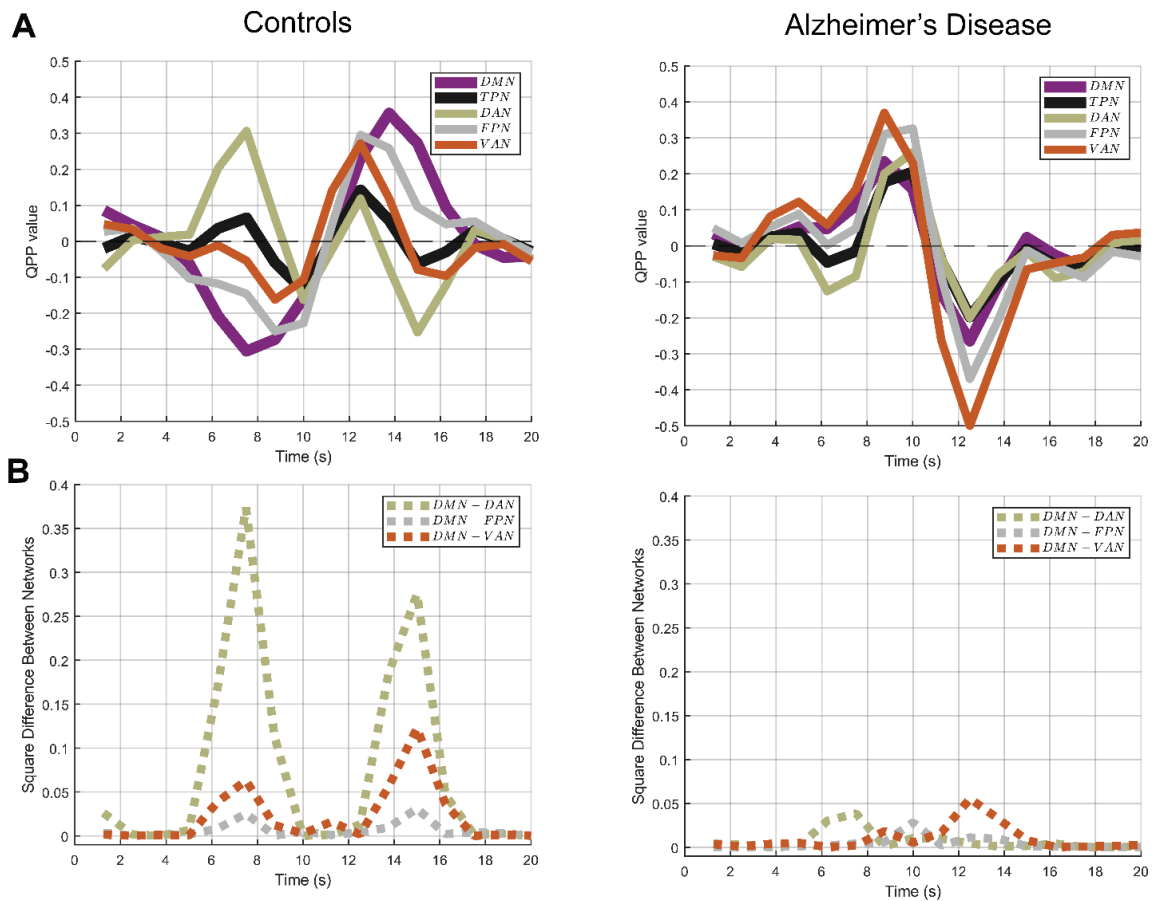


**Figure 4.2.** A) Waveforms of sliding-window QPP focused on attentional networks and DMN only, note the near complete loss of anticorrelation that normally occurs between the DMN and DAN in the AD group. B) Plot of the squared difference between networks over the same QPP cycles shown in A. Completely anticorrelated networks would show a squared difference of 1, while completely correlated networks would show a squared difference of 0. In the bottom right, the squared difference in AD subjects is near zero and quite clear (n = 20 controls, 20 AD, 50/50 male/female, mean age ~ 72 years).

Further analysis of the ADNI dataset is an active area of exploration, including validation of the ADNI results with an AD dataset obtained from collaborating professors at imaging centers from Emory University and the Georgia Institute of Technology.

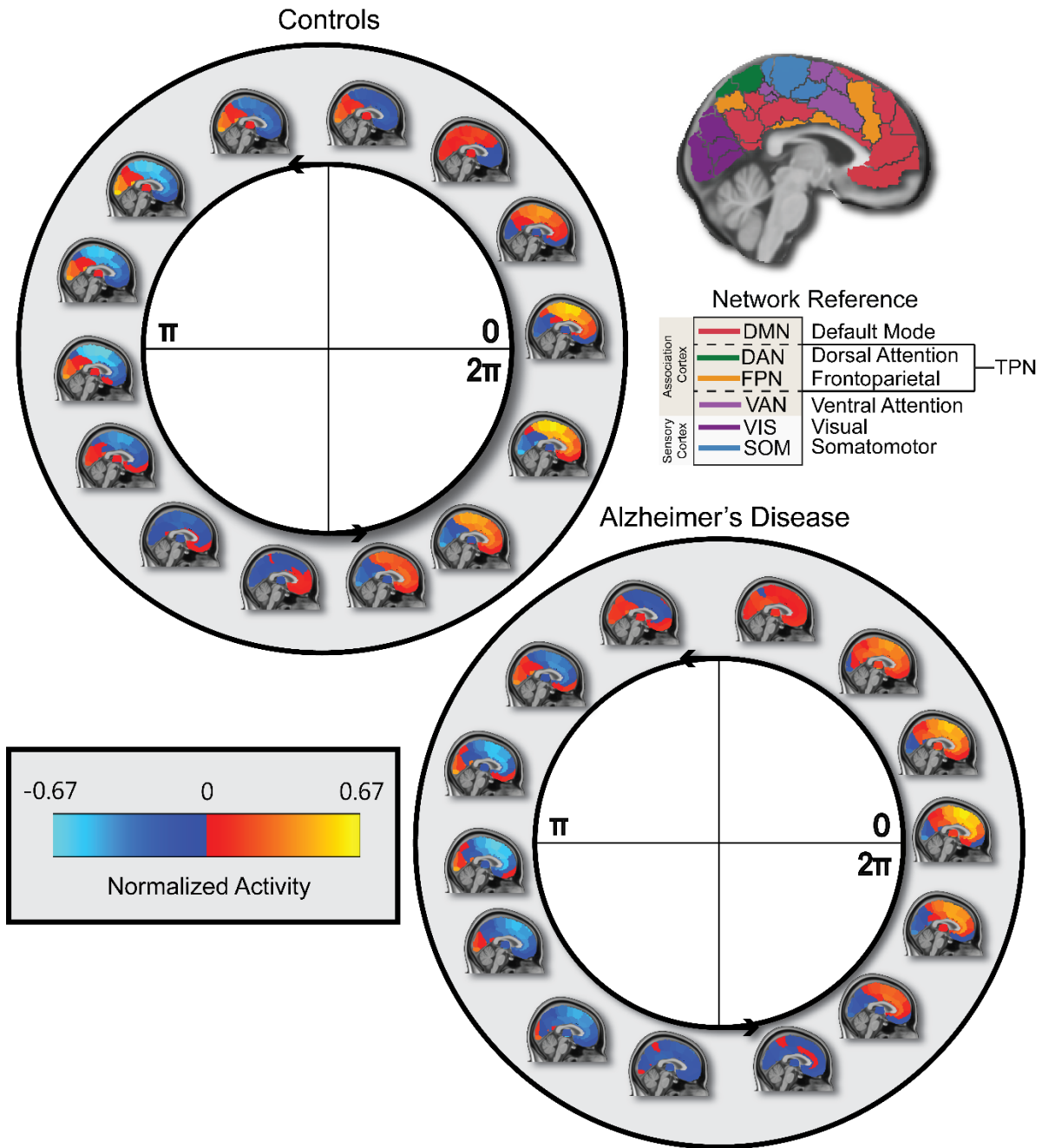


**Figure 4.3.** Spatial-temporal visualization of QPPs detected with cPCA on AD vs control subjects from the ADNI database. Shown are 15 time points (half of total timepoints generated) at close approximations of their phase around 1 full QPP cycle (from zero to  $2\pi$ ). Note (qualitatively) the substantially longer dwell times with loss of anticorrelation in the AD group.

In addition to validating our results in AD subjects from another dataset, active studies related to this project seek to apply additional methods of dynamic analysis that provide complimentary results including cPCA (Figure 4.3) (49) and Hopfield network analysis. Recent work by Englert and colleagues (186) has demonstrated that macro-scale brain dynamics, such as cortical network dynamics, can be faithfully modeled as Hopfield Neural Networks (HNN). In this model, cortical dynamics can be explained as part of an energetic landscape, where networks represent attractor states of low energy configuration (186). For example, the “internal” attractor state observed in their study shows considerable spatial overlap with the canonical default mode network described in the present study, while the “external” attractor state is analogous to task positive regions discussed here.

In the introductory chapter of this dissertation, a hypothesis was presented to explain DMN-TPN anticorrelation based on cortical resource allocation, as several studies suggest that anticorrelated networks governing internal vs external models were forced to evolve due to limited cortical resources (10, 15, 35). The conception of cortical network dynamics as attractor states offers a complimentary explanation for the phenomenon of anticorrelated networks as well as providing insight into the loss of QPP anticorrelation seen in AD patients. If default mode and task related regions act as basins of attraction, then it makes good sense why they exhibit anticorrelated dynamics in cognitively neurotypical subjects. The internal and external attractor states serve mutually exclusive functions, and if their basins of attraction were to begin overlapping, it stands to reason the computational resolution between the respective networks would be lost.

Explaining anticorrelated networks as attractor states is consistent with changes seen in brain states where anticorrelation as well as normal cognitive capacity is eroded, such as sleep deprivation (33). Consumption of strong psychedelics like LSD and psilocybin has also been shown

to decrease anticorrelation between DMN and task networks as well as flatten the energetic landscape of the brain, increasing spontaneous state transitions (38, 41, 187-191).

Based on the results of lost DMN-DAN anticorrelation in AD patients from the present study and the established literature, it is likely that modeling dynamic cortical networks as Hopfield attractor networks will show a decrease in the energetic barrier between typically separate basins of attraction. If this hypothesis should bear out, it offers significant mechanistic insight into the ultimate adaptive function of anticorrelated networks. Additionally, it offers a unifying hypothesis that helps to link activity across scales, providing a consistent model of dynamics from single neurons to whole-brain activity.

---

## **Appendix A: CPAC processing pipeline**

All functional and anatomical MRI scans were formatted according to BIDS standards and processed using the configurable pipeline for the analysis of connectomes (CPAC) (192-194). The use of a high efficiency processing pipeline helps to minimize noise introduced from processing variation between toolsets and groups. CPAC is run via Docker container and contains many formerly separate fMRI tools and processing packages housed within a single software, allowing for streamlined processing. These include but are not limited to steps for skull stripping, functional to anatomical registration, and motion correction. As the name implies, the pipeline has a default version, but has a wide range of parameters which are configurable to meet the needs and experimental interests of the researcher. For this study, an identical version of the configurable pipeline was used for all datasets, which included motion correction, slice-timing correction, global signal regression, and registration to an anatomical template. The complete version of the pipeline used can be made available upon request.

## Appendix B: Supplementary Tables

Supplementary Table 1. Scan sources and parameters.

Dataset	Source:	T1 Anatomical	Functional Scan
<b>Video Gamer Task (VG)</b> N=47, 4 task scans per subject	Dr. Mukeshwar Dhamala (Georgia State University) and Timothy Jordan (UCLA). Georgia State/Georgia Tech Center for Advanced Brain Imaging (CABI).	3T S Magnetom Prisma MRI scanner; TR=2530ms; TE1-4: 1.69–7.27ms; flip angle:7°;Voxel Size:1mm <sup>3</sup>	3T S Magnetom Prisma MRI scanner; TR=535ms; TE=30ms; flip angle:46°; FOV:240mm; Voxel Size: 3.8x3.8x4mm; slices:32
<b>Visual Working (VWM)</b> Memory Task N=19 (13M 6F) Mean Age: 22.4, 3 task scans per subject	OpenNeuro (Hampshire, Adam and Soreq, Eyal (2019)	Siemens 3T MRI TrioTim scanner; TR=2500ms; TE=2.9ms; flip angle: 9°; Voxel Size:1mm <sup>3</sup>	Siemens 3T MRI TrioTim scanner; TR=2000ms; TE=30ms; flip angle:45°; FOV:240mm; Voxel Size: 3mm <sup>3</sup> ; slices:36
<b>Simon Task</b> N=21, 2 task scans per subject	OpenNeuro (Kelly AMC and Milham MP (2018). Simon task. OpenNeuro).	Siemens Allegra 3T scanner; TR=2500ms; TE=3.93ms; flip angle:8°; FOV:256mm; Voxel Size:1mm <sup>3</sup>	Siemens Allegra 3T scanner; TR=2000ms; TE=30ms; flip angle:80°; FOV:192mm; Voxel Size: 3x3x4mm; slices:40
<b>Stroop Task</b> N=28 (20M 10F) Mean Age: 31yr, 1 task	OpenNeuro (Timothy D. Verstynen (2018). Stroop Task. OpenNeuro).	Siemens Verio 3T scanner	Siemens Verio 3T scanner; TR=1500ms; TE=20ms; flip angle:90°; FOV:240mm; Voxel Size: 3.5mm isotropic; slices:30

scan per subject			
<b>Flanker Task</b> N=26, 2 task scans per subject	OpenNeuro (Kelly AMC and Uddin LQ and Biswal BB and Castellanos FX and Milham MP (2018). Flanker task (event-related). OpenNeuro.	Siemens Allegra 3T scanner; TR=2500ms; TE=3.93ms; flip angle:8°; FOV:256mm; Voxel Size:1mm <sup>3</sup>	Siemens Allegra 3T scanner; TR=2000ms; TE=30ms; flip angle:80°; FOV:192mm; Voxel Size: 3x3x4mm; slices:40
<b>CABI Rest</b> N=99 Mean Age: 26yr, 1 rest scan per subject, 2 rest scans for most subjects	Dr. Eric Schumacher, Georgia Institute of Technology. Georgia State/Georgia Tech Center for Advanced Brain Imaging (CABI).	Siemens 3T Trio MRI scanner; TR=2250ms; TE=3.98ms; flip angle:9°; FOV:256mm; Voxel Size:1mm <sup>3</sup>	Siemens 3T Trio MRI scanner; TR=2000ms; TE=30ms; flip angle:90°; FOV:240mm; Voxel Size: 3x3x3mm; slices:37
<b>HCP Rest/Task</b> N = 50 Ages 26-36, 2 rest and 2 task scans per subject	Human Connectome Project. Washington University. (Van Essen et al., 2012).	Siemens Skyra 3T; 3D MPRAGE sequence; TR = 2400 ms, TE = 2.14 ms, TI = 1000 ms, FA = 8°, FOV = 224 mm × 224 mm, voxel size 0.7 mm <sup>3</sup>	Siemens Skyra 3T; Gradient-echo Echo Planar Imaging; TR = 720 ms, TE = 33.1 ms, FA = 52°, FOV = 208 mm × 180 mm (RO x PE), matrix = 104 × 90 (RO x PE), slice thickness = 2.0 mm; 72 slices; 2.0 mm isotropic voxels, multi-band factor = 8, echo spacing 0.58 ms
<b>Meditations</b> N=14 (3M 11F)	Dr. Wendy Hasenkamp and Dr. Larry Barsalou, Dr. Christine Wilson-Mendenhall, Emory University. (Hasenkamp et al., 2012).	Siemens 3T Trio MRI scanner; TR=2600ms; TE=3.9ms; FOV:240mm	Siemens 3T Trio MRI scanner; TR=1500ms; TE=30ms; flip angle:90°; FOV:192mm; Voxel

Ages 28-66, 1 rest and 1 meditation task scan per subject			Size: 4x3x3mm; slices:18
<b>Twilight Zone</b> N=24, 1 task (watching Twilight Zone) per subject	OpenNeuro. (J. Chen and C. J. Honey and E. Simony and M. J. Arcaro and K. A. Norman and Hasson, U. (2019). Twilight Zone Movie Watching Dataset. OpenNeuro. doi: 10.18112/openneuro.ds001145.v1.0.0).	Siemens 3T Skyra scanner; Voxel Size:0.89mm <sup>3</sup>	Siemens 3T Skyra scanner; TR=1500ms; TE=28ms; flip angle:64°; FOV:192mm; Voxel Size: 4x3x3mm; slices:27
<b>THC data,</b> N=12	Dr. Linda Klumpers, University of Vermont. Data Originally obtained in the Netherlands at the Center for Human Drug Research.	3 T Achieva scanner (Philips Medical System, Best, The Netherlands)	3 T Achieva scanner. T2*-weighted, 220 gradient echo 'echo planar imaging' (EPI) volumes (repetition time interval = 2180 ms; echo time interval = 30 ms; flip angle = 80°; 38 axial slices; 64 × 64 × 38 isotropic resolution 3.44 mm; scan time = 8.1 min)
<b>LSD Data</b>	Robin Carhart-Harris et al. (2020). Neural correlates of the LSD experience revealed by multimodal neuroimaging. OpenNeuro. [Dataset] doi: 10.18112/openneuro.ds003059.v1.0.0	3T GE HDx system. 3D fast spoiled gradient echo scans in an axial orientation, with field of view = 256 × 256 × 192 and matrix = 256 × 256 × 20 192 to yield 1mm isotropic voxel resolution. TR/TE = 7.9/3.0ms; inversion time = 450ms; flip angle = 20°.	3T GE HDx system. TR/TE = 2000/35ms, field-of-view = 220mm, 64 × 64 acquisition matrix, 90° flip angle. 35 oblique axial slices, 3.4mm thick (3.4mm isotropic voxels). BOLD scan duration 7:20 minutes.

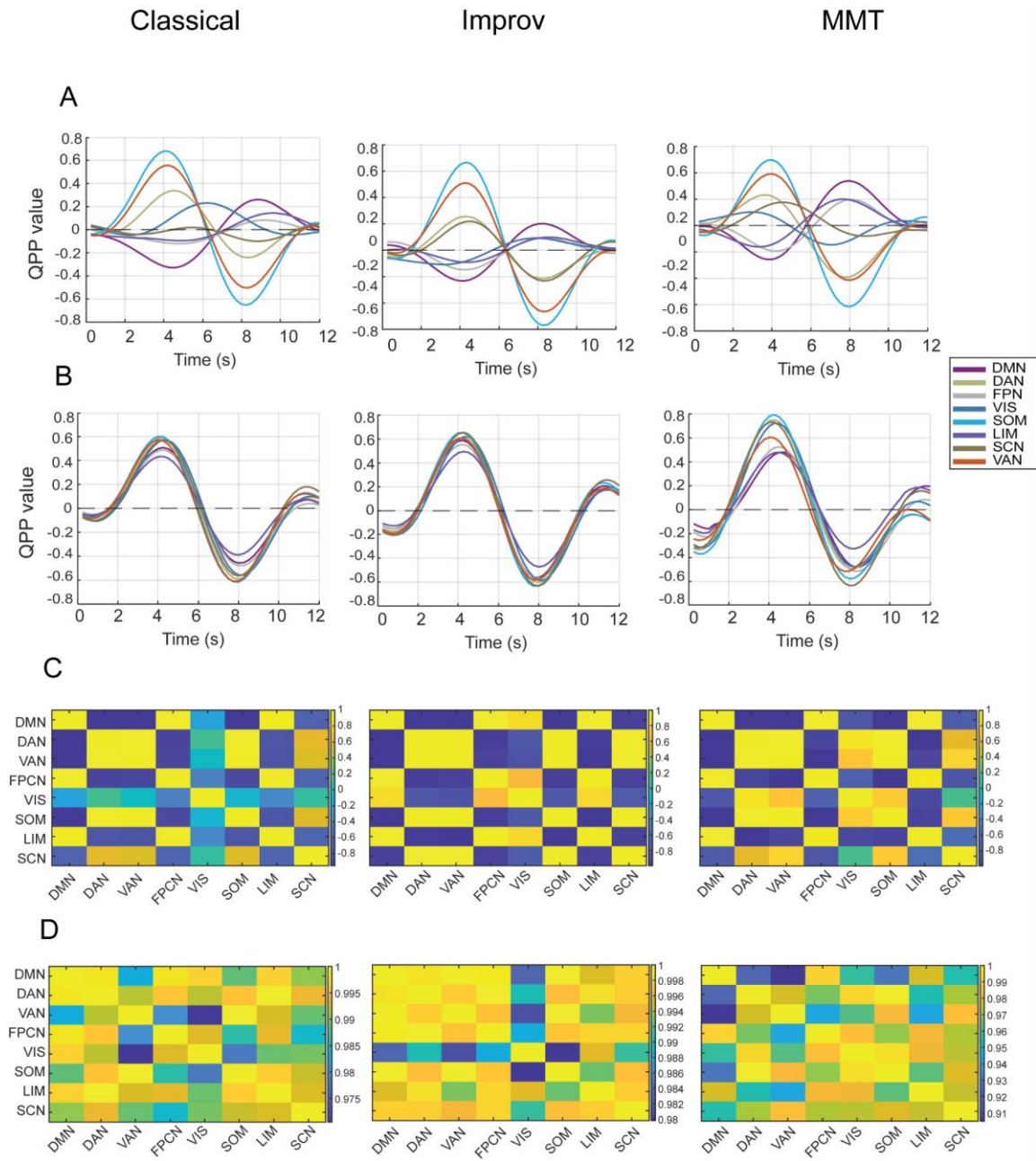
<b>Musician Data</b>	Alex Belden and Pysche Loui from Northeastern University. 1. A. Belden <i>et al.</i> , Improvising at rest: Differentiating jazz and classical music training with resting state functional connectivity. <i>Neuroimage</i> <b>207</b> , 116384 (2020).	T1-weighted sequences: 3D magnetization prepared rapid-acquisition gradient-echo (MPRAGE) with a voxel size of 0.8 x 0.8 x 0.8 mm <sup>3</sup> (TR = 2.4 s, TE = 2.09 ms, flip angle = 8°, FOV = 256 mm).	Duration of 7.5 minutes. Echo-planar imaging (EPI) sequence. 947 volumes (TR = 475 ms; TE = 30 ms; flip angle = 90, 48 slices; FOV = 240 mm; acquisition voxel size = 3 × 3 × 3 mm <sup>3</sup> ).

Supplementary Table 2. Brainnetome coordinates of ROIs assigned to each network.

	<b>DMN</b>	<b>DAN</b>	<b>FPN</b>	<b>VAN</b>	<b>VIS</b>	<b>SOM</b>
3	7	1	2	105	9	
5	8	4	15	106	10	
6	25	12	37	108	53	
11	26	16	38	112	54	
13	30	17	39	113	57	
14	55	18	40	114	58	
23	56	19	61	119	59	
33	63	20	62	120	60	
34	64	21	65	135	66	
35	85	22	123	136	67	
41	86	24	124	151	68	
42	91	28	167	152	71	
43	92	29	168	182	72	
44	97	31	169	189	73	
51	98	32	170	190	74	
52	107	36	173	191	75	
79	125	46	174	192	76	
80	126	82	180	193	131	
81	127	99	183	194	132	

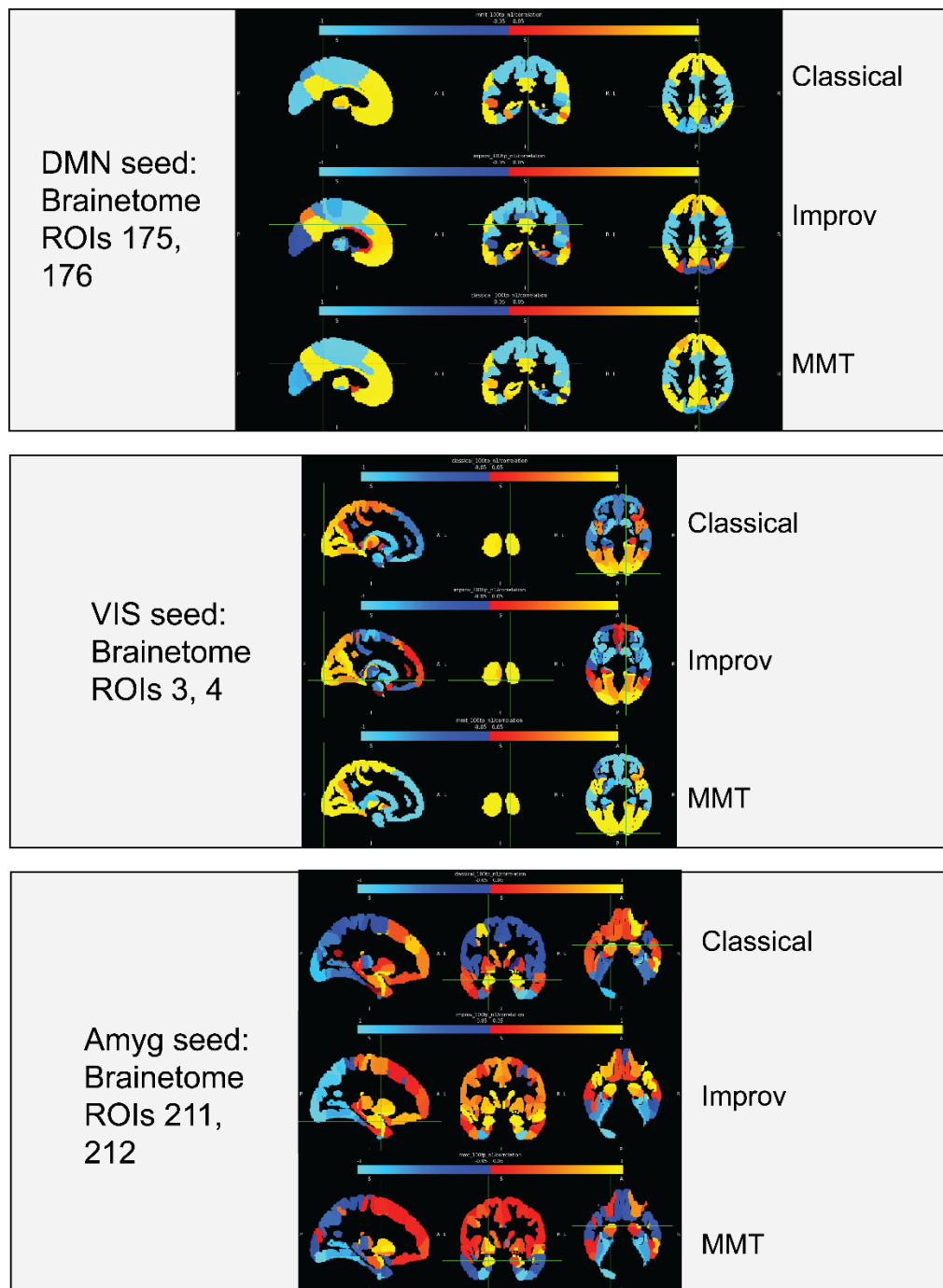
83	128	100	184	195	145
84	129	137	185	196	146
87	130	138	186	197	149
88	133	142		198	155
95	134	147		199	156
121	139	148		200	157
122	140	166		202	158
141	143			203	160
144	150			204	161
<b>153</b>	159			205	162
154	201			206	163
<b>175</b>				207	164
176				208	171
179				209	172
181				210	
187					
188					

## Appendix C: Supplemental Figures



**Supplemental figure 1.** Global signal regressed (GSR) vs non-GSR data for Music data. QPP waveforms with GSR (A) and without GSR (B) for the 3 musical training groups. FC matrices showing correlations between 8x8 Yeo's networks during the QPP for GSR (C), and non-GSR (D) scans. Note

the near complete loss of anticorrelation in non-GSR data. These results are typical for non-GSR data.



**Supplemental figure 2.** Seed voxel locations within major ROIs analyzed with cPCA for Musician Data. A) DMN, B), VIS, and C) Amygdala. Color bar indicates correlation to seed region of normalized

BOLD signal during 1 cycle of cPCA based QPP between -1 and +1. Note the very high correlation (bright yellow) of all voxels within each ROI to the seed voxels.

### **Funding Acknowledgements**

This research was funded by grants from the National Institutes of Health: 1R01Ns078095, 1R01AG062581, 1R01EB029857. Additional financial support was received from the Laney Graduate School at Emory University and the NRSA T32 training grant program.

## References

1. M. E. Raichle, Two views of brain function. *Trends Cogn Sci* **14**, 180-190 (2010).
2. M. E. Raichle, The restless brain. *Brain Connect* **1**, 3-12 (2011).
3. B. Biswal, F. Z. Yetkin, V. M. Haughton, J. S. Hyde, Functional connectivity in the motor cortex of resting human brain using echo-planar MRI. *Magn Reson Med* **34**, 537-541 (1995).
4. B. B. Biswal, J. Van Kylen, J. S. Hyde, Simultaneous assessment of flow and BOLD signals in resting-state functional connectivity maps. *NMR Biomed* **10**, 165-170 (1997).
5. L. Q. Uddin, B. T. T. Yeo, R. N. Spreng, Towards a Universal Taxonomy of Macro-scale Functional Human Brain Networks. *Brain Topogr* **32**, 926-942 (2019).
6. M. E. Raichle, A. Z. Snyder, A default mode of brain function: a brief history of an evolving idea. *Neuroimage* **37**, 1083-1090; discussion 1097-1089 (2007).
7. M. D. Fox *et al.*, The human brain is intrinsically organized into dynamic, anticorrelated functional networks. *Proc Natl Acad Sci U S A* **102**, 9673-9678 (2005).
8. M. E. Raichle, The restless brain: how intrinsic activity organizes brain function. *Philos Trans R Soc Lond B Biol Sci* **370** (2015).
9. B. T. Yeo *et al.*, Functional Specialization and Flexibility in Human Association Cortex. *Cereb Cortex* **25**, 3654-3672 (2015).
10. B. T. Yeo *et al.*, The organization of the human cerebral cortex estimated by intrinsic functional connectivity. *J Neurophysiol* **106**, 1125-1165 (2011).
11. R. L. Buckner, F. M. Krienen, The evolution of distributed association networks in the human brain. *Trends Cogn Sci* **17**, 648-665 (2013).
12. P. A. Bandettini, Sewer pipe, wire, epoxy, and finger tapping: the start of fMRI at the Medical College of Wisconsin. *Neuroimage* **62**, 620-631 (2012).
13. P. A. Bandettini, E. C. Wong, R. S. Hinks, R. S. Tikofsky, J. S. Hyde, Time course EPI of human brain function during task activation. *Magn Reson Med* **25**, 390-397 (1992).
14. L. Q. Uddin, A. M. Kelly, B. B. Biswal, F. X. Castellanos, M. P. Milham, Functional connectivity of default mode network components: correlation, anticorrelation, and causality. *Hum Brain Mapp* **30**, 625-637 (2009).
15. R. L. Buckner, L. M. DiNicola, The brain's default network: updated anatomy, physiology and evolving insights. *Nat Rev Neurosci* **20**, 593-608 (2019).
16. R. L. Buckner, The serendipitous discovery of the brain's default network. *Neuroimage* **62**, 1137-1145 (2012).
17. K. Murphy, M. D. Fox, Towards a consensus regarding global signal regression for resting state functional connectivity MRI. *Neuroimage* **154**, 169-173 (2017).
18. M. E. Raichle *et al.*, A default mode of brain function. *Proc Natl Acad Sci U S A* **98**, 676-682 (2001).
19. M. E. Raichle, The brain's default mode network. *Annu Rev Neurosci* **38**, 433-447 (2015).
20. M. D. Greicius, B. Krasnow, A. L. Reiss, V. Menon, Functional connectivity in the resting brain: a network analysis of the default mode hypothesis. *Proc Natl Acad Sci U S A* **100**, 253-258 (2003).
21. J. Smallwood *et al.*, The default mode network in cognition: a topographical perspective. *Nat Rev Neurosci* **22**, 503-513 (2021).
22. J. Smallwood, K. Brown, B. Baird, J. W. Schooler, Cooperation between the default mode network and the frontal-parietal network in the production of an internal train of thought. *Brain Res* **1428**, 60-70 (2012).

23. S. Tommasin *et al.*, Task-Related Modulations of BOLD Low-Frequency Fluctuations within the Default Mode Network. *Front Phys* **5** (2017).
24. D. Vatansever, D. K. Menon, A. E. Manktelow, B. J. Sahakian, E. A. Stamatakis, Default mode network connectivity during task execution. *Neuroimage* **122**, 96-104 (2015).
25. C. Fassbender *et al.*, A lack of default network suppression is linked to increased distractibility in ADHD. *Brain Res* **1273**, 114-128 (2009).
26. M. M. Owens *et al.*, Investigation of Psychiatric and Neuropsychological Correlates of Default Mode Network and Dorsal Attention Network Anticorrelation in Children. *Cereb Cortex* **30**, 6083-6096 (2020).
27. M. Corbetta, G. L. Shulman, Control of goal-directed and stimulus-driven attention in the brain. *Nat Rev Neurosci* **3**, 201-215 (2002).
28. R. Esposito *et al.*, Modifications in resting state functional anticorrelation between default mode network and dorsal attention network: comparison among young adults, healthy elders and mild cognitive impairment patients. *Brain Imaging Behav* **12**, 127-141 (2018).
29. K. N. Meyer, F. Du, E. Parks, J. B. Hopfinger, Exogenous vs. endogenous attention: Shifting the balance of fronto-parietal activity. *Neuropsychologia* **111**, 307-316 (2018).
30. S. Qian *et al.*, Disrupted Anti-correlation Between the Default and Dorsal Attention Networks During Hyperthermia Exposure: An fMRI Study. *Front Hum Neurosci* **14**, 564272 (2020).
31. T. Eichele *et al.*, Prediction of human errors by maladaptive changes in event-related brain networks. *Proc Natl Acad Sci U S A* **105**, 6173-6178 (2008).
32. J. T. Wu *et al.*, Aging-related changes in the default mode network and its anti-correlated networks: a resting-state fMRI study. *Neurosci Lett* **504**, 62-67 (2011).
33. J. A. De Havas, S. Parimal, C. S. Soon, M. W. Chee, Sleep deprivation reduces default mode network connectivity and anti-correlation during rest and task performance. *Neuroimage* **59**, 1745-1751 (2012).
34. C. Dai *et al.*, Effects of Sleep Deprivation on Working Memory: Change in Functional Connectivity Between the Dorsal Attention, Default Mode, and Fronto-Parietal Networks. *Front Hum Neurosci* **14**, 360 (2020).
35. S. Weber, A. Aleman, K. Hugdahl, Involvement of the default mode network under varying levels of cognitive effort. *Sci Rep* **12**, 6303 (2022).
36. R. B. Mars *et al.*, On the relationship between the "default mode network" and the "social brain". *Front Hum Neurosci* **6**, 189 (2012).
37. V. Menon, 20 years of the default mode network: A review and synthesis. *Neuron* **111**, 2469-2487 (2023).
38. C. Letheby, P. Gerrans, Self unbound: ego dissolution in psychedelic experience. *Neurosci Conscious* **2017**, nix016 (2017).
39. M. M. Owens *et al.*, Urinary tetrahydrocannabinol is associated with poorer working memory performance and alterations in associated brain activity. *Neuropsychopharmacology* **44**, 613-619 (2019).
40. J. S. Siegel *et al.*, Psilocybin desynchronizes brain networks. *medRxiv* 10.1101/2023.08.22.23294131 (2023).
41. D. Stoliker *et al.*, Effective Connectivity of Functionally Anticorrelated Networks Under Lysergic Acid Diethylamide. *Biol Psychiatry* **93**, 224-232 (2023).
42. C. M. Garin *et al.*, An evolutionary gap in primate default mode network organization. *Cell Rep* **39**, 110669 (2022).
43. Y. Yeshurun, M. Nguyen, U. Hasson, The default mode network: where the idiosyncratic self meets the shared social world. *Nat Rev Neurosci* **22**, 181-192 (2021).

44. A. Zadbood, J. Chen, Y. C. Leong, K. A. Norman, U. Hasson, How We Transmit Memories to Other Brains: Constructing Shared Neural Representations Via Communication. *Cereb Cortex* **27**, 4988-5000 (2017).
45. G. J. Stephens, L. J. Silbert, U. Hasson, Speaker-listener neural coupling underlies successful communication. *Proc Natl Acad Sci U S A* **107**, 14425-14430 (2010).
46. S. Dikker, L. J. Silbert, U. Hasson, J. D. Zevin, On the same wavelength: predictable language enhances speaker-listener brain-to-brain synchrony in posterior superior temporal gyrus. *J Neurosci* **34**, 6267-6272 (2014).
47. R. Hyon, A. M. Kleinbaum, C. Parkinson, Social network proximity predicts similar trajectories of psychological states: Evidence from multi-voxel spatiotemporal dynamics. *Neuroimage* **216**, 116492 (2020).
48. C. Parkinson, A. M. Kleinbaum, T. Wheatley, Similar neural responses predict friendship. *Nat Commun* **9**, 332 (2018).
49. T. Bolt *et al.*, A parsimonious description of global functional brain organization in three spatiotemporal patterns. *Nat Neurosci* **25**, 1093-1103 (2022).
50. C. Chang, G. H. Glover, Time-frequency dynamics of resting-state brain connectivity measured with fMRI. *Neuroimage* **50**, 81-98 (2010).
51. X. Di, B. B. Biswal, Dynamic brain functional connectivity modulated by resting-state networks. *Brain Struct Funct* **220**, 37-46 (2015).
52. R. M. Hutchison *et al.*, Dynamic functional connectivity: promise, issues, and interpretations. *Neuroimage* **80**, 360-378 (2013).
53. L. Meyer-Baese, H. Watters, S. Keilholz, Spatiotemporal patterns of spontaneous brain activity: a mini-review. *Neurophotonics* **9**, 032209 (2022).
54. M. E. Belloy *et al.*, Dynamic resting state fMRI analysis in mice reveals a set of Quasi-Periodic Patterns and illustrates their relationship with the global signal. *Neuroimage* **180**, 463-484 (2018).
55. W. Majeed *et al.*, Spatiotemporal dynamics of low frequency BOLD fluctuations in rats and humans. *Neuroimage* **54**, 1140-1150 (2011).
56. W. Majeed, M. Magnuson, S. D. Keilholz, Spatiotemporal dynamics of low frequency fluctuations in BOLD fMRI of the rat. *J Magn Reson Imaging* **30**, 384-393 (2009).
57. B. Yousefi, J. Shin, E. H. Schumacher, S. D. Keilholz, Quasi-periodic patterns of intrinsic brain activity in individuals and their relationship to global signal. *Neuroimage* **167**, 297-308 (2018).
58. X. Liu, N. Zhang, C. Chang, J. H. Duyn, Co-activation patterns in resting-state fMRI signals. *Neuroimage* **180**, 485-494 (2018).
59. A. Abbas *et al.*, Quasi-periodic patterns contribute to functional connectivity in the brain. *Neuroimage* **191**, 193-204 (2019).
60. S. Keilholz, C. Caballero-Gaudes, P. Bandettini, G. Deco, V. Calhoun, Time-Resolved Resting-State Functional Magnetic Resonance Imaging Analysis: Current Status, Challenges, and New Directions. *Brain Connect* **7**, 465-481 (2017).
61. B. Yousefi, S. Keilholz, Propagating patterns of intrinsic activity along macroscale gradients coordinate functional connections across the whole brain. *Neuroimage* **231**, 117827 (2021).
62. A. Abbas, Y. Bassil, S. Keilholz, Quasi-periodic patterns of brain activity in individuals with attention-deficit/hyperactivity disorder. *Neuroimage Clin* **21**, 101653 (2019).
63. D. T. Seeburger *et al.*, Time-varying functional connectivity predicts fluctuations in sustained attention in a serial tapping task. *Cogn Affect Behav Neurosci* **24**, 111-125 (2024).

64. Y. Arif *et al.*, Modulation of attention networks serving reorientation in healthy aging. *Aging (Albany NY)* **12**, 12582-12597 (2020).
65. M. L. Dixon *et al.*, Heterogeneity within the frontoparietal control network and its relationship to the default and dorsal attention networks. *Proc Natl Acad Sci U S A* **115**, E1598-E1607 (2018).
66. S. Vossel, J. J. Geng, G. R. Fink, Dorsal and ventral attention systems: distinct neural circuits but collaborative roles. *Neuroscientist* **20**, 150-159 (2014).
67. J. Zhao, J. Wang, C. Huang, P. Liang, Involvement of the dorsal and ventral attention networks in visual attention span. *Hum Brain Mapp* **43**, 1941-1954 (2022).
68. B. Avelar-Pereira, L. Backman, A. Wahlin, L. Nyberg, A. Salami, Age-Related Differences in Dynamic Interactions Among Default Mode, Frontoparietal Control, and Dorsal Attention Networks during Resting-State and Interference Resolution. *Front Aging Neurosci* **9**, 152 (2017).
69. S. A. Cutts, J. Faskowitz, R. F. Betzel, O. Sporns, Uncovering individual differences in fine-scale dynamics of functional connectivity. *Cereb Cortex* **33**, 2375-2394 (2023).
70. S. D. Keilholz, The neural basis of time-varying resting-state functional connectivity. *Brain Connect* **4**, 769-779 (2014).
71. A. Kucyi, K. D. Davis, Dynamic functional connectivity of the default mode network tracks daydreaming. *Neuroimage* **100**, 471-480 (2014).
72. D. J. Lurie *et al.*, Questions and controversies in the study of time-varying functional connectivity in resting fMRI. *Netw Neurosci* **4**, 30-69 (2020).
73. N. Xu *et al.*, The interaction between random and systematic visual stimulation and infraslow quasiperiodic spatiotemporal patterns of whole brain activity. *Imaging Neurosci (Camb)* **1**, 1-19 (2023).
74. N. Franzmeier *et al.*, Resting-State Connectivity of the Left Frontal Cortex to the Default Mode and Dorsal Attention Network Supports Reserve in Mild Cognitive Impairment. *Front Aging Neurosci* **9**, 264 (2017).
75. Y. H. Hsu *et al.*, Prospective Memory and Default Mode Network Functional Connectivity in Normal and Pathological Aging. *J Alzheimers Dis* **86**, 753-762 (2022).
76. Y. I. Sheline, M. E. Raichle, Resting state functional connectivity in preclinical Alzheimer's disease. *Biol Psychiatry* **74**, 340-347 (2013).
77. J. Wang *et al.*, Dysfunctional interactions between the default mode network and the dorsal attention network in subtypes of amnesic mild cognitive impairment. *Aging (Albany NY)* **11**, 9147-9166 (2019).
78. D. H. Geschwind, P. Rakic, Cortical evolution: judge the brain by its cover. *Neuron* **80**, 633-647 (2013).
79. D. Mantini, M. Corbetta, G. L. Romani, G. A. Orban, W. Vanduffel, Evolutionarily novel functional networks in the human brain? *J Neurosci* **33**, 3259-3275 (2013).
80. M. A. Garcia-Cabezas, B. Zikopoulos, Evolution, development, and organization of the cortical connectome. *PLoS Biol* **17**, e3000259 (2019).
81. S. E. Petersen, M. I. Posner, The attention system of the human brain: 20 years after. *Annu Rev Neurosci* **35**, 73-89 (2012).
82. C. M. Adler *et al.*, Changes in neuronal activation with increasing attention demand in healthy volunteers: an fMRI study. *Synapse* **42**, 266-272 (2001).
83. P. Fransson, Spontaneous low-frequency BOLD signal fluctuations: an fMRI investigation of the resting-state default mode of brain function hypothesis. *Hum Brain Mapp* **26**, 15-29 (2005).

84. M. F. Mason *et al.*, Wandering minds: the default network and stimulus-independent thought. *Science* **315**, 393-395 (2007).
85. R. N. Spreng *et al.*, Goal-congruent default network activity facilitates cognitive control. *J Neurosci* **34**, 14108-14114 (2014).
86. S. Spadone *et al.*, Dynamic reorganization of human resting-state networks during visuospatial attention. *Proc Natl Acad Sci U S A* **112**, 8112-8117 (2015).
87. V. Menon, L. Q. Uddin, Saliency, switching, attention and control: a network model of insula function. *Brain Struct Funct* **214**, 655-667 (2010).
88. G. L. Shulman *et al.*, Common Blood Flow Changes across Visual Tasks: II. Decreases in Cerebral Cortex. *J Cogn Neurosci* **9**, 648-663 (1997).
89. R. L. Buckner, J. R. Andrews-Hanna, D. L. Schacter, The brain's default network: anatomy, function, and relevance to disease. *Ann N Y Acad Sci* **1124**, 1-38 (2008).
90. C. Grady, S. Sarraf, C. Saverino, K. Campbell, Age differences in the functional interactions among the default, frontoparietal control, and dorsal attention networks. *Neurobiol Aging* **41**, 159-172 (2016).
91. R. N. Spreng, W. D. Stevens, J. D. Viviano, D. L. Schacter, Attenuated anticorrelation between the default and dorsal attention networks with aging: evidence from task and rest. *Neurobiol Aging* **45**, 149-160 (2016).
92. M. G. Bossong *et al.*, Effects of delta9-tetrahydrocannabinol on human working memory function. *Biol Psychiatry* **71**, 693-699 (2012).
93. K. C. S. Adam, M. K. Doss, E. Pabon, E. K. Vogel, H. de Wit, Delta(9)-Tetrahydrocannabinol (THC) impairs visual working memory performance: a randomized crossover trial. *Neuropsychopharmacology* **45**, 1807-1816 (2020).
94. J. Smallwood *et al.*, Insulation for daydreams: a role for tonic norepinephrine in the facilitation of internally guided thought. *PLoS One* **7**, e33706 (2012).
95. J. Smallwood, J. W. Schooler, The science of mind wandering: empirically navigating the stream of consciousness. *Annu Rev Psychol* **66**, 487-518 (2015).
96. N. Petridou, C. C. Gaudes, I. L. Dryden, S. T. Francis, P. A. Gowland, Periods of rest in fMRI contain individual spontaneous events which are related to slowly fluctuating spontaneous activity. *Hum Brain Mapp* **34**, 1319-1329 (2013).
97. G. J. Thompson *et al.*, Short-time windows of correlation between large-scale functional brain networks predict vigilance intraindividually and interindividually. *Hum Brain Mapp* **34**, 3280-3298 (2013).
98. M. G. Preti, T. A. Bolton, D. Van De Ville, The dynamic functional connectome: State-of-the-art and perspectives. *Neuroimage* **160**, 41-54 (2017).
99. N. Xu *et al.*, QPPLab: A generally applicable software package for detecting, analyzing, and visualizing large-scale quasiperiodic spatiotemporal patterns (QPPs) of brain activity. *bioRxiv* 10.1101/2023.09.25.559086 (2023).
100. E. J. Sonuga-Barke, F. X. Castellanos, Spontaneous attentional fluctuations in impaired states and pathological conditions: a neurobiological hypothesis. *Neurosci Biobehav Rev* **31**, 977-986 (2007).
101. T. Jordan, M. Dhamala, Enhanced Dorsal Attention Network to Salience Network Interaction in Video Gamers During Sensorimotor Decision-Making Tasks. *Brain Connect* **13**, 97-106 (2023).
102. A. Hampshire, E. Soreq, Visual working memory: Study one Task fMRI and Behavioural response.
103. D. C. Van Essen *et al.*, The Human Connectome Project: a data acquisition perspective. *Neuroimage* **62**, 2222-2231 (2012).

104. T. D. Verstynen, Stroop Task. .
105. A. Kelly, L. Q. Uddin, B. B. Biswal, F. X. Castellanos, M. P. Milham, Flanker task (event-related). OpenNeuro.
106. A. Kelly, M. P. Milham, Simon task. .
107. W. Hasenkamp, C. D. Wilson-Mendenhall, E. Duncan, L. W. Barsalou, Mind wandering and attention during focused meditation: a fine-grained temporal analysis of fluctuating cognitive states. *Neuroimage* **59**, 750-760 (2012).
108. J. Chen *et al.*, Twilight Zone Movie Watching Dataset. .
109. X. Zhang, E. A. Maltbie, S. D. Keilholz, Spatiotemporal trajectories in resting-state FMRI revealed by convolutional variational autoencoder. *Neuroimage* **244**, 118588 (2021).
110. S. S. Craddock C, Cheung B, Khanuja R, Ghosh SS, Yan C, Li Q, Lurie D, Vogelstein J, Burns R, Colcombe S, Mennes M, Kelly C, Di Martino A, Castellanos FX, Milham M., Towards automated analysis of connectomes: the configurable pipeline for the analysis of connectomes (C-PAC). *In: Presented at the Front. Neuroinform. Conference Abstract 10.3389/conf.fninf.2013.09.00042. Stockholm, Sweden (2013).*
111. J. Zhang, G. Northoff, Beyond noise to function: reframing the global brain activity and its dynamic topography. *Commun Biol* **5**, 1350 (2022).
112. T. J. VanderWeele, M. B. Mathur, Some Desirable Properties of the Bonferroni Correction: Is the Bonferroni Correction Really So Bad? *Am J Epidemiol* **188**, 617-618 (2019).
113. W. Gao, W. Lin, Frontal parietal control network regulates the anti-correlated default and dorsal attention networks. *Hum Brain Mapp* **33**, 192-202 (2012).
114. D. M. Barch *et al.*, Function in the human connectome: task-fMRI and individual differences in behavior. *Neuroimage* **80**, 169-189 (2013).
115. D. S. Margulies *et al.*, Situating the default-mode network along a principal gradient of macroscale cortical organization. *Proc Natl Acad Sci U S A* **113**, 12574-12579 (2016).
116. M. Golesorkhi, J. Gomez-Pilar, S. Tumati, M. Fraser, G. Northoff, Temporal hierarchy of intrinsic neural timescales converges with spatial core-periphery organization. *Commun Biol* **4**, 277 (2021).
117. A. Wolff *et al.*, Intrinsic neural timescales: temporal integration and segregation. *Trends Cogn Sci* **26**, 159-173 (2022).
118. G. Northoff, D. Vatansever, A. Scalabrini, E. A. Stamatakis, Ongoing Brain Activity and Its Role in Cognition: Dual versus Baseline Models. *Neuroscientist* **29**, 393-420 (2023).
119. J. L. Vincent, I. Kahn, A. Z. Snyder, M. E. Raichle, R. L. Buckner, Evidence for a frontoparietal control system revealed by intrinsic functional connectivity. *J Neurophysiol* **100**, 3328-3342 (2008).
120. R. N. Spreng, J. Sepulcre, G. R. Turner, W. D. Stevens, D. L. Schacter, Intrinsic architecture underlying the relations among the default, dorsal attention, and frontoparietal control networks of the human brain. *J Cogn Neurosci* **25**, 74-86 (2013).
121. S. M. Szczepanski, M. A. Pinsk, M. M. Douglas, S. Kastner, Y. B. Saalman, Functional and structural architecture of the human dorsal frontoparietal attention network. *Proc Natl Acad Sci U S A* **110**, 15806-15811 (2013).
122. W. Yang *et al.*, Memory Suppression Ability can be Robustly Predicted by the Internetwork Communication of Frontoparietal Control Network. *Cereb Cortex* **31**, 3451-3461 (2021).
123. T. M. Morin, K. N. Moore, K. Isenburg, W. Ma, C. E. Stern, Functional reconfiguration of task-active frontoparietal control network facilitates abstract reasoning. *Cereb Cortex* **33**, 5761-5773 (2023).
124. J. Smallwood, J. W. Schooler, The restless mind. *Psychol Bull* **132**, 946-958 (2006).

125. K. Christoff, Z. C. Irving, K. C. Fox, R. N. Spreng, J. R. Andrews-Hanna, Mind-wandering as spontaneous thought: a dynamic framework. *Nat Rev Neurosci* **17**, 718-731 (2016).
126. M. Corbetta, G. Patel, G. L. Shulman, The reorienting system of the human brain: from environment to theory of mind. *Neuron* **58**, 306-324 (2008).
127. L. Q. Uddin, Salience processing and insular cortical function and dysfunction. *Nat Rev Neurosci* **16**, 55-61 (2015).
128. D. Sridharan, D. J. Levitin, V. Menon, A critical role for the right fronto-insular cortex in switching between central-executive and default-mode networks. *Proc Natl Acad Sci U S A* **105**, 12569-12574 (2008).
129. R. Solis-Vivanco, O. Jensen, M. Bonnefond, New insights on the ventral attention network: Active suppression and involuntary recruitment during a bimodal task. *Hum Brain Mapp* **42**, 1699-1713 (2021).
130. C. Sripada *et al.*, Disrupted network architecture of the resting brain in attention-deficit/hyperactivity disorder. *Hum Brain Mapp* **35**, 4693-4705 (2014).
131. J. Smallwood, Distinguishing how from why the mind wanders: a process-occurrence framework for self-generated mental activity. *Psychol Bull* **139**, 519-535 (2013).
132. R. V. Bretas, M. Taoka, H. Suzuki, A. Iriki, Secondary somatosensory cortex of primates: beyond body maps, toward conscious self-in-the-world maps. *Exp Brain Res* **238**, 259-272 (2020).
133. P. Qin *et al.*, Higher-order sensorimotor circuit of the brain's global network supports human consciousness. *Neuroimage* **231**, 117850 (2021).
134. R. Chin, S. W. C. Chang, A. J. Holmes, Beyond cortex: The evolution of the human brain. *Psychol Rev* **130**, 285-307 (2023).
135. P. R. Steffen, D. Hedges, R. Matheson, The Brain Is Adaptive Not Triune: How the Brain Responds to Threat, Challenge, and Change. *Front Psychiatry* **13**, 802606 (2022).
136. J. Cesario, D. J. Johnson, H. L. Eisthen, Your Brain Is Not an Onion With a Tiny Reptile Inside. *Current Directions in Psychological Science* **29**, 255-260 (2020).
137. M. Oldehinkel *et al.*, Altered Connectivity Between Cerebellum, Visual, and Sensory-Motor Networks in Autism Spectrum Disorder: Results from the EU-AIMS Longitudinal European Autism Project. *Biol Psychiatry Cogn Neurosci Neuroimaging* **4**, 260-270 (2019).
138. B. Chen *et al.*, Greater functional connectivity between sensory networks is related to symptom severity in toddlers with autism spectrum disorder. *J Child Psychol Psychiatry* **62**, 160-170 (2021).
139. J. Wang *et al.*, Atypical Resting-State Functional Connectivity of Intra/Inter-Sensory Networks Is Related to Symptom Severity in Young Boys With Autism Spectrum Disorder. *Front Physiol* **12**, 626338 (2021).
140. H. Hjelmervik, M. Hausmann, B. Osnes, R. Westerhausen, K. Specht, Resting states are resting traits--an fMRI study of sex differences and menstrual cycle effects in resting state cognitive control networks. *PLoS One* **9**, e103492 (2014).
141. C. A. Godwin *et al.*, Functional connectivity within and between intrinsic brain networks correlates with trait mind wandering. *Neuropsychologia* **103**, 140-153 (2017).
142. R. N. Spreng, The fallacy of a "task-negative" network. *Front Psychol* **3**, 145 (2012).
143. L. Q. Uddin *et al.*, Network homogeneity reveals decreased integrity of default-mode network in ADHD. *J Neurosci Methods* **169**, 249-254 (2008).
144. K. Konrad, S. B. Eickhoff, Is the ADHD brain wired differently? A review on structural and functional connectivity in attention deficit hyperactivity disorder. *Hum Brain Mapp* **31**, 904-916 (2010).

145. E. B. Liddle *et al.*, Task-related default mode network modulation and inhibitory control in ADHD: effects of motivation and methylphenidate. *J Child Psychol Psychiatry* **52**, 761-771 (2011).
146. T. S. Hale *et al.*, Visual Network Asymmetry and Default Mode Network Function in ADHD: An fMRI Study. *Front Psychiatry* **5**, 81 (2014).
147. E. Hoekzema *et al.*, An independent components and functional connectivity analysis of resting state fMRI data points to neural network dysregulation in adult ADHD. *Hum Brain Mapp* **35**, 1261-1272 (2014).
148. J. Golchert *et al.*, Individual variation in intentionality in the mind-wandering state is reflected in the integration of the default-mode, fronto-parietal, and limbic networks. *Neuroimage* **146**, 226-235 (2017).
149. M. Mittner, G. E. Hawkins, W. Boebel, B. U. Forstmann, A Neural Model of Mind Wandering. *Trends Cogn Sci* **20**, 570-578 (2016).
150. J. Smallwood, A. Fitzgerald, L. K. Miles, L. H. Phillips, Shifting moods, wandering minds: negative moods lead the mind to wander. *Emotion* **9**, 271-276 (2009).
151. A. Fink *et al.*, Enhancing creativity by means of cognitive stimulation: evidence from an fMRI study. *Neuroimage* **52**, 1687-1695 (2010).
152. S. Liu *et al.*, Neural correlates of lyrical improvisation: an FMRI study of freestyle rap. *Sci Rep* **2**, 834 (2012).
153. R. E. Beaty, M. Benedek, S. B. Kaufman, P. J. Silvia, Default and Executive Network Coupling Supports Creative Idea Production. *Sci Rep* **5**, 10964 (2015).
154. S. L. Bengtsson, M. Csikszentmihalyi, F. Ullén, Cortical regions involved in the generation of musical structures during improvisation in pianists. *J Cogn Neurosci* **19**, 830-842 (2007).
155. P. Loui, Rapid and flexible creativity in musical improvisation: review and a model. *Ann N Y Acad Sci* **10.1111/nyas.13628** (2018).
156. D. L. Zabelina, G. Ganis, Creativity and cognitive control: Behavioral and ERP evidence that divergent thinking, but not real-life creative achievement, relates to better cognitive control. *Neuropsychologia* **118**, 20-28 (2018).
157. J. Li *et al.*, Flexible reconfiguration of functional brain networks as a potential neural mechanism of creativity. *Brain Imaging Behav* **15**, 1944-1954 (2021).
158. A. Belden *et al.*, Improvising at rest: Differentiating jazz and classical music training with resting state functional connectivity. *Neuroimage* **207**, 116384 (2020).
159. S. Roumeliotis *et al.*, Be careful with ecological associations. *Nephrology (Carlton)* **26**, 501-505 (2021).
160. J. D. Horel, Complex Principal Component Analysis: Theory and Examples.

*Journal of Applied Meteorology and Climatology* **23**, 1660–1673 (1984).

161. Anonymous (2023) The MathWorks Inc. (2023). MATLAB version: 9.13.0 (R2023b), Natick, Massachusetts: The MathWorks Inc. <https://www.mathworks.com>.
162. Anonymous (R Core Team (2023). R: A language and environment for statistical computing. R Foundation for Statistical Computing, Vienna, Austria. URL <https://www.R-project.org/>.
163. M. Jenkinson, C. F. Beckmann, T. E. Behrens, M. W. Woolrich, S. M. Smith, Fsl. *Neuroimage* **62**, 782-790 (2012).
164. B. Diedenhofen, J. Musch, cocor: a comprehensive solution for the statistical comparison of correlations. *PLoS One* **10**, e0121945 (2015).
165. T. Chou, D. D. Dougherty, A. A. Nierenberg, T. Deckersbach, Restoration of default mode network and task positive network anti-correlation associated with mindfulness-based cognitive therapy for bipolar disorder. *Psychiatry Res Neuroimaging* **319**, 111419 (2022).

166. Y. He, T. Xu, W. Zhang, X. N. Zuo, Lifespan anxiety is reflected in human amygdala cortical connectivity. *Hum Brain Mapp* **37**, 1178-1193 (2016).
167. C. M. Sylvester *et al.*, Individual-specific functional connectivity of the amygdala: A substrate for precision psychiatry. *Proc Natl Acad Sci U S A* **117**, 3808-3818 (2020).
168. S. Ogawa, T. M. Lee, A. R. Kay, D. W. Tank, Brain magnetic resonance imaging with contrast dependent on blood oxygenation. *Proc Natl Acad Sci U S A* **87**, 9868-9872 (1990).
169. H. Petsche, Approaches to verbal, visual and musical creativity by EEG coherence analysis. *Int J Psychophysiol* **24**, 145-159 (1996).
170. H. Takeuchi *et al.*, White matter structures associated with creativity: evidence from diffusion tensor imaging. *Neuroimage* **51**, 11-18 (2010).
171. A. Zamm, G. Schlaug, D. M. Eagleman, P. Loui, Pathways to seeing music: enhanced structural connectivity in colored-music synesthesia. *Neuroimage* **74**, 359-366 (2013).
172. Y. Wang *et al.*, Spontaneous Activity in Primary Visual Cortex Relates to Visual Creativity. *Front Hum Neurosci* **15**, 625888 (2021).
173. J. Pearson, The human imagination: the cognitive neuroscience of visual mental imagery. *Nat Rev Neurosci* **20**, 624-634 (2019).
174. D. M. Eagleman, D. A. Vaughn, The Defensive Activation Theory: REM Sleep as a Mechanism to Prevent Takeover of the Visual Cortex. *Front Neurosci* **15**, 632853 (2021).
175. M. Schredl, D. Erlacher, Self-reported effects of dreams on waking-life creativity: an empirical study. *J Psychol* **141**, 35-46 (2007).
176. D. Barrett, Dreams and creative problem-solving. *Ann N Y Acad Sci* **1406**, 64-67 (2017).
177. D. M. Bashwiler, C. J. Wertz, R. A. Flores, R. E. Jung, Musical Creativity "Revealed" in Brain Structure: Interplay between Motor, Default Mode, and Limbic Networks. *Sci Rep* **6**, 20482 (2016).
178. M. J. McPherson, F. S. Barrett, M. Lopez-Gonzalez, P. Jiradejvong, C. J. Limb, Emotional Intent Modulates The Neural Substrates Of Creativity: An fMRI Study of Emotionally Targeted Improvisation in Jazz Musicians. *Sci Rep* **6**, 18460 (2016).
179. B. Thirion *et al.*, Analysis of a large fMRI cohort: Statistical and methodological issues for group analyses. *Neuroimage* **35**, 105-120 (2007).
180. K. S. Button *et al.*, Power failure: why small sample size undermines the reliability of neuroscience. *Nat Rev Neurosci* **14**, 365-376 (2013).
181. R. J. Daker, R. A. Cortes, I. M. Lyons, A. E. Green, Creativity anxiety: Evidence for anxiety that is specific to creative thinking, from STEM to the arts. *J Exp Psychol Gen* **149**, 42-57 (2020).
182. I. Carlsson, Anxiety and Flexibility of Defense Related to High or Low Creativity. *Creativity Research Journal* **14**, 341-349 (2002).
183. O. Vartanian, S. A. Saint, N. Herz, P. Suedfeld, The Creative Brain Under Stress: Considerations for Performance in Extreme Environments. *Front Psychol* **11**, 585969 (2020).
184. S. Yin, Y. Li, A. Chen, Functional coupling between frontoparietal control subnetworks bridges the default and dorsal attention networks. *Brain Struct Funct* **227**, 2243-2260 (2022).
185. B. O. Turner, E. J. Paul, M. B. Miller, A. K. Barbey, Small sample sizes reduce the replicability of task-based fMRI studies. *Commun Biol* **1**, 62 (2018).
186. R. Englert *et al.*, Connectome-Based Attractor Dynamics Underlie Brain Activity in Rest, Task, and Disease. *bioRxiv* 10.1101/2023.11.03.565516, 2023.2011.2003.565516 (2024).
187. P. Bedford *et al.*, The effect of lysergic acid diethylamide (LSD) on whole-brain functional and effective connectivity. *Neuropsychopharmacology* **48**, 1175-1183 (2023).

188. R. L. Carhart-Harris *et al.*, Neural correlates of the LSD experience revealed by multimodal neuroimaging. *Proc Natl Acad Sci U S A* **113**, 4853-4858 (2016).
189. A. I. Luppi *et al.*, LSD alters dynamic integration and segregation in the human brain. *Neuroimage* **227**, 117653 (2021).
190. D. E. Nichols, Dark Classics in Chemical Neuroscience: Lysergic Acid Diethylamide (LSD). *ACS Chem Neurosci* **9**, 2331-2343 (2018).
191. T. F. Varley, R. Carhart-Harris, L. Roseman, D. K. Menon, E. A. Stamatakis, Serotonergic psychedelics LSD & psilocybin increase the fractal dimension of cortical brain activity in spatial and temporal domains. *Neuroimage* **220**, 117049 (2020).
192. K. J. Gorgolewski *et al.*, The brain imaging data structure, a format for organizing and describing outputs of neuroimaging experiments. *Sci Data* **3**, 160044 (2016).
193. R. A. Poldrack *et al.*, The Past, Present, and Future of the Brain Imaging Data Structure (BIDS). *ArXiv* (2024).
194. X. Li *et al.*, Moving Beyond Processing and Analysis-Related Variation in Neuroscience. *bioRxiv* 10.1101/2021.12.01.470790, 2021.2012.2001.470790 (2024).